博士学位論文

Elemental Distribution Analysis of Lithium Ion Battery Electrodes with Glow Discharge Optical Emission Spectroscopy

グロー放電発光分析法によるリチウムイオン二次電池電極の元素分布分析

平成 **26** 年 **9** 月

兵庫県立大学　工学研究科

高原　晃里

博士学位論文

Elemental Distribution Analysis of Lithium Ion Battery Electrodes with Glow Discharge Optical Emission Spectroscopy

グロー放電発光分析法によるリチウムイオン二次電池電極の元素分布分析

平成 **26** 年 **9** 月

兵庫県立大学　工学研究科

高原　晃里

Contents

1. Introduction

1.1 The background of this study

Lithium ion battery (LIB) has been successfully applied to portable electronics for the last decade. Recently, application of LIB in the field of energy vehicles and stationary storage systems has attracted considerable attention, in order to efficiently utilize renewable energies such as solar and wind energies. As higher energy capacity and power, long–term stability, safety, and lower costs are required, further development and studies are carried out around the globe. Materials and configurations of battery are being developed, and fundamental behaviors of the electrochemical reactions and the interphase phenomena of the electrode and electrolyte are being studied.

The schematic illustration of a lithium ion cell is shown in Fig.1.1 [1]. It is composed of a positive electrode, a negative electrode, organic liquid electrolyte with lithium–ion conductivity, and an electrically insulating polymer separator. Lithium insertion compounds such as $LiCoO_2$, $LiMn_2O_4$, and $LiFePO_4$ are typically employed for the positive electrode. Graphite is typical for a negative electrode, and more recently Si or Sn alloy having higher energy capacities and $Li_4Ti_5O_{12}$ with an advantage in safety are also used. During the charge process, the lithium ion migrates from the positive electrode material to the negative electrode material through the electrolyte and the electron flows through the external circuit from the positive electrode to the negative electrode. An inverse reaction occurs during the discharge process. It follows that the number of lithium ions migrating between the electrodes determines the energy capacity of the cell, and the mobility and the repeatability on the migration of lithium ion affect the power and lifespan of the cell, respectively.

An important subject related to LIB development is cell deterioration in the energy capacity and power during long–term and high–temperature operations. The cell deterioration mechanism has been studied extensively to date. The cell can be degraded for numerous and various reasons: formation of inactive layer so–called solid electrolyte interphase (SEI) [2], structural change of electrode materials, decomposition of organic liquid electrolytes, gas evolution, and so on. Especially, SEI growth on the negative electrode is well known to contribute strongly to capacity fading during cycles. Formation of the SEI layer on the negative electrode causes irreversible capacity loss in the first few cycles. Even in additional cycles, lithium is consumed continuously as a result of continuous reduction of the electrolyte on the electrode. The numerous studies on characterization of SEI with x–ray photoelectron spectroscopy

(XPS), Fourier–transform infrared spectroscopy (FT–IR), and nuclear magnetic resonance spectroscopy –decomposed solvents such as $Li_xPF_yO_z$ originated from $LiPF_6$. The formation of SEI could occur inhomogeneously in–plane direction and in–depth direction in graphite electrode. However, there are a little distribution analysis methods, especially for in–depth direction. Pretreatment by a cross–section polisher (CP) with Ar ion beam is commonly used to exposure the measuring face [3]. Then the versatile tools for surface analysis such as scanning electron microscope (SEM), electron probe micro analyzer (EPMA), XPS, and auger electron spectroscopy (AES) become available for in–depth direction mapping. However, the pretreatment with CP could make the analyzing sample surface unstable and reacted in some cases. The light and volatile elements such as Li, C, N, O, and F are difficult to preserve from the mechanical polishing. Therefore we had objects to evaluate and apply glow discharge optical emission spectroscopy (GD–OES) to improve the in–depth direction characterization for LIB electrodes. GD–OES is a direct depth profiling technique with nm to 100 μm scale. The elements from light elements including H, Li, C, O, and F to heavy elements are possible to analyze. The general outlines of GD–OES are described in the next section.

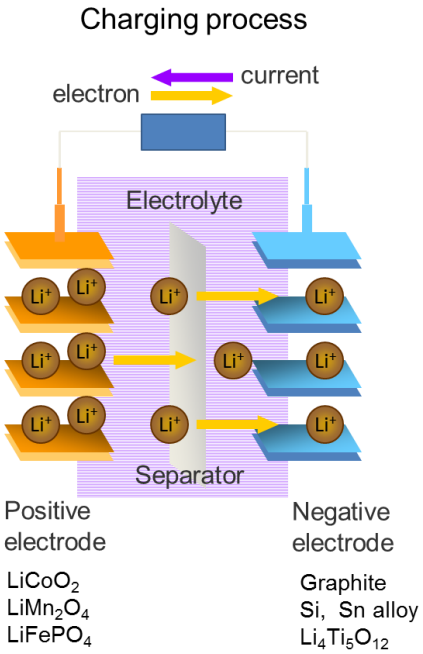

Figure 1.1. Schematic illustration of lithium ion cell.

1.2 The basic principle and characteristics of glow discharge optical emission spectroscopy [4]

Glow discharge is defined as a stable gaseous discharge generated under a reduced pressure, which is distinguished from arc and spark discharges generated at atmospheric pressure. The plasma induced with glow discharge performs sputtering phenomena. The sputtering with glow discharge has been indispensable in microelectronics and material industrial fields and extensively utilized as thin−film deposition, coating, and surface etching. Analytically relevant glow discharge was first described by Grimm in 1967. The Grim type lamp enables placing the cathode out of the discharge source and ablating it layer−by−layer by sputtering. This type of discharge is useful for bulk and depth profiling analysis for a bulk solid. Glow discharge optical emission spectroscopy (GD−OES) was used for a trace elemental analysis of bulk in steel industry in 1970s. In 1980s, it was applied to depth profiling in a metal−plating such as zinc alloy. Once radio frequency (rf) potential alternative to conventional direct current (dc) potential was mounted in the equipment in 1990s, GD−OES has broaden to microelectronics field such as semiconductors, thin films, glasses and polymers in the benefit of rf potential, which enables sputtering either conductive or non−conductive material because of the self−bias potential.

Figure 1.2 shows schematic drawing of GD−OES equipment and the detail of the glow discharge source. Its equipment is furnished with a grim type glow discharge lump, where a sample is mounted facing as a cathode. When argon is introduced into the source with low pressure (a few hundreds Pa) and a high voltage (500 − 1000 V) is applied to the cathode, the gas is ionized and then the electrical discharge plasma is generated from positively−charged ions (Ar^+) and free electrons (e^-). Then sample sputtering (cathodic sputtering) by Ar^+ bombardment is induced according to the potential between the electrodes. When the atoms are sputtered away from sample surface, they are excited to the various atomic and ionic excited states by the complex collisions with Ar^+ and e^- in the plasma discharge, and then the optical emissions are induced in the relaxation processes. The optical emissions are element−specific radiations ranging over ultraviolet, visible, and near infrared wave regions. In the analytical equipment (Fig. 1.2(a)), the emissions are taken through a lens into the spectrometer located behind it, diffracted by a grating, and then detected using photomultipliers or CCDs.

The optical emissions are characteristic lines and the intensities are proportional to the numbers of the atoms, bringing the qualitative and quantitative capabilities of GD−OES. The aperture of the anode in the glow discharge lump is typically a few mm in diameter, which decides the measurement spot size. A typical sputtering rate is around 1 μm min^{-1} for metallic sample. This property makes possible much faster

and much deeper depth profiling than other techniques of AES and SIMS (1 μm h^{-1} in typical sputtering rate)[5]. The sputtering rate varies with sample composition. Figure 1.3 exhibits a comparison of sputtering yield for various elements under 400 eV Ar ions bombardment which is close to a sputtering condition in GD–OES [6]. The sputtering yield is theoretically dependent on the ion–atom mass ratio. However, it is likely more complicated in practice, though the sputtering yield seems to vary according to the d–shell filling.

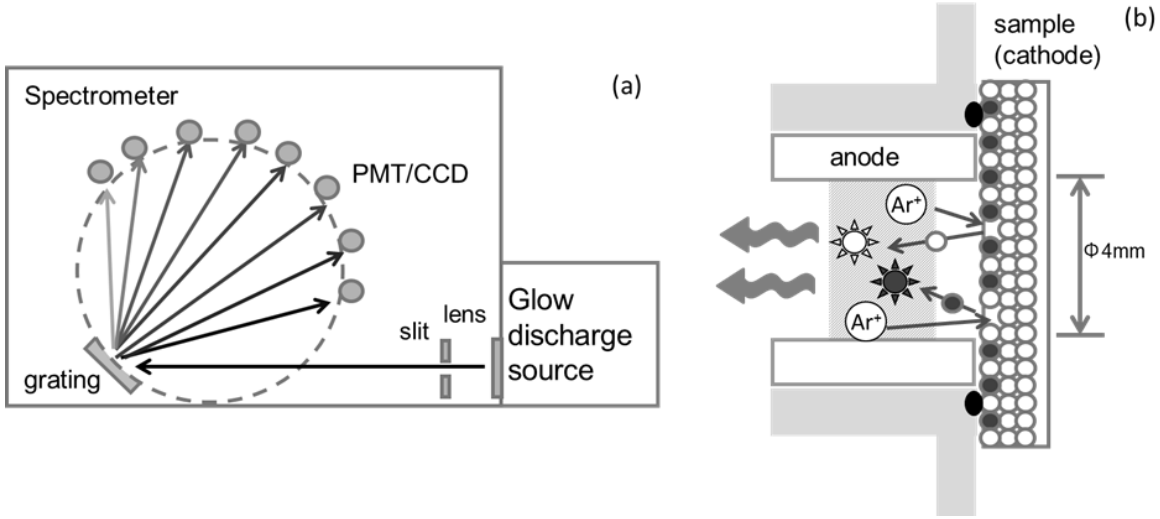

Figure 1.2. Schematic drawing of GD-OES equipment (a) and details of the glow discharge source (b).

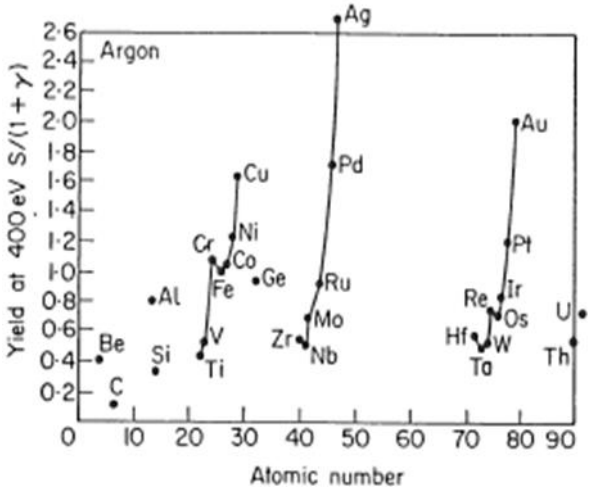

Figure 1.3. Sputter yields for various elements under bombardment of 400–eV Ar ions [6].

1.3 The aim of the present study and the contents of the doctoral thesis

The aim of the present study is evaluating the capability of GD–OES analysis technique in order to characterize LIB electrodes.

In chapter 2: Elemental distribution analysis of $LiFePO_4$/graphite cells studied with glow discharge optical emission spectroscopy [7], GD–OES capability was investigated for depth profiling of positive and negative electrodes. $LiFePO_4$/graphite cells with an aging state and several capacity fading levels were studied using GD–OES. Depth profiles were obtained from the surface to the collector in positive and negative electrodes. The Li profiles were changed with degree of degradation and the behavior of Li in degraded electrodes was discussed. It is proposed that GD–OES is useful for degradation analysis.

In chapter 3: Quantification of lithium in LIB electrodes with glow discharge optical emission spectroscopy [8], GD–OES quantification ability of Li was evaluated for LIB electrodes. The glow discharge conditions were adjusted and the sample surface features in sputtering were investigated in detail with SEM and XPS. The Li intensities obtained from GD–OES were correlated with the Li components determined by inductively coupled plasma–mass spectroscopy (ICP–MS) for both positive and negative electrodes. The results confirmed that GD–OES is a potential technique for quantitative analysis of Li in the electrodes.

In chapter 4: Depth profiling of graphite electrode in lithium ion battery using glow discharge optical emission spectroscopy with small quantities of hydrogen or oxygen addition to argon [9], the improvement for graphite electrode measurement was examined. In the preceded study described in chapter 3, it was found out that carbon–based electrode was difficult to measure stably with the conventional Ar–ion sputtering because of its low sputtering rate and the redeposition phenomenon. The measurement of carbon–based electrode was improved with reactive sputtering with adding small quantities of hydrogen or oxygen addition to Ar.

In the chapter 5 [10]: Analysis of solid electrolyte interphase in Mn–based cathode/graphite Li–ion battery with glow discharge optical emission spectroscopy, the improved GD–OES method, described in chapter 4, was applied to the degraded graphite electrodes in commercially available batteries. The distributions of Li and Mn in graphite electrodes were indicated in the depth profiles, and the deterioration mechanism was discussed from the results.

In the chapter 6: Conclusion, the results obtained from this study were summarized.

1.4 References

[1] G–A. Nazri and G. Pistoia (Ed), *LITHIUM BATTERIES Science and Technology*, Springer, New York, pp.3 – 41 (2009).

[2] P. B. Balbuena and Y. Wang (Ed), *Lithium–Ion Batteries, Solid–Electrolyte Interphase*, Imperial College press, London (2004).

[3] J. C. Rivier and S. Myhra (Ed), *Handbook of surface and interface analysis*, Marcel Dekker, Inc., New York, pp.650 – 653 (1998).

[4] R. K. Marcus (Ed), *Glow Discharge Spectroscopies (Modern Analytical Chemistry)*, Plenum pub Corp, New York (1993).

[5] R. K. Marcus and J. A. C. Broekaert (Ed), *Glow Discharge plasmas in Analytical Spectroscopy*, John Wiley & Sons Ltd., England pp.253 – 272 (2003).

[6] R. K. Marcus (Ed), *Glow Discharge Spectroscopies*, pp. 30–31, Plenum Press, New York (1993).

[7] H. Takahara, H. Miyauchi, M. Tabuchi, T. Nakamura, *J. Electrochem. Soc.*, **160**, A272 (2013).

[8] H. Takahara, M. Shikano, H. Kobayashi, *J. Power Sources*, **244**, 252 (2013).

[9] H. Takahara, A. Kojyo, K. Kodama, T. Nakamura, K. Shono, Y. Kobayashi, M, Shikano, H. Kobayashi, *J. Anal. At. Spectrom*., **29**, 95 (2014).

[10] H. Takahara, Y. Kobayashi, K. Shono, H. Kobayashi, M. Shikano, T. Nakamura, *J. Electrochem. Soc.*, **161**, A1716, (2014).

2. Elemental distribution analysis of $LiFePO_4$/graphite cells studied with glow discharge optical emission spectroscopy (GD–OES)

$LiFePO_4$/graphite cells with an aging state and several capacity fading levels were studied using GD–OES. Depth profiles were obtained from the surface to the collector in positive and negative electrodes. Results show that Li is distributed homogeneously in terms of depth in $LiFePO_4$ and graphite electrodes for cells with 85–100% capacity retention. For a cell that deteriorated to 44% capacity retention after only 50 cycles, the Li amount was apparently slightly lower toward the current collector in the positive electrode. Deposits formed on the graphite electrode surface (SEI) comprise Li, H, C, F, O, and P, with a large amount of Li for the cell with sudden deterioration. The deposition amount increases with progression of capacity fading, suggesting that deposits on the negative electrode are related to cell deterioration. The deposition surface shows Fe, implying that Fe dissolved and migrated from the positive electrode during charge–discharge cycles at 45 ˚C. The Li intensities obtained from GD–OES spectra of all cells were correlated with Li contents obtained using induced coupled plasma – optical emission spectroscopy (ICP–OES) and atomic absorption spectroscopy (AAS), which enable us to ascertain the Li contents of the electrodes quantitatively.

2.1 Introduction

Lithium ion batteries (LIB) have been applied to portable electronics for the last two decades. Recently, application of LIB in the field of electric vehicles and stationary storage systems has attracted considerable attention for use in renewable energy applications such as electrical generation at solar and wind installations. Because their wider use demands energy capacity and power, long-term stability, safety, and lower costs, further development and studies are being conducted worldwide. Extensive research related to materials and battery configurations is being accelerated to reach this goal. Moreover, characterization techniques are strongly required because it is important to ascertain the fundamental behavior of materials in the electrochemical reaction, the cell deterioration mechanism, and interphase phenomena of the electrode and electrolyte. In addition to conventional and basic uses of laboratory analysis tools, spatially resolved and temporally resolved functions might be used to study interfacial reactions, reaction

distributions, and the LIB reaction mechanism. In−situ analysis techniques examine conditions that closely resemble actual operating conditions [1−5]. Among those techniques, synchrotron radiation provides the highest sensitivity and resolution. The characterization of lithium is also crucial because the behavior of lithium ions in the electrodes and interface to the electrolyte is the key to LIB cell performance. Li is consumed for the formation of solid electrolyte interphase (SEI) in the negative electrode. Furthermore, Li might remain in the discharged negative electrode (or charged positive electrode) if reversible Li^+ de−intercalation and/or intercalation in either electrode is prevented by side reactions, structural deterioration, or another phenomenon.

Glow discharge optical emission spectroscopy (GD−OES) is an in−depth analytical technique by which the sample sputtering and atomic emissions take place simultaneously in an argon plasma atmosphere. It has been used in steel and metal−plating industries for trace elemental analysis and the depth profiling with direct current (dc) potential. Recently it has been applied widely in the microelectronics field for semiconductors, thin films, glasses, and polymers in the benefit of the radio frequency (rf) potential, which makes it possible to sputter either conductive or non−conductive material because of the self−bias potential [6]. Numerous analytical works have examined for example, boron phosphorous silicate glass (BPSG) film on silicon wafers in semiconductor industry and a barrier oxide film formed in anodic oxidation of aluminum [7]. Also in the advanced field of lithium ion batteries, depth profiling of positive electrodes was attempted using rf−GD−OES [8]. The lithium composition is evaluated comprehensively from the surface to the interface of the current collector for a few SOC states of $LiAl_{0.05}$ $Co_{0.15}Ni_{0.8}O_2$ electrode. The results agree well with those obtained from induced coupled plasma−mass spectroscopy (ICP−MS), which suggests that GD−OES is useful for quantification of Li in LIB electrodes.

The depth profiling capability of GD−OES is applicable not only to the bulk solid but also to the surface of the LIB electrodes. A surface passivation film called solid electrolyte interphase (SEI) is well known to be formed at the electrode−electrolyte interface. The layer is necessary to protect the negative electrode from further side reaction with electrolytes. However, it simultaneously raises impedance and engenders capacity loss. Therefore, the SEI plays an important role in battery characteristics and failure mechanisms. The SEI is formed by a decomposition reaction that occurs among the Li ion, solvent anion, and/or alkyl carbonate solution during reduction of the negative electrode [9]. Numerous studies with X−ray photoelectron spectroscopy (XPS), Fourier transform − infrared spectroscopy (FT−IR), and nuclear

magnetic resonance (NMR) analysis have indicated that the SEI comprises LiF, Li_2CO_3, lithium alkyl carbonates $ROCO_2Li$. In addition, decomposed solvents such as $Li_xPF_yO_z$, Li_xAsF_y, and $Li_xSO_yCF_z$ originated respectively from $LiPF_6$, LiAsF, and $LiC(SO_2CF_3)_3$ [10, 11]. In this study, we attempt to use GD–OES to analyze the SEI composition on the negative electrode surface.

Lithium iron phosphate $LiFePO_4$ [12] is a candidate for use in large battery applications such as electric and hybrid electric vehicles because of its benefits of safety characteristics of poly–anion compounds. Although $LiFePO_4$ presents the shortcoming of poor rate capability because of low electronic conductivity and low lithium ion mobility, it is overcome by synthesized approaches of the reduction of the particle size and carbon coating of particle surfaces [13–16]. In this work, a GD–OES depth profiling technique was applied to analyze the capacity fading process of C–coated $LiFePO_4$ ($LiFePO_4$/C) and graphite cells. The $LiFePO_4$/C was prepared by gas–solid phase reaction and was coated homogeneously with a 2 nm carbon layer (1.5–2.5 wt% of C coating weight) through reaction with hydrocarbon gas, which enhanced the high–rate capability and stable cycling performance. The cells, which comprised $LiFePO_4$/C composite and graphite, were subjected to charge–discharge cycling at 45 °C. Both the positive and negative electrodes under different levels of cell deterioration processes were measured using GD–OES technique. Depth profiling was performed for the whole electrode, from the surface to the current collector. Detailed surface profiles of the graphite electrodes were also analyzed.

2.2 Experimental

2.2.1 Sample preparation

Positive electrode materials of carbon coated $LiFePO_4$ ($LiFePO_4$/C) were synthesized using a gas–solid phase reaction as reported previously[17]. The precursor $LiFePO_4$ compound was prepared with an initial mixing of Li_2CO_3, $FeC_2O_4{\cdot}2H_2O$, and $(NH_4)_2HPO_4$ and by calcination at 350 °C in a N_2 atmosphere. Then it was heated under a constant flow of hydrocarbon gas, which is a source of elemental carbon. The heating temperatures were 720 °C for sample cells A–0, A–50, and A–100 and 660 °C for a B–100 sample cell. The amounts of carbon for the $LiFePO_4$/C powder materials were analyzed using a carbon/sulfur analyzer (EMIA–2200; Horiba Ltd.). The negative electrode material of graphite (OMAC) was provided by Osaka Gas Chemicals Co., Ltd. (Osaka, Japan). The positive and negative electrodes were prepared by mixing the active materials, acetylene black and poly(vinylidene fluoride) (PVdF) binder in

N−methyl−2−pyrrolidone (NMP) solvent, which were coated respectively onto Al and Cu current collectors. The positive electrode was 86:7:7 (wt%) in composition of $LiFePO_4$/C: acetylene black: PVdF, 7.8 mg cm^{-2} of loading and 40 μm thickness. The 29 μm−thick negative electrode was 93:2:5 (wt%) in composition of graphite: acetylene black: PVdF, 3.8 mg cm^{-2} of loading. The electrode sizes were 50 mm × 50 mm. The laminated cells were assembled with the $LiFePO_4$/C electrode, the graphite electrode, polyolefin separator (Hipore; Asahi−Kasei Chemicals Corp.), and 1 mol dm^{-3} $LiPF_6$ in ethylene carbonate – diethyl carbonate electrolyte (EC: DEC, 3:7 in volume, Kishida Chemical Co. Ltd.) in an Ar−filled glove box. Charge–discharge cycle tests were conducted at 45 °C. The cut−off voltages of 2.5 and 4.0 V under the current rate of 1 C, where the current was defined for the $LiFePO_4$ cathode (1 C current corresponding to 170 mA g^{-1}). The sample cell A−0 was aged during the same period as cell A−100 for reference. The cells were disassembled after 50 cycles for sample cell A−50 and 100 cycles for A−100 and B−100. The electrodes were rinsed with dimethyl carbonate solvent (DMC; Kishida Chemical Co. Ltd.) in an Ar−filled glove box, and were then analyzed using GD−OES. Moreover, SEM micrographs were taken (JSM 5500 LV; JEOL) with 15 kV accelerating voltage. In addition to GD−OES measurements, the Li contents in the sample electrodes were analyzed using ICP−OES (SPS4000; SII Nano Technology Inc.) and AAS (Z2300; Hitachi High−Technologies Corp.).

2.2.2 GD−OES measurement

The GD−OES depth profiles in this study were collected (GDA750; Rigaku/Spectruma) with application of the radio frequency power and pulsed glow discharge. The cells after aging or charge–discharge cycling were disassembled in an Ar−filled glove box. The sample electrodes were transferred to the apparatus with an experimental vessel without exposure to ambient atmosphere. The analyzed spot was of 4−mm diameter. The discharged gas (Ar or Ne) was selected under consideration of the sensitivity of the elements: Ne gas was chosen when including fluorine in the analytical elements because Ne gas discharge provides much higher sensitivity for fluorine analysis than Ar gas discharge does [18]. Source conditions chosen to obtain static sputtering were 500–600 V and 200–350 Pa for Ar gas discharge, and 1000 V and 1500 Pa for Ne gas discharge. The following elements and their emission lines were applied in this study: H (121.57 nm), Li (610.41 nm or 670.78 nm), C (156.14 nm), O (130.22 nm), F (685.60 nm), P (177.50 nm), Al (396.15 nm), Fe (238.20 nm), and Cu (327.40 nm).

2.3 Results and Discussion

2.3.1 Charge–discharge cycle test results for samples

Positive electrode materials of carbon–coated $LiFePO_4$ ($LiFePO_4$/C) were synthesized at two temperatures: 720 °C for sample cells A–0, A–50, and A–100; and 660 °C for sample cell B–100. The amounts of carbon for the $LiFePO_4$/C sintered at 720 and 660 °C were, respectively, 2.5 and 1.5 wt%. Figure 2.1 depicts the discharge capacities in charge–discharge cycles, for sample cells A–50, A–100, and B–100, which were $LiFePO_4$/C and graphite electrodes. The initial discharge capacities were 127.7 and 140.6 mAh g^{-1}. The capacity retention values after 100 cycles were 95 and 85%, respectively, for A–100 and B–100. Reportedly, the carbon content, conductivity and ferromagnetic impurities such as α–Fe and Fe_2P vary concomitantly with the sintering temperatures of $LiFePO_4$/C [17]. The initial discharge capacity decreases and the capacity retention increases continuously with increasing sintering temperature from 660 °C to 720 °C, which is a similar trend to that shown by the present charge–discharge result. The sample cell A–50 showed 44% capacity retention after the 50th cycle. The sudden decrease of its discharge capacity at the 50th cycle is probably related to partial shorting because the charge–discharge curves were noisy at the beginning of the cycle. The sample cell A–0 was aged during the same period as cell A–100 for use as a reference. Table 2.1 presents a summary of the capacity retention values obtained for sample cells A–50, A–100, and B–100. The Li contents of the positive and negative electrodes were determined using ICP–OES and AAS chemical analyses. The Li content for the as–prepared $LiFePO_4$/C positive electrode was estimated as 0.34 mg cm^{-2} (calculated based on the composition and loading density).

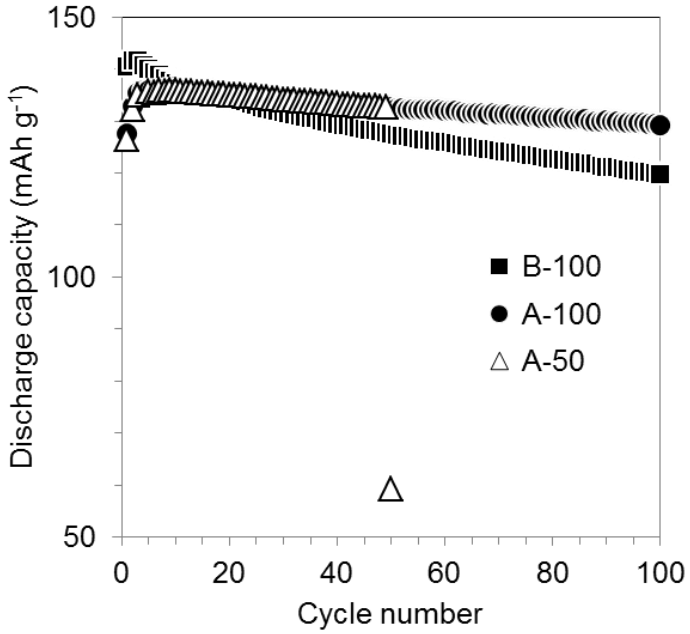

Figure 2.1. Variation in the discharge capacity with cycle number for sample cells A-50, A-100, and B-100 of $LiFePO_4$/C and graphite. The cell A-50 capacity decreased suddenly at the 50th cycle.

Table 2.1 Sintering temperatures and carbon contents for $LiFePO_4$/C of the positive electrode materials, cycle numbers, capacity retentions, Li contents with ICP-OES and AAS for sample cells A-0, A-50, A-100, and B-100

Sample cell	Sintering temperature (°C)	Carbon content (%)	Cycle number	Capacity retention (%)	Li contents by chemical analysis (mg cm^{-2})	
					positive	negative
A-0	720	2.5	0 (aging)	-	0.30	0.001
A-50	720	2.5	50	44	0.16	0.036
A-100	720	2.5	100	95	0.27	0.011
B-100	660	1.5	100	85	0.27	0.015

2.3.2 Depth profile and quantification of lithium in the electrodes

Figure 2.2 shows a GD–OES depth profile for $LiFePO_4$/C positive electrode of sample cell B–100. The intensities of Li, Fe, P, O, C, H, and Al are shown as a function of the sputtering time instead of the distance from the surface. Actually, $LiFePO_4$ contributes with Li, Fe, P, and O, whereas the carbon coating

and acetylene black contribute with C, and the PVdF binder contributes with C and H. It is only after 1800 s that the sputtering reaches the Al current collector. This point is reflected by a rapid increase of the Al intensity. Figure 2.2 shows that the Li, Fe, P, and O were distributed homogeneously in the electrode because all of their intensities are almost constant in the middle region. In contrast, the H and C intensities decrease continuously with increasing depth. Moreover, it is likely that the binder and/or acetylene black are not uniform and that more of each is contained in the outer layer [19]. It can also be considered that the peaks of P, C, H, and O at the top region, which are observed around 150 s, suggest surface film formation. Figure 2.3 (a) and (b) respectively display Li and Fe profiles for the four samples of A–0, A–50, A–100, and B–100. All samples show similar flat profiles of Fe. The Fe intensity is almost constant, but it increased slightly concomitantly with increasing sputtering time, probably because the sputtering rate is slightly enhanced gradually as sputtering proceeds. Sample A–0 had a higher sputtering rate, so that the Fe intensity was somewhat higher at the plateau and dropped down earlier. Figure 2.3 (a) shows that the plateau intensity of Li varies with the Li contents in the samples. It decreases within the order of A–0, A–100 which is almost equal to B–100 and A–50. The samples A–0, A–100, and B–100 show an almost constant profile of Li intensity in the middle region (or slightly increasing profile because of the gradual increase of the sputtering rate, as suggested also on the Fe profiles), which suggests that, except for the top layer, Li is distributed uniformly in terms of depth after 100 cycles of insertion and de–insertion into the positive electrode. The Li intensity exhibits a trend of a slight decrease that occurs with increasing depth for sample A–50, which suggests that the inner layers can contain less lithium than the outer layers for that sample. Such non–uniform distribution of Li, which was inferred for sample A–50, is probably correlated with the sudden deterioration. Recently, the reaction distribution and its relaxation process were investigated using depth–resolved X–ray absorption spectroscopy (XAS) and other methods. Results show that the lithium ionic diffusion in electrode bulk is affected by the potential slope of the charge–discharge reactions. The Li diffusion might be extremely slow in $LiFePO_4$ electrode because of its flat potential profile, which can at least partially explain the inhomogeneous distribution of Li in the GD–OES depth profile.

The feasibility of the lithium quantification was evaluated using Li intensities obtained using GD–OES. In GD–OES, the emission intensity of the analytical line depends on the concentration of the corresponding element and on the sputtering rate of the sample. Therefore, it is clear that the Li intensity

can vary not only with the Li content in the sample but also with the sputtering rates of respective samples. To avoid the influence of the sputtering rate variation, the intensity ratio of Li to the matrix element Fe was recorded. Figure 2.4 depicts the intensity ratio of Li to Fe versus Li contents obtained by chemical analyses of ICP–OES and AAS. The intensities of Li and Fe were averaged from the beginning up to the inflection point of Al increment for each datum. A linear relation was obtained with a coefficient of determination r^2 = 0.996, which is a great improvement over the relation between Li contents and Li intensity averaged without correction using Fe intensity (r^2 = 0.903).

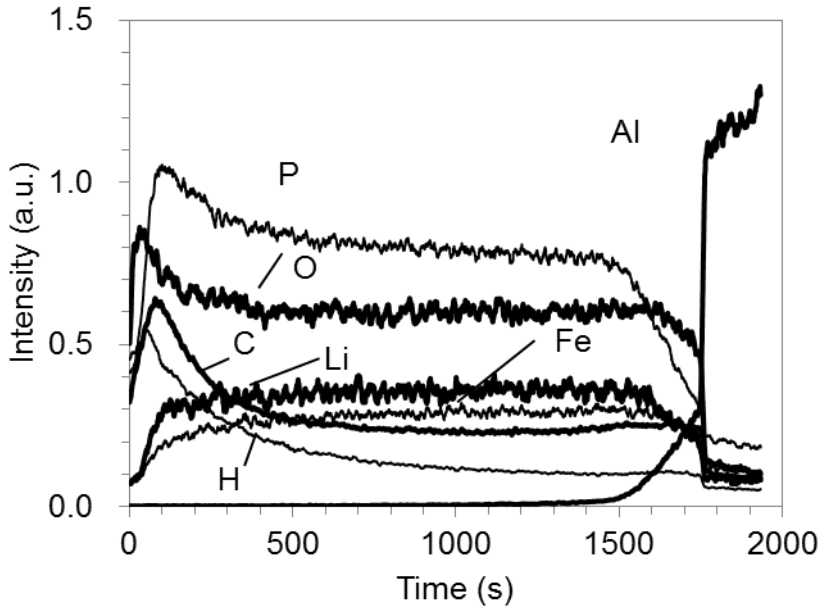

Figure 2.2. GD-OES depth profile for a $LiFePO_4$ electrode of sample cell B-100.

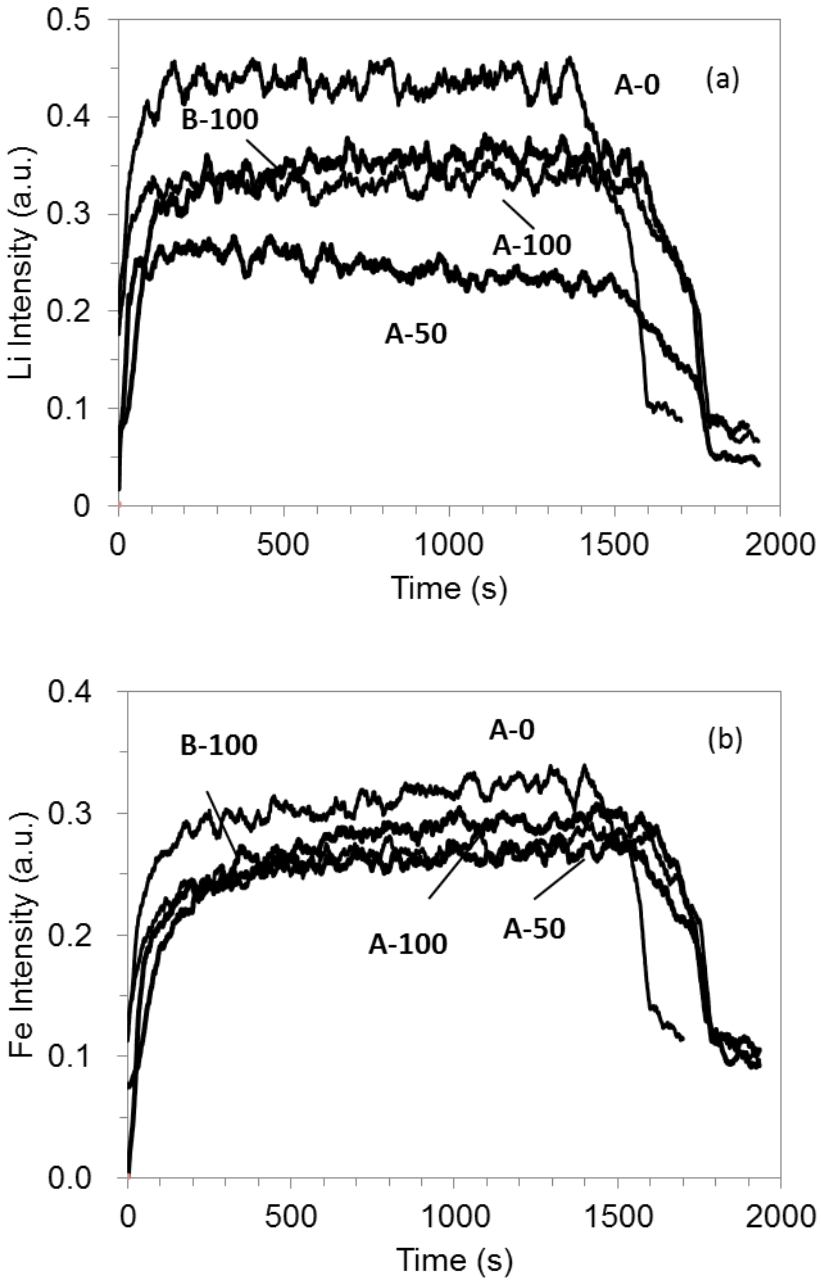

Figure 2.3. Variation of depth profiles of Li (a) and Fe (b) for $LiFePO_4$ electrodes in sample cells A-0, A-50, A-100, and B-100.

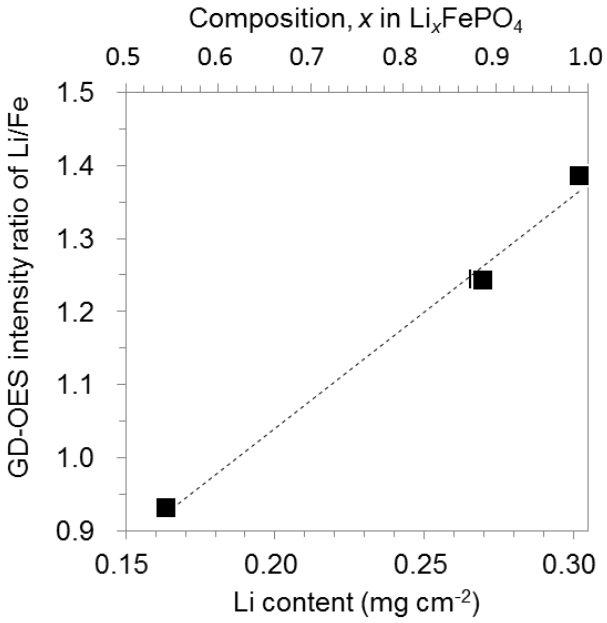

Figure 2.4. Relation between intensity ratios of Li/Fe obtained using GD-OES, and Li contents analyzed using AAS and ICP-OES for $LiFePO_4$ electrodes in sample cells A-0, A-50, A-100, and B-100. The broken line is shown as a visual guide. The linear coefficient r^2 is estimated as 0.996.

Figure 2.5 shows the GD–OES depth profile of Li, C, and Cu for the graphite electrode of sample B–100. The Li intensity is almost constant in the middle region, which suggests that Li is distributed homogeneously in the negative electrode. The rapid increase of Cu intensity after 6500 s indicates that the sputtering reaches the Cu current collector. Considering a factor of sputtering yield, which is defined as the ratio between the number of atoms sputtered from the surface and the number of incident ion (Ar^+ in this measurement), carbon possesses an extremely low sputtering yield (for example: 0.12 atoms/ion toward 1.0 for Fe, at 400 eV Ar ions [20]). Therefore, to reach the current collector of negative electrode, it is necessary to sputter for a longer time than with the positive electrode. Figure 2.5 shows that the intensity of Cu increased gradually from 3000 s before the rapid increment at 6500 s. Because of its high sputtering yield, Cu (1.6 atoms/ion at 400 eV Ar ions [20]) is likely to be sputtered slightly through the carbon–based electrode layer with a low sputtering rate when the electrode layer thickness is reduced by sputtering. Results also show that the intensity of C is depressed from 2500 s, as shown in Figure 2.5, which implies that the C profile is not as stable as the Li profile. To demonstrate the morphological change of the electrode after sputtering, SEM analysis was performed. Figure 2.6 presents an SEM micrograph of the

pristine graphite electrode after 3000 s of measurement. Although the electrode sample is sputtered smoothly for the most part, redeposition of the sputtered material and exposure of Cu are observed in places. These can contribute to the instability of C and Cu intensities. The redeposited materials can depress the C intensity caused by its lower sputtering efficiency. The exposure of Cu might cause the false onset of Cu intensity before reaching the interface between the electrode and the current collector. Furthermore, in the depth profile of Figure 2.5, both the intensities of Li and C are enhanced near the Cu current collector. This enhancement probably occurs because the sputtering rate of the electrode layer is enhanced in the presence of Cu. The positive electrode presents a depth profile that is commonly observed in GD–OES, where the intensities of Li, Fe, and P dropped while the Al (0.8 atoms/ion at 400 eV Ar ions [20]) intensity increased at the interface between the electrode and the current collector (Figure 2.2). In the profile of the graphite electrode, the rapid increases of Li and C intensities seem to present an extraordinary change at the interface of electrode layer and Cu current collector, which might be true because C and Cu have completely different sputtering yield characteristics from one another. Figure 2.7 portrays Li profiles of the stable intensity region before the rapid intensity enhancement because of the Cu layer for all samples A–0, A–50, A–100, and B–100. The plateau intensity of Li increases with Li content in the sample, in the order of A–0, A–100, B–100, and A–50. The Li intensity is almost constant in the middle region for each sample, suggesting that Li was distributed uniformly in depth during cycling of the insertion and de–insertion into the negative electrode, except the top layer. It is noteworthy that sample A–50 shows a uniform distribution of Li irrespective of the remarkable capacity fading, although it is suggested that the Li amount decreases slightly in the inner layers of the positive electrode of the sample (Figure 2.3 (a)).

For all negative electrode samples A–0, A–50, A–100, and B–100, the Li intensities determined using GD–OES have been compared to the Li contents evaluated using chemical analyses. A good linear relation was obtained between the averaged Li intensities from GD–OES (with no correction of sputtering rate variation) and Li contents from chemical analyses of ICP–OES and AAS analyses (r^2 = 0.992). For each datum, we considered the average intensity between the beginning and the inflection point of Cu increment. The averaged intensity ratio, Li/C, did not improve the relation (r^2 = 0.98), probably because the profile of C is not as stable as the Li profile shown in Figure 2.5. Therefore, the integration of Li intensity was performed as another means to correct the sputtering rate, irrespective of the C intensity. The total intensity integrated from the surface up to the current collector is expected to correspond to the total

amount of Li in the electrode. Figure 2.8 depicts the integrated intensity of Li versus Li contents obtained by chemical analyses for the negative electrode samples A–0, A–50, A–100, and B–100. Integration of the intensity is effective to improve the relation with the Li contents. It gives a better linear coefficient: r^2 = 0.998.

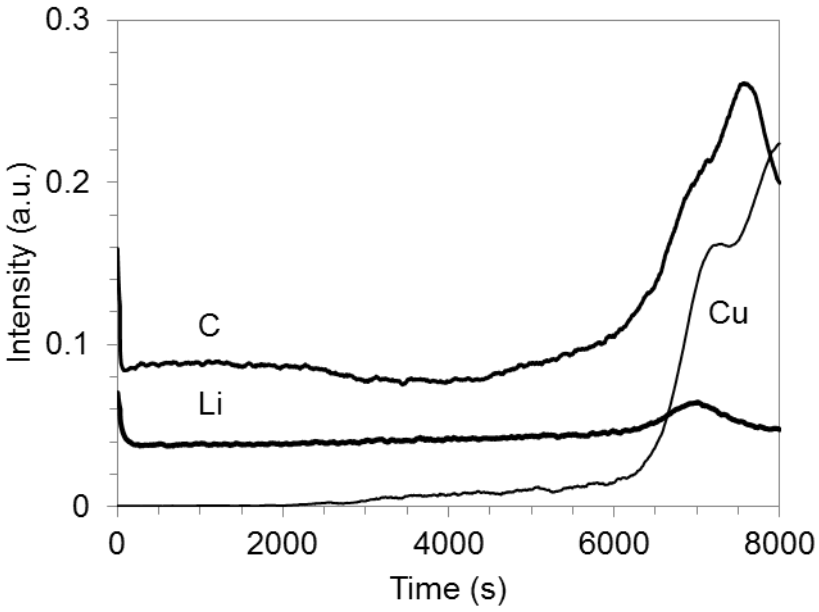

Figure 2.5. GD-OES depth profile for a graphite electrode of sample cell B-100.

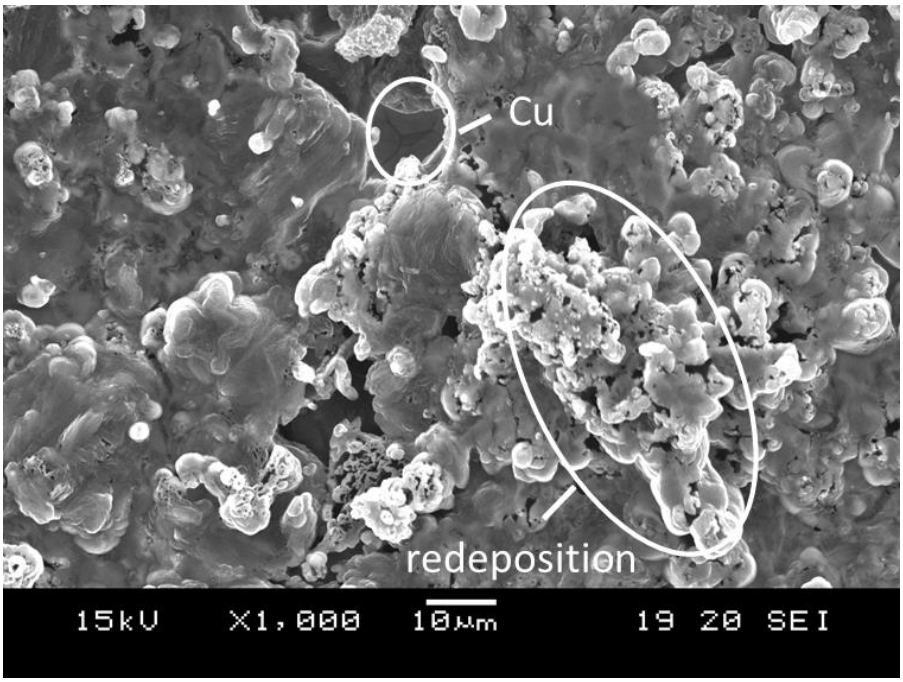

Figure 2.6. SEM micrograph of a pristine electrode after sputtering for 3000 s.

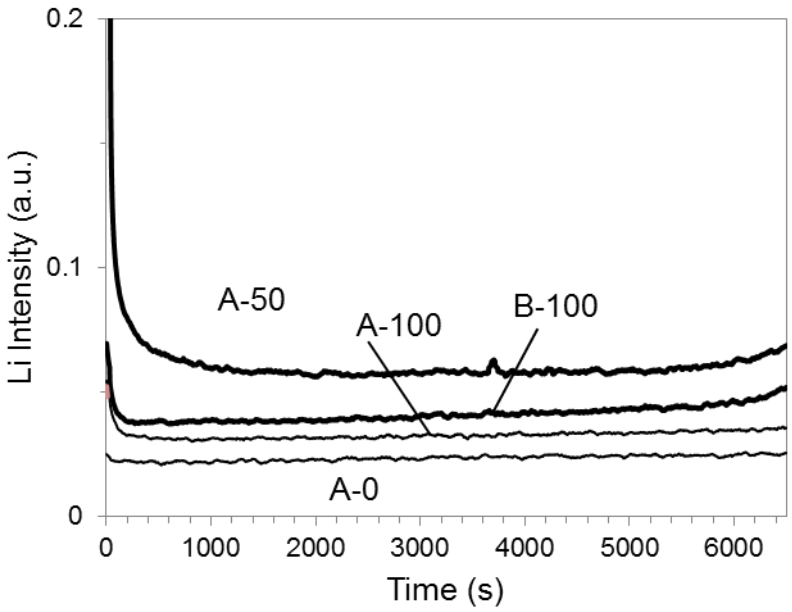

Figure 2.7. Variation of depth profiles of Li for the graphite electrode in sample cells A-0, A-50, A-100, and B-100.

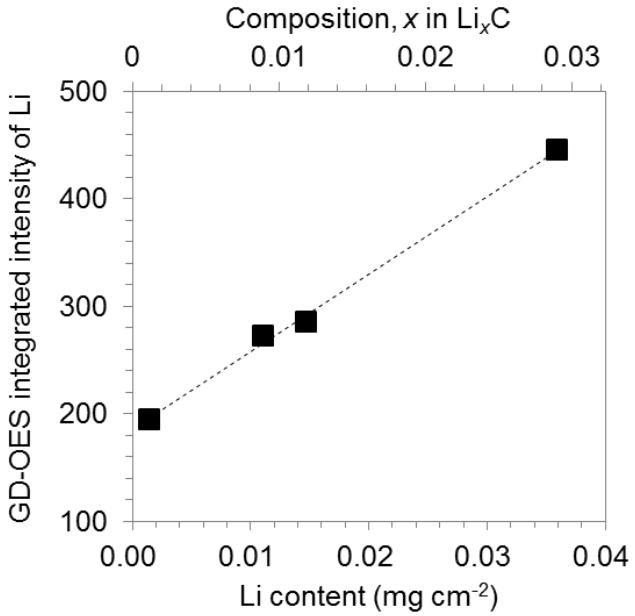

Figure 2.8. GD-OES integrated intensities of Li versus Li contents analyzed with AAS and ICP-OES for graphite electrodes in sample cells A-0, A-50, A-100, and B-100. The broken line is shown as a visual guide. The linear coefficient r^2 is estimated as 0.998.

2.3.3 Analysis of deposition on the negative electrodes

For detailed investigation of the surface of the negative electrode, slow sputtering was conducted with the lower pulse in the glow discharge condition. Figure 2.9 presents the surface profile of the graphite electrode of sample B−100. Peaks at the beginning of the profile originated from a layer deposited onto the electrode surface. When sputtering permeates the bulk of the electrode, the emission intensities are reduced drastically because the sputtering rate is much lower in the packed carbon matrix than it is with surface deposition, which has a lower atomic density. These peaks on the electrode surface imply the presence of solid state interphase (SEI), which was formed through the interface reaction with the electrolyte. Results obtained using different techniques (XPS, FT−IR and NMR) have shown that the SEI consists of decomposed materials of electrolytes such as LiF, Li_2CO_3, $ROCO_2Li$, and $Li_xPF_yO_z$ [21]. These findings show agreement with the GD−OES analyses of the surface layer, which reflect the presence of Li, F, O, C, P, and H, as depicted on Figure 2.9. Furthermore, Fe is detected at the surface, which indicates a possible dissolution of Fe from the positive electrode $LiFePO_4$ during the charge–discharge cycles followed by migration to the negative electrode. Reportedly, the migration of Fe from the positive electrode to the negative electrode surface contributes to cell degradation and the cell aging processes for $LiFePO_4$/Graphite cells [22−24].

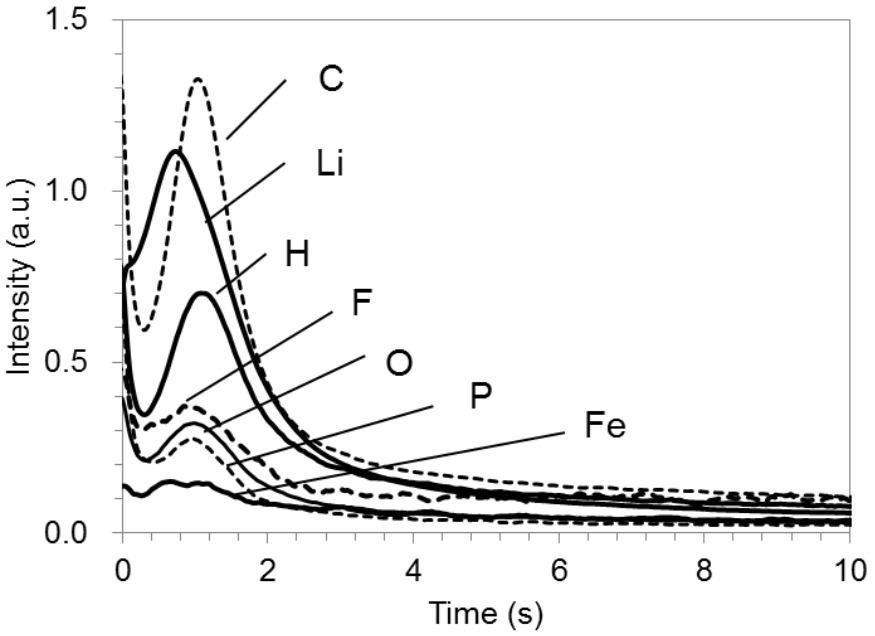

Figure 2.9. Detailed surface profiles obtained for graphite electrodes of sample cell B-100.

To elucidate changes in the amount of the deposition on the negative electrode samples qualitatively, the integrated peak intensities for the individual elements are presented as a function of the capacity retention for all cells (Figure 2.10). Here the integrated intensities are normalized by those of sample A−100, having the least capacity fading. The integrated intensities for all elements increase with a decrease of the capacity retention, which indicates a strong relation between cell deterioration and the amount of deposition on the graphite electrode surface. Figure 2.11 presents the variations of the Li, C, and Fe intensities in the different samples. For sample A−0, which was aged without cycling, no Li peaks are apparent, as shown in Figure 2.11(a), whereas the other elements form peaks (Figs. 2.11(b) and (c)), which suggests that some passivation layer is formed on the negative electrode when it is just countered to the positive electrode through the electrolyte, but only a small amount of Li is precipitated on it before charge–discharge cycling. The Li peak increases concomitantly with the decrease of the capacity retention. For sample B, the profiles were measured for two sampling positions, designated as A−50−1 and A−50−2 (Figure 2.11), from the same electrode. The 50 mm × 50 mm sample electrode size made several sampling positions available for the 4−mm−diameter spot size of GD−OES measurements. The Li peak profile collected at A−50−1 is much wider than that at A−50−2, whereas the Li peak at A−50−2 is similar to those from the A−100 and B−100 cells, which indicates inhomogeneous deposition at the surface of sample A−50. The SEI measurement reproducibility for the other samples was about 40% in the intensity integration for three repetitions of this deposition analysis. Therefore such a large difference observed between A−50−1 and A−50−2 is attributed to the sampling position dependence.

We can also see in the surface profile of A−50−1 (Figure 2.12) that the top surface region (up to around 20 s) is composed mainly of Li and the intensities of C, O, F, and others rise beneath the top layer. This fact implies that in sample A−50−1, metallic Li, without counter anions, can be deposited on the top surface on the deposition composed of Li, C, O, F, and so on. The sudden deterioration of sample A−50 after 50 cycles, probably because of a partial shorting, might have engendered the non−uniformity at the surface and precipitation of the metallic Li on the top surface of the graphite electrode.

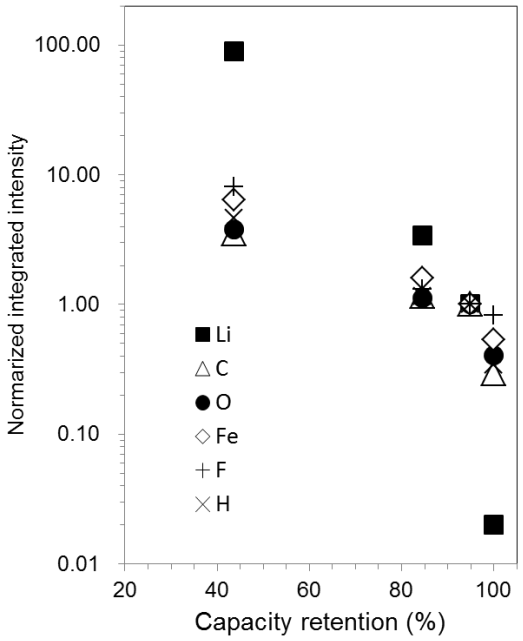

Figure 2.10. Integrated intensities for various elements in the surface profiles of negative electrodes are shown as a function of the capacity retentions for sample cells A-0, A-50, A-100, and B-100.

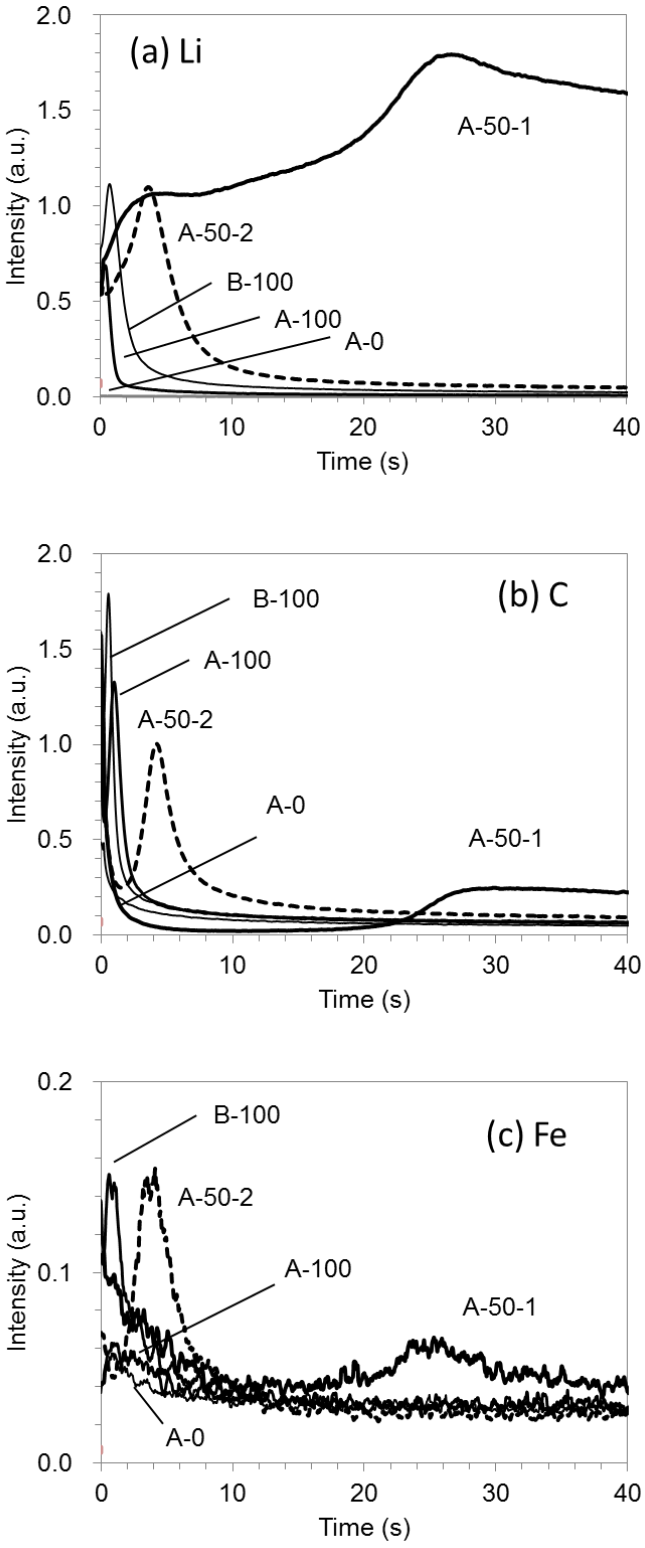

Figure 2.11. Detailed surface profiles of (a) Li, (b) C, and (c) Fe obtained for graphite electrodes from sample cells A-0, A-50, A-100, and B-100.

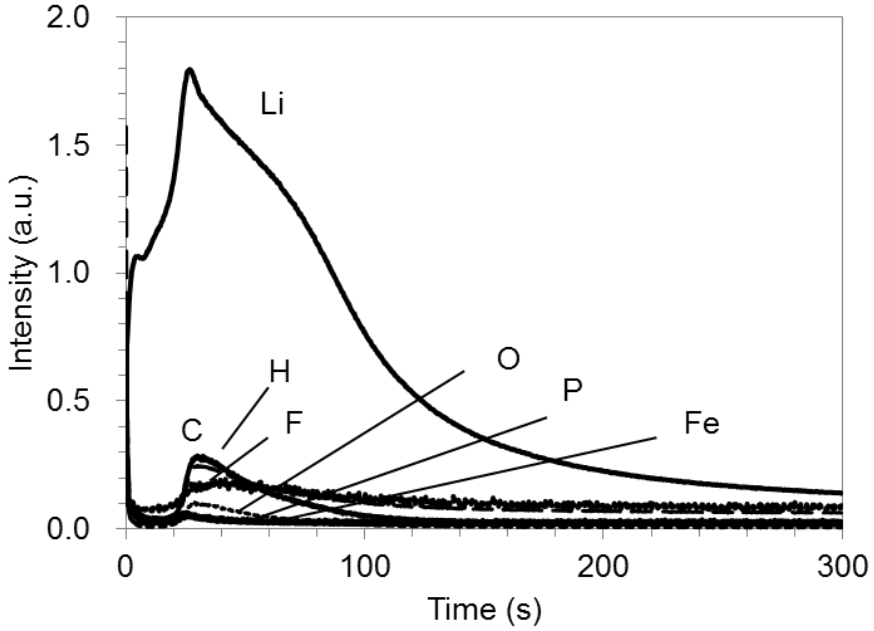

Figure 2.12. Detailed surface profile obtained for graphite electrodes of sample A-50-2. Sample A-50 gives different profiles in positions, which are designated as A-50-1 and A-50-2.

2.4 Conclusion

GD–OES was applied to $LiFePO_4$/graphite cells with various capacity failure conditions. Depth profiles were obtained from the surface to the current collector for both positive and negative electrodes. Additionally, detailed surface profiles of the graphite electrodes were obtained to investigate the deposition formed on the surface (SEI). These results suggest that Li is distributed homogeneously in terms of depth from the surface to the current collector, except for the top layer of $LiFePO_4$. Graphite electrodes for the cells have 85–100% capacity retention. However, for the cell with 44% capacity retention, the Li amount decreased slightly to the current collector in the $LiFePO_4$ electrode, whereas in the negative electrode, Li was distributed homogeneously in depth of the electrode, but a large amount of Li was deposited on the surface. Detailed surface profiles of the graphite electrodes show that deposition comprising Li, H, C, F, O, P, and Fe was formed on the electrode surface. Only a slight amount of Li was precipitated when aging without cycling. However, the amount of Li deposition increased with the degree of capacity–fading. The Li intensity in the GD–OES depth profile shows a good linear relation with respect to Li contents from AAS and ICP–OES analyses for both $LiFePO_4$ and graphite electrodes, which confirms that GD–OES can quantify Li in the electrodes. Therefore, results show that the surface profile of GD–OES is useful to study

SEI, as are other techniques such as XPS and NMR.

2.5 References

[1] S. J. Harris, A. Timmons, D. R. Baker, and C. Montoe, *Chem. Phys. Lett*., **485**, 265 (2010).

[2] W. Luo, X. Li, and J. R. Dahn, *J. Electrochem. Soc*., **157(9)**, A993 (2010).

[3] I. Nakai and T. Nakagome, Electrochem. *Solid-State Lett.*, **1**, 259 (1998).

[4] D. Takamatsu, T. Nakatsutsumi, S. Mori, Y. Orikasa, M. Mogi, H. Yamashige, K. Sato, T. Fujimoto, Y. Takanashi, H. Murayama, M. Oishi, H. Tanida, T. Uruga, H. Arai, Y. Uchimoto, and Z. Ogumi, *J. Phys. Chem. Lett*., **2**, 2511 (2011).

[5] H. Tanida, H. Yamashige, Y. Orikasa, M. Oishi, Y. Takanashi, T. Fujimoto, K. Sato, D. Takamatsu, H. Murayama, H. Arai, E. Matsubara, Y. Uchimoto and Z. Ogumi, *J. Synchrotron Rad.*, **18**, 919 (2011).

[6] M. Winchester and R. Payling, *Spectrochemica Acta B*, **59**, 607 (2004).

[7] R. Payling, P. Chapon, K. Shimizu, R. Passetemps, A. Jadin, Y. Bourgeois, K. Crener, M. Aeberhard, and J. Michler, *Glow Discharge Plasma in Analytical Spectroscopy*, R. K. Marcus and J. A. C. Broekaert, Editors, p.231-251, John Wiley & Sons, England (2003).

[8] Y. Saito and M. K. Rahman, *J. Power Sources*, **174**, 877 (2007).

[9] M. Winter, K-C. Moeller, and J. O. Besenhard, *Lithium Batteries Science and Technology*, G. Nazri and G. Pistoia, Editors, p.171-179, Springer, New York (2009).

[10] D. Aurbach, B. Markovsky, I. Weissman, E. Levi, and Y. Ein-Eli, *Electrochim Acta*, **45**, 67 (1999).

[11] B. M. Meyer, N. Leifer, S. Sakamoto, S. G. Greenbaum, and C. P. Grey, *Electrochem. Solid-State Lett.*, **8(3)**, A145 (2005).

[12] A. K. Padhi, K. S. Nanjundaswamy, C. Masquelier, S. Okada, and J. B. Goodenough, *J. Electrochem. Soc.*, **144**, 1188 (1997).

[13] A. Yamada, S. C. Chung, and K. Hinokuma, *J. Electrochem. Soc.*, **148**, A224 (2001).

[14] S. Y. Chung and Y. M. Chiang, Electrochem. *Solid-State Lett*., **6**, A278 (2003).

[15] P. P. Prosini, M. Lisi, D. Zane, and M. Pasquali, *Solid State Ionics*, **148**, 45 (2002).

[16] D. Morgan, A. Van der Ven, and G. Ceder, Electrochem. *Solid-State Lett*., **7**, A30 (2004).

[17] T. Nakamura, Y. Shima, H. Matsui, Y. Yamada, S. Hashimoto, H. Miyauchi, and N. Koshiba, *J. Electrochem. Soc*., **157(4)** , A544 (2010).

[18] K. Wagatsuma, K. Hirokawa, and N. Yamashita, *Analytica Chimica Acta*, **324**, 147 (1996).

[19] C. C. Li and Y. W. Wang, *J. Electrochem. Soc.*, **158(12)**, A1361 (2011).

[20] D. Fang and R. K. Marcus, *Glow Discharge Spectroscopies*, R. K. Marcus, Editor, p.30-31, Plenum Press, New York (1993).

[21] D. Aurbach, A. Zaban, O. Chusid, and I. Weissman, *Electrochim. Acta*, **39**, 51 (1994).

[22] K. Striebel, J. Shim, A. Sierra, H. Yang, X. Song, R. Kostecki, and K. McCarthy, *J. Power Sources*, **146**, 33 (2005).

[23] K. Amine, J. Liu, and I. Belharouak, *Electrochem. Commun.*, **7**, 669 (2005).

[24] K. Zaghib, N. Ravet, M. Gauthier, F. Gendron, A. Mauger, J. B. Goodenough, and C. M. Julien, *J. Power Sources*, **163**, 560 (2006).

3. Quantification of lithium in LIB electrodes with glow discharge optical emission spectroscopy

GD–OES was applied to quantification of Li in both positive and negative electrodes. Depth profiles of $Li_{1.03}Ni_{0.32}Co_{0.33}Mn_{0.32}O_2$ (NCM) and hard carbon based electrodes in the range of state of charge (SOC) 0–100 % were measured throughout from the surface to the current collector within a few hours. The flat crater shapes, although slightly concave at the edge for NCM, suggested a good depth resolution in the profiles. The sample surfaces sputtered during the GD–OES measurement were smooth in SEM observation, suggesting that remarkable preferential sputtering of the composite materials did not occur. The Li intensities obtained from GD–OES were correlated with the Li components determined using ICP–MS for both positive and negative electrode samples. The correlation coefficients of the linear relationship were improved by considering intensity ratio of Li to the matrix element, Li/Co and Li/C for NCM and hard carbon electrodes, respectively, to correct the sputtering rate variation of samples. These results confirm that GD–OES is a potential technique for quantitative analysis of Li in the electrodes.

3.1 Introduction

Lithium ion battery (LIB) has become an indispensable technology for portable electronic devices for the last two decade. Recently, the demands for LIB in wider applications such as energy vehicles and stationary storage systems are drastically increasing, so that many researches have been studied to improve its energy density, long−term stability, safety, and so on. To understand the fundamental behavior of the material in the electrochemical reaction is essential for the further development of LIB. Especially, characterization of lithium in the electrodes is crucial, because the behaviors of lithium such as reversible lithium in the electrodes and irreversible lithium consumed in solid electrolyte interphase (SEI) are the keys to influence the cell performance. Conventional analysis techniques such as X−ray diffraction (XRD), X−ray fluorescence (XRF), and electron probe micro analyzer (EPMA) are insufficient to characterize Li. X−ray photoelectron spectroscopy (XPS) [1–3], and nuclear magnetic resonance (NMR) [4–6], and scanning transmission electron energy loss (STEM−EELS) [7] have been well accepted for characterizing Li in the electrode so far.

Glow discharge optical emission spectroscopy (GD–OES) is an elemental analysis and a direct in–depth analysis technique for a bulk solid and thin film. Its equipment is furnished with a grim type glow discharge lump, where a sample is mounted facing as a cathode [8]. When argon is introduced into the source with low pressure (a few hundreds Pa) and a high voltage (500–1000 V) is applied to the cathode, electrical discharge plasma generates between the electrodes. The sample is atomized and excited in the plasma discharge away from sample surface, as is cathodic sputtering of the sample. At the same time the characteristics emissions by the excited atoms are generated in plasma, which enables us optical elemental analysis. The aperture of the anode in the glow discharge lump is typically a few mm in diameter, which decides the measurement spot size. A typical sputtering rate is around 1 μm min^{-1} for stainless steel samples for example. GD–OES was previously utilized in steel and metal–plating industries for the trace elemental analysis and the depth profiling with direct current (dc) potential. Furthermore it has broaden to microelectronics field such as semiconductors, thin films, glasses and polymers in the benefit of the radio frequency (rf) potential which enables sputtering either conductive or non–conductive material because of the self–bias potential [9]. Also in the advanced field of lithium ion battery, the depth profiling of positive electrodes was attempted by rf–GD–OES [10]. The lithium composition is evaluated from surface to the interface of the current collector totally for degraded $LiNi_{0.8}Co_{0.15}Al_{0.05}O_2$ electrodes with various states of charge (SOC). The results show that the distributions of lithium are uniform in the degraded electrodes and that lithium compositions obtained by GD–OES well agree with those from induced coupled plasma–mass spectroscopy (ICP–MS). GD–OES is proposed as a potential analysis technique for depth profiling and quantification of Li in LIB electrode. On the basis of the proceeding study, we had objects to investigate the potential of GD–OES analysis in positive electrodes in detail and expand it to carbon negative electrodes. In the present study, the quantification of Li in both positive and negative electrodes was aimed using GD–OES technique. The $Li_{1.03}Ni_{0.32}Co_{0.33}Mn_{0.32}O_2$ (NCM) and hard carbon based batteries [11–12] were adjusted to the range of SOC 0–100 % after pre–determined cycling, and the both electrode samples were measured with GD–OES. The sample surfaces sputtered in GD–OES measurement were investigated with scanning electron microscope (SEM) and XPS. The correlation between Li intensity obtained from GD–OES and Li components determined by ICP–MS was confirmed for the positive and negative electrode samples.

3.2 Experimental

$Li_{1.03}Ni_{0.32}Co_{0.33}Mn_{0.32}O_2$ (NCM) powder, provided by Toda Kogyo, was used as the positive electrode material [11]. The slurry consisting of 90 % active material, 6 % acetylene black, and 4 % poly(vinylidene difluoride) (PVdF) were prepared by mixing in N–methyl–2–pyrrolidone (NMP) solvent and coated onto both sides of Al current collector. The loading and the thickness were 9.5 mg cm^{-2} and 31 μm on either side. Hard carbon powder was provided by Kureha for the negative electrode material. The negative electrode was prepared by casting the slurry consisting of 90.5 % active material and 9.5 % PVdF binder onto both sides of Cu current collector. The loading and the thickness were 3.8 mg cm^{-2} and 29 μm on either side. The cylindrical cells were assembled with the positive and negative electrodes, polymer separator (Asahi–Kasei Chemicals), and 1mol dm^{-3} $LiPF_6$ in ethylene carbonate – diethyl carbonate electrolyte (EC:DMC, 1:2 in volume, Toyama–Chemical) in an Ar–filled glove box. Charge–discharge cycles were carried out for the cells at 3.0 and 4.3 V in cut–off voltages under 1C in current rate at 25˚C. After the prevdetermined cycles, the SOC of the cells were set to 0, 25, 50, 75, and 100 % by a constant current charge with C/3 current rate. Here the current rate was defined to the NCM positive electrode. The cells adjusted to the various SOCs were disassembled and the obtained electrodes were rinsed with dimethyl carbonate (DMC) in an Ar–filled grove box and dried in vacuum.

GD–OES measurement was performed with GDA750 (Rigaku/Spectruma) for the positive and negative electrode samples. The samples were transferred to the apparatus using an experimental vessel without exposing to the air. Argon gas was employed for a discharging gas. Radio frequency power and pulsed glow discharge were applied with 500 V (or 20 W) electric voltage (or power) and 200 Pa gas pressure. The analyzed spot size was 4 mm in diameter for positive electrode samples. Alternative spot size of 2.5 mm was taken for negative electrode samples to gain the sputtering rate, because the sputtering rate of carbon electrode was several tens of times lower than that of positive electrode samples. The lower sputtering rate of negative electrode could be explained from a factor of elemental sputtering yield, which is defined as the ratio between the number of atoms sputtered from the surface and the number of incident ion (Ar^+ in this measurement). The sputtering yield of C is very low; 0.12 atoms/ion toward 1.0 atoms/ion for Fe, at 400 eV Ar ions [14], whereas those of Mn, Co, and Ni were 0.8–1.3 atoms/ion at 400 eV Ar ions [14]. The following elements and their emission lines are applied in this study; H (121.57 nm), Li (610.41 or 670.78 nm), C (156.14 nm), O (130.22 nm), Al (396.15 nm), Mn (403.45 nm), Co (345.35 nm), Ni

(341.48 nm), and Cu (219.22 nm). SEM imaging and XPS surface characterization were performed for the electrode samples before and after GD–OES measurement. The SEM micrographs were taken (JSM 5500 LV; JEOL) with 15 kV accelerating voltage. XPS data were collected with Al Kα radiation source operated at 46.95 eV and an applied power of 25 W (PHI 5000 VersaProbe; Ulvac–Phi). The energies associated with each spectra were calibrated to the C1s (284.6 eV), which is assigned mainly to C–C of acethylene black and hard carbon in the composite electrode. Besides the GD–OES measurement, the Li contents in the sample electrodes were determined by ICP–MS analysis (Table 3.1).

Table 3.1 Li Compositions for NCM and hard carbon electrodes with various SOC % determined by ICP-MS.

SOC %	x in $Li_x(NiMnCo)O_2$	x in Li_xC
0	0.70	0.050
25	0.63	0.076
50	0.54	0.093
75	0.46	0.11
100	0.38	0.12

3.3 Results and Discussion

3.3.1 GD–OES measurement of positive electrode samples

Figure 3.1 shows a depth profile of a NCM electrode sample with 0% SOC obtained from GD–OES measurement. The intensities of Li, Mn, Ni, Co, O, C, H and Al are plotted as a function of the sputtering time instead of the distance from the surface. The NCM active material contributes with Li, Mn, Ni, Co and O, whereas the acetylene black and PVdF binder contribute with C and H. The sputtering pierced the electrode layer with 31 μm thickness and reached the Al current collector after 2600 s, which is reflected by a rapid increase of the Al intensity. The intensities of Li, Mn, Ni, Co, and O are almost constant in the whole region. Figure 3.2(a) shows a crater shape for NCM sample with 100 % SOC after 2000 s of measurement. The sputtering proceeded to about 25 μm depth from surface. The crater presents a smooth bottom whereas slightly concave at the edge, which allows depth profiling with good depth resolution [13]. In order to demonstrate the impact of sputtering for the NCM electrodes, SEM observation was performed. Figures 3.2(b) and (c) show SEM micrographs for the sample with 100 % SOC, before and

after 2000 s of measurement respectively. The surface features after 60 s and 600 s of measurement were similar to after 2000 s (not shown). It seems the boundaries of the primary particles are not sharply defined and sticking mutually after measurement in Fig. 3.2(c). This is probably caused by the collision of Ar ions and the generation of heat in the sputtering process. However, the morphology of secondary particles of NCM remained, furthermore binder and acetylene black filling the space between the secondary particles also likely remained. This suggested that a remarkable preferential sputtering could not occur for the constituents of active material, binder, and acetylene black, and it followed by that the measured depth profile would not be distorted extremely. In the depth profile of NCM electrode (Fig. 3.1), however, the H and C intensities decreased with increasing depth, especially at the surface region to 500s, though the intensities of Li, Ni, Co, Mn, and O from NMC components were homogeneous. Because preferential sputtering of the constituents were not intense on the SEM observation results, it was considered that PVdF binder and/or acetylene black were in–homogeneously distributed in depth and more of them existed in the outer layer in the NCM electrode.

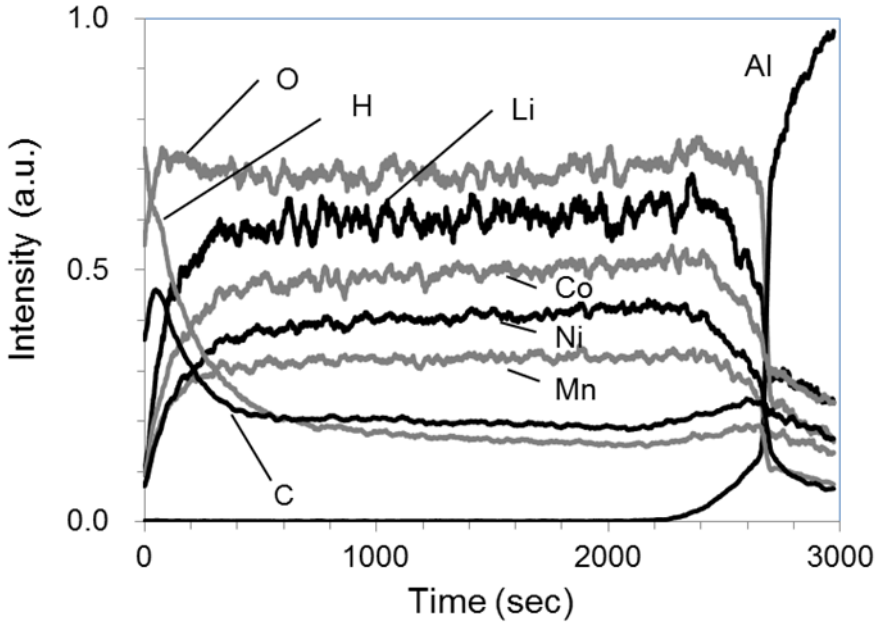

Figure 3.1. GD-OES depth profile for NCM electrode with 0% SOC (The intensity ratio among the elements is not equivalent to molar ratio).

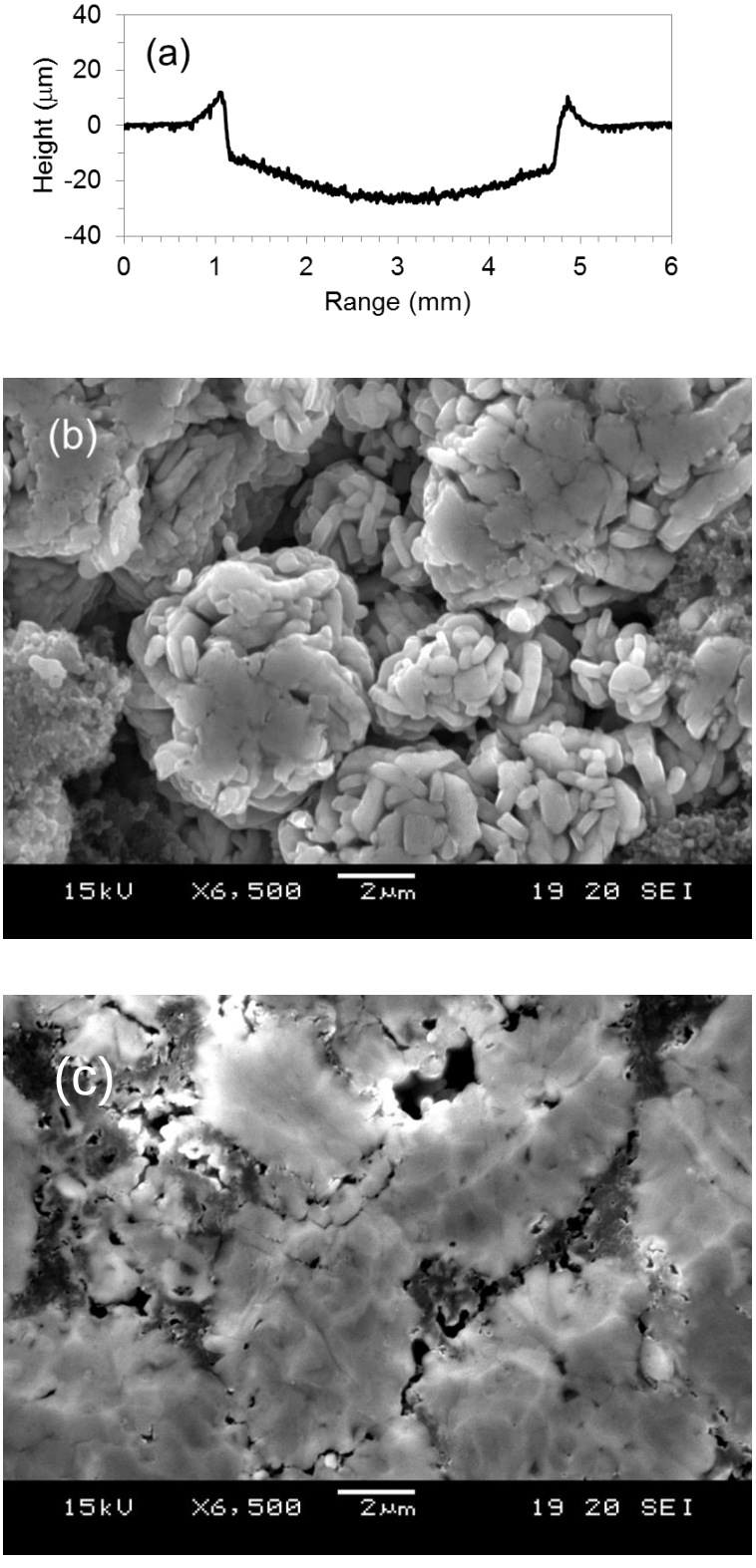

Figure 3.2. Crater shape after 2000 s of GD-OES measurement (a) and SEM micrographs before (b) and after (c) 2000 s of GD-OES measurement for NCM electrode with 100 % SOC.

For more detailed investigation of the sputtered surface, XPS measurement was conducted. Figure 3.3 shows XPS F1s and C1s spectra for a pristine NCM electrode sample before and after the GD–OES measurement. A strong peak at 687.8 eV in F1s spectra, which is obtained for the sample before GD–OES, is assigned to C–F of PVdF. [1–3] This peak is disappeared for the sample after GD–OES measurement. The peaks at 290.8 and 286.1 eV in C1s spectra, which are assigned to C–F and C–H of PVdF [1–3], are also disappeared after GD–OES measurement. Instead of those peaks, new peaks at 684.3 eV in F1s and 289.7 eV in C1s appeared after GD–OES measurement. These peaks could be assigned to Li–F and carbonate functional groups, respectively. Therefore it was suggested that some recombination products of PVdF binder and NCM could be formed on the sputtered sample surface, which would not be reflected to elemental analysis in GD–OES.

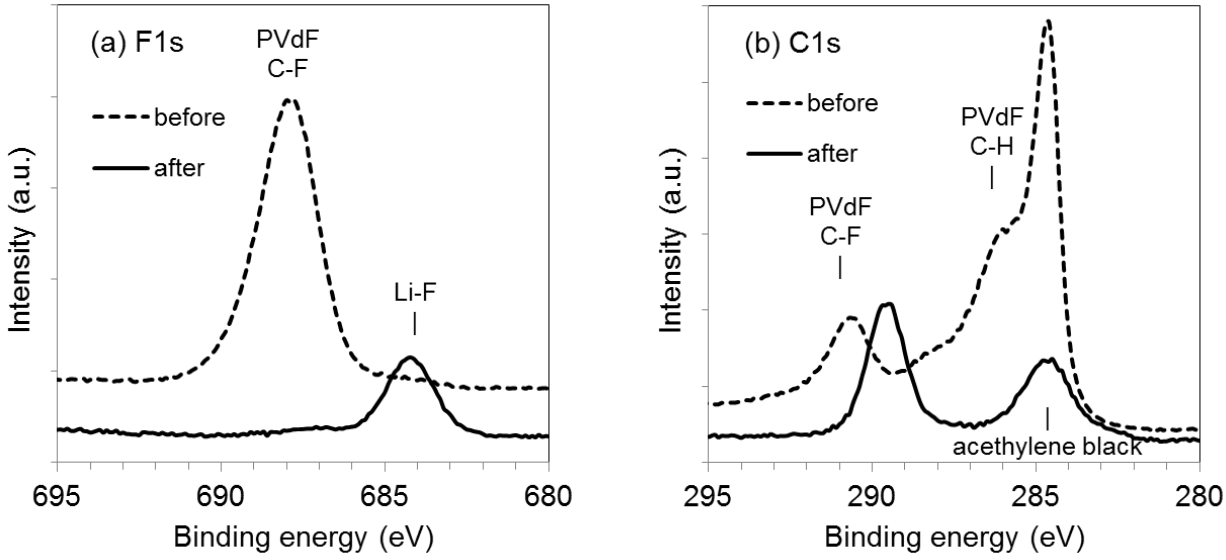

Figure 3.3. F1s (a) and C1s (b) XPS spectra of a pristine NCM electrode sample before and after 2000 s of GD-OES measurement.

3.3.2 GD–OES measurement of negative electrode samples

Figure 3.4 displays a GD–OES profile of Li, C, and Cu for a hard carbon electrode sample controlled to 0 % SOC. Both Li and C intensities are almost constant in the middle region. The rapid increase of Cu intensity, after 4500 s, indicates that the sputtering reaches Cu current collector. The Li and C intensities are enhanced in the vicinity of the Cu current collector. This is because the sputtering rate of

the sample is influenced in the presence of Cu which has a quite high sputtering yield (1.6 atoms/ion at 400 eV Ar ions [14]). The positive electrode shows a depth profile commonly seen in GD–OES, where the intensities of Mn, Co, and Ni dropped down whereas the Al (0.8 atoms/ion at 400 eV Ar ions [14]) intensity increased at the interface between the electrode and the current collector (Fig. 3.1). In the profile of hard carbon electrode, Li and C intensities show extraordinary change at the interface of electrode layer and Cu current collector, C intensity is once drastically increased before dropping down in the vicinity of increase of Cu intensity. This might be because C and Cu have completely different characteristics in sputtering yield from each other. Figures 3.5(a) and (b) show a crater shape and a SEM micrograph for the hard carbon electrode sample with 100 % SOC after 3000 s measurement. The sputtering proceeded to about 15 μm depth from the surface. The crater shape with flat bottom is mostly ideal, which is necessary for a reliable depth resolution. The sputtered surface shown in SEM micrograph was smooth and the particle structure remained. These results support reliable GD–OES measurement for hard carbon electrode with SOC.

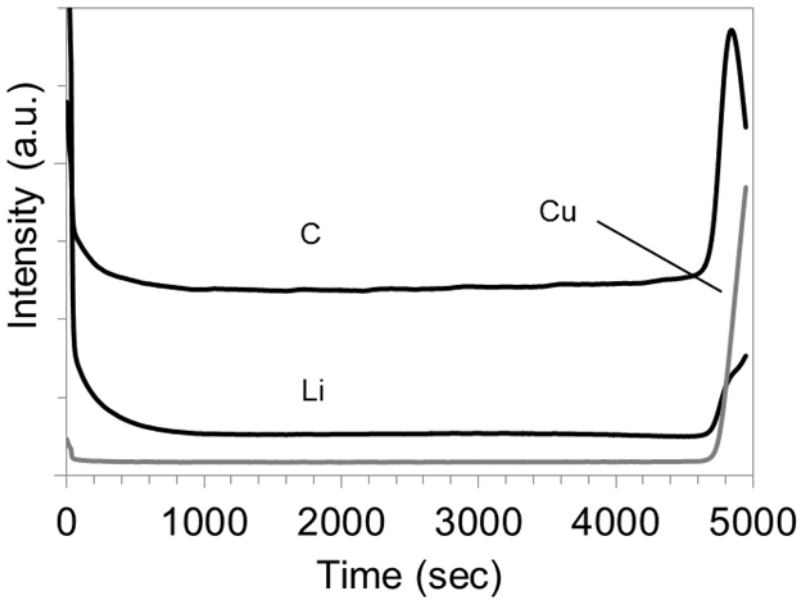

Figure 3.4. GD-OES depth profile for hard carbon electrode with 0 % SOC (The intensity ratio among the elements is not equivalent to molar ratio).

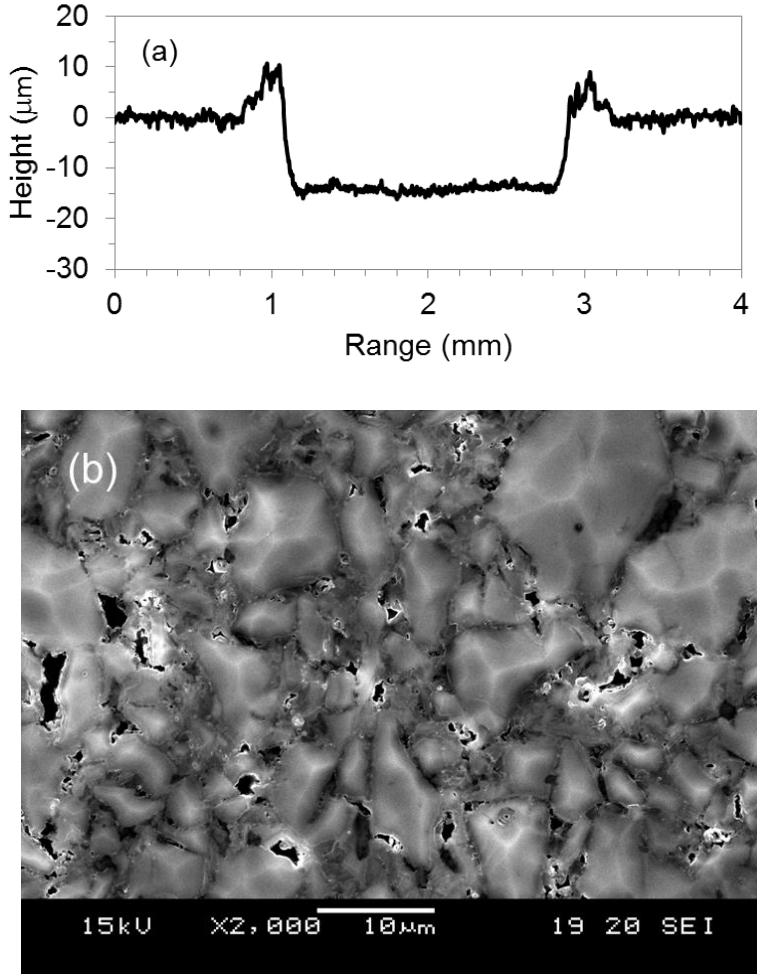

Figure 3.5. Crater shape (a) and SEM micrograph (b) after 3000 s of GD-OES measurement for hard carbon electrode with 0 % SOC.

In order to understand GD–OES measurement of a carbon electrode sample deeply, the difficulty found in measuring pristine hard carbon electrode should be complemented here. Figure 3.6 shows a crater shape and SEM micrographs for the pristine hard carbon electrode sample before and after 3000 s measurement. The crater shape formed on the pristine hard carbon electrode shows a terribly jagged bottom in contrast to SOC sample (Fig. 3.5(a)). The SEM micrograph reveals that redeposited material is formed on the sputtered surface of the pristine sample, which probably brings about the rough bottom of the crater. In the depth profiling of pristine electrode, C intensity unstably decreased with sputtering time and a longer sputtering time (8000 s) was taken to reach Cu current collector (not shown). This was considered because the redeposition covering the surface area could reduce the sputtering efficiency.

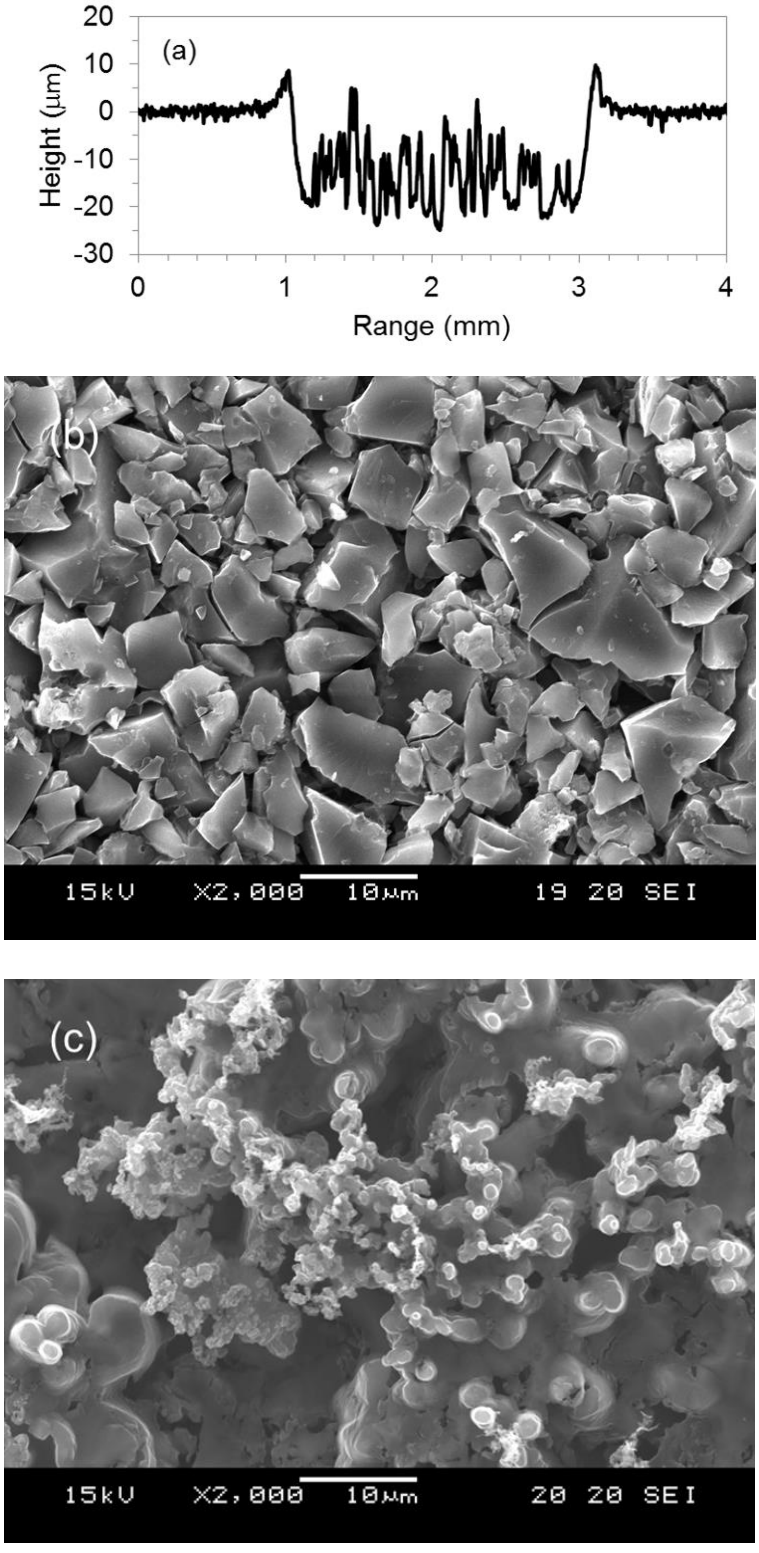

Figure 3.6. Crater shape after 3000 s of GD-OES measurement (a) and SEM micrographs before (b) and after (c) 3000 s of GD-OES measurement for hard carbon electrode with 0 % SOC.

Figure 3.7 shows F1s and C1s XPS spectra for a pristine hard carbon electrode sample before and after 3000 s of GD–OES measurement. The strong peak observed at 687.8 eV for the sample before GD–OES is assigned to C–F of PVdF. The peak at 290.8 and 286.1 eV in C1s spectra are assigned to C–F and C–H of PVdF. These peaks related to PVdF are disappeared and only a peak at 284.7 eV, which is assigned to C–C in hard carbon, remains after GD–OES measurement. These results suggested that the content of PVdF binder was lower in the sputtered surface and the redeposition material was mainly composed of carbon probably maintaining hard carbon structure. Generally redeposition will happen in sputtering process; the sputtered material is returned to the sample by losing its momentum through elastic collisions in the discharge plasma. In GD–OES analysis tool, however, the gas flow is controlled in the discharge anode to lead the redeposition material to outside of the crater. Therefore the redeposition is commonly observed as a projection around the crater edge, as is shown in Fig. 3.5(a). It is interesting that redeposition is brought about only for a pristine carbon electrode (not only hard carbon electrode but graphite electrode), though it is suppressed for SOC samples of them. We have also found it for neither pristine nor SOC samples of NCM and other positive electrodes such as $LiFePO_4$, $LiCoO_2$, and $LiMn_2O_4$. Further studies are needed to understand the mechanism of redeposition brought about only for a pristine carbon electrode sample.

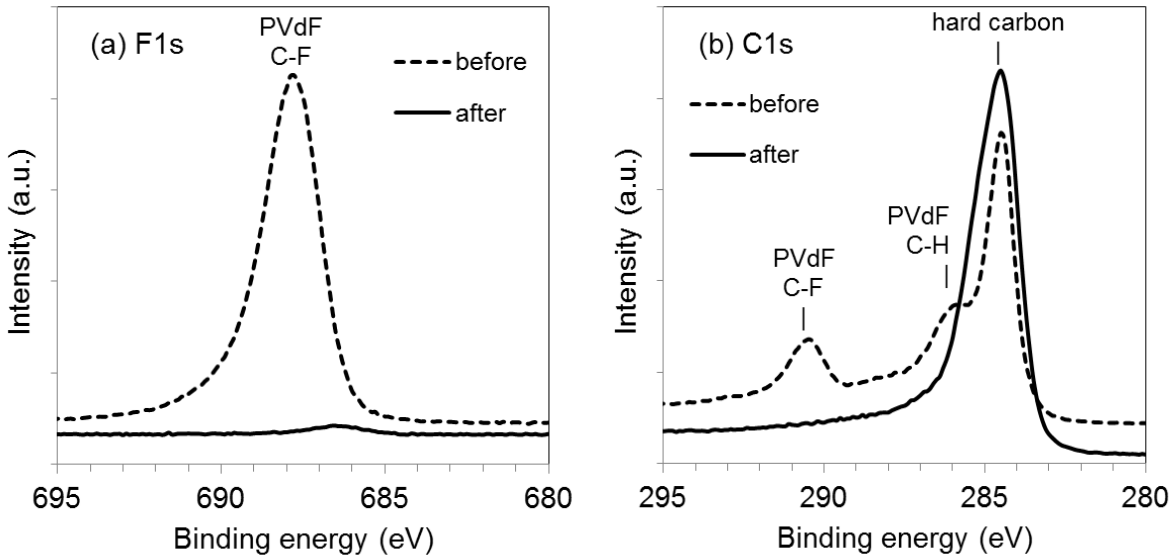

Figure 3.7. F1s (a) and C1s (b) XPS spectra of a pristine hard carbon electrode sample before and after 3000 s of GD-OES measurement.

3.3.3 Quantification of lithium in the electrodes

The capability of GD−OES technique for Li quantification was evaluated with use of Li intensities in the depth profiles. Figure 3.8 plots Li intensities obtained from GD−OES versus Li contents by ICP−MS for the NCM electrode samples with 0−100% SOC (marked with open squares). The Li intensities were averaged from the beginning up to the inflection point of Al increment in each depth profile. A linear relationship with the correlation coefficient $r^2 = 0.94$ was obtained for the averaged intensity of Li, similar to a previous report by Saito et al [10]. In GD−OES, the emission intensity depends on the concentration of the corresponding element and the sputtering rate of the sample. Therefore, it is clear that the Li intensity can vary not only with the Li content in the sample but also with the sputtering rate of respective samples. To avoid the influence of the sputtering rate variation, the intensity ratio of Li to Co, which was one of the representative matrix elements, was recorded. The intensity ratio of Li to Co, Li/Co, versus Li contents obtained from ICP−MS is plotted with filled squares in Fig. 3.8. The correlation coefficient $r^2 = 0.998$ was surely improved comparing to the correlation between averaged Li intensity and ICP−MS Li contents. As an alternative mean to correct the sputtering rate variation, the integration of Li intensity was also tried. The integration of Li intensity also improved the correlation coefficient ($r^2 = 0.996$), as plotted with filled circles in Fig. 3.8. The reproducibilities for three time repeated measurement were 1.0 % and 2.7 % in the intensity ratio Li/Co and integrated Li intensity, respectively, for 75 % SOC samples, whereas it was 6.6 % in averaged Li intensity. By use of the calibration curve with the intensity ratio of Li/Co, which gave the best result in correlation coefficient and reproducibility, the depth profiles of Li were quantified for the NCM electrode samples with 0−100% SOC (Fig. 3.9). The Li contents in the middle region of profiles are constant in depth and trend to decrease with increasing SOC. At the surface region, it was found that Li contents decreased for 50 to 100 % SOC samples. This suggested that Li contents were low at the surface of highly charged state over 50 % of the NCM electrode samples.

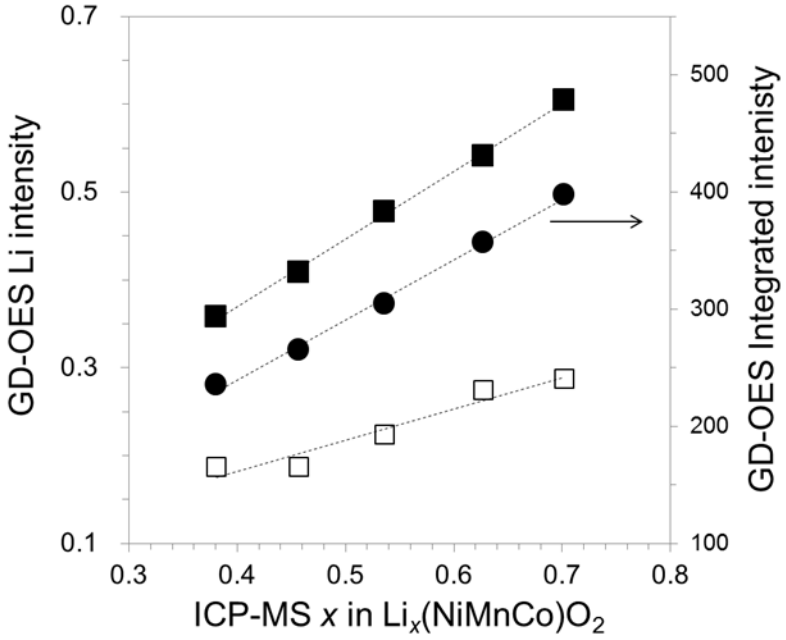

Figure 3.8. Relationship between Li intensities obtained from GD-OES and Li contents determined by ICP-MS for NCM samples with 0–100 % SOC. Averaged Li intensities, the intensity ratios of Li/Co, and integrated Li intensities are plotted with open squares, filled squares, and filled circles, respectively.

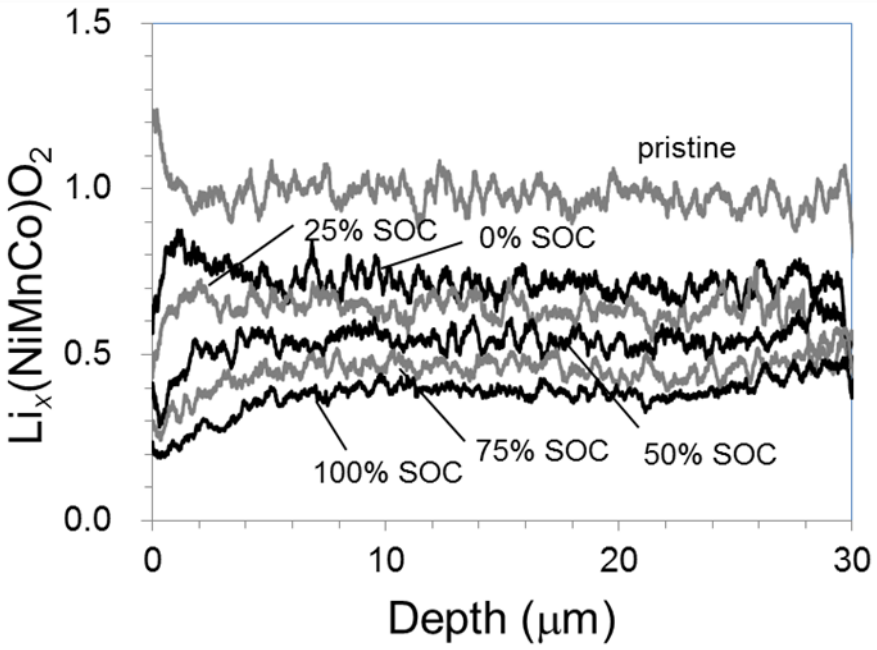

Figure 3.9. Depth profiles of Li for NCM samples with 0 – 100 % SOC which were quantified with the calibration curve using Li/Co intensity ratio, shown in Fig 3.8.

Similarly, the Li quantification by GD–OES was evaluated for the hard carbon electrode samples. Fig. 3.10 plots Li intensities obtained from GD–OES versus Li contents by ICP–MS for the samples with 0–100% SOC, marked with open squares. The Li intensities were taken average from the beginning up to the inflection point of Cu increment for each data. A good linear relationship was obtained, and the correlation coefficient was r^2 = 0.97. Either intensity ratio of Li to C as a matrix element, Li/C, or integration of Li intensity improved the correlation coefficient of the relationship with ICP–MS Li contents (r^2 = 0.98), which were plotted with filled squares and filled circles, respectively, in Fig. 3.10. The reproducibilities for three time repeated measurement were 2.0 % and 2.7 % in the intensity ratio Li/C and integrated Li intensity, respectively, for 75 % SOC samples, whereas it was 3.7 % in averaged Li intensity. Recording intensity ratio of Li/C would enable the most reliable quantification of Li in hard carbon electrode from the points of correlation in the calibration curve and reproducibility.

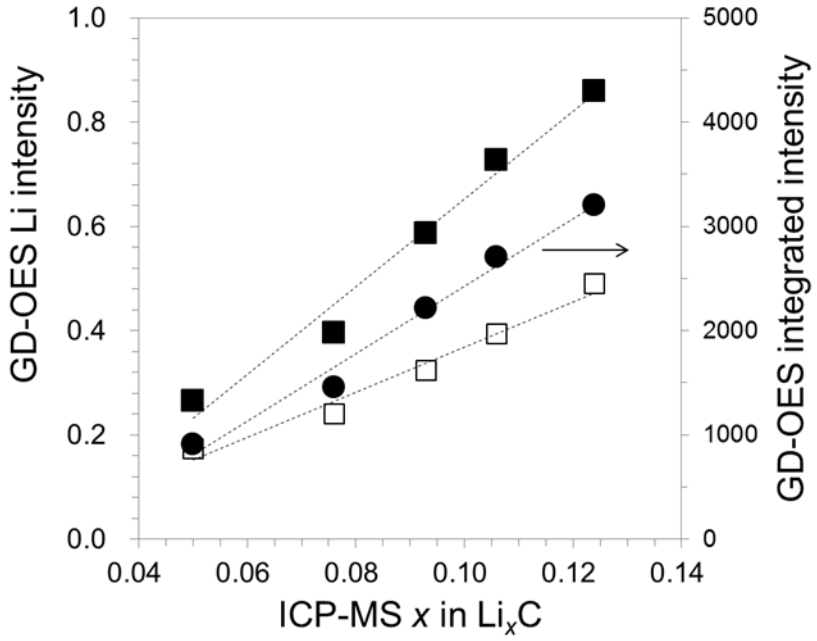

Figure 3.10. Relationship between Li intensities obtained from GD-OES and Li contents determined by ICP-MS for hard carbon electrode samples with 0–100 % SOC. Averaged Li intensities, the intensity ratios of Li/C, and integrated Li intensities are plotted with open squares, filled squares, and filled circles, respectively.

Figure 3.11 shows Li depth profiles for the hard carbon electrode samples with 0−100% SOC quantified with the Li/C calibration curve. The contents in the middle region of profiles trend to increase with increasing SOC %. At the top surface region, high contents of Li were observed for all samples. This top surface peak could be attributed to the deposition formed on the negative electrode surface, which is called SEI. The variation in surface profile showed that the thickness of the surface deposition was increased for highly charged states of the electrode samples. Recently depth profile of SEI film on graphite electrode surface was investigated using photoelectron spectroscopy (PES) [15]. The results indicate that the SEI of charged negative electrode is thicker than that of discharged one, since the PES graphite peak does not appear until bulk sensitive measurement at high kinetic energy for the charged electrode. The thickness variation of the surface deposition shown in GD−OES profiles might agree with the PES study. Except for the top surface region, Li content was almost constant for 0 % SOC electrode, which suggested homogeneous distribution of Li in the electrode. In contrast, Li contents gradually decreased in depth for the electrodes from 25 to 100 % SOC. It likely appeared that the decreasing slop was high for 75 % SOC especially. These suggested that large amount of Li was present in the outer layer and inhomogeneous distribution of Li was happened in the electrodes with highly charged state. We examined separately the possibility of preferential sputtering of Li over C which can be responsible for the decreasing slope in the depth profiles. For a graphite electrode with a certain amount of Li_3PO_4, which was prepared by mixing the chemical regent in the composite slurry, the depth profile exhibited almost constant concentration of Li in whole electrode region (not shown). Therefore it was concluded that no apparent preferential sputtering of Li over C could occur in GD−OES and the Li profile for the 25 to 100 % SOC suggested inhomogeneous distribution of Li in depth. We also attempted to evaluate a few graphite electrode samples which were set to 0 and 100 % SOCs for references (Fig. 3.12). The results showed that Li was homogeneously present in the graphite electrode with 0 % SOC similarly to the corresponding hard carbon electrode sample. For 100 % SOC sample, however, it was suggested that Li content was almost constant in the outer layer and abruptly decreased in the inner layer.

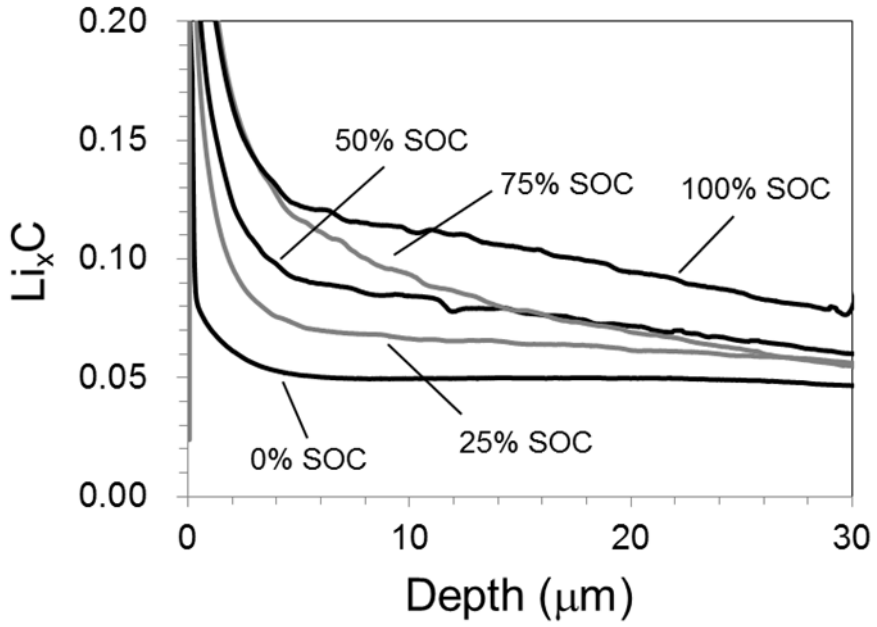

Figure 3.11. Depth profiles of Li for hard carbon samples with 0 – 100 % SOC which were quantified with the calibration curve using GD-OES Li/C intensity ratio, shown in Fig 3.10.

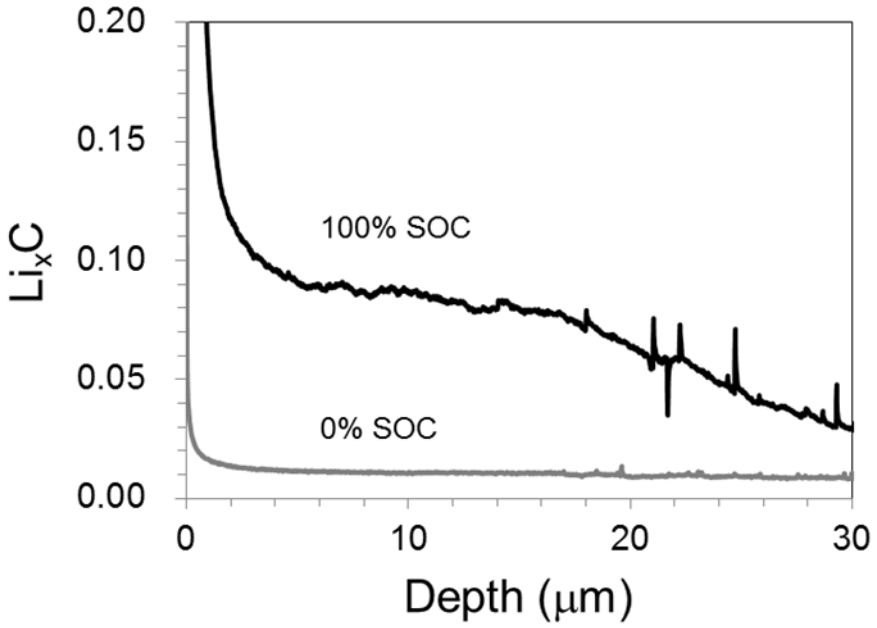

Figure 3.12. Depth profiles of Li for graphite electrode samples with 0 and 100 % SOC. Li compositions determined by ICP-MS are respectively x = 0.021 and 0.12 in Li_xC.

3.4 Conclusion

GD–OES analysis technique was applied to NCM and hard carbon electrodes with 0 – 100 % range of SOC. The NCM positive electrode samples were measured in depth from the surface to the Al current collector around 2000–3000 s. The hard carbon electrodes were also successfully measured up to the Cu current collector, though it took longer time than the positive electrode, 5000–8000 s, because of the low sputtering yield of carbon. The crater shapes were flat, whereas slightly concave at the edge for NCM samples, suggesting a good depth resolution in the profiles for both positive and negative electrodes. SEM images show the electrode surfaces after the GD–OES measurement were smooth and traceable to the original form, suggesting that remarkable preferential sputtering of the composite materials does not occur for the samples. Only for pristine hard carbon electrode sample, redeposition during sputtering process was observed. The GD–OES intensity of Li was linearly correlated to the Li components determined by ICP–MS for the positive and negative electrode samples. The correlation coefficients of the linear relationship were improved when the intensities were corrected on sputtering rate by taking intensity ratio of the Li to the intensity of matrix element, Li/Co and Li/C for NCM and hard carbon electrodes, respectively, or by integrating Li intensity.

3.5 References

[1] A. M. Andersson, D. P. Abraham, R. Haasch, S. MacLaren, J. Liu, and K. Amine, *J. Electrochem. Soc.*, **149**, A1358 (2002).

[2] R. Dedryvere, S. Laruelle, S. Grugeon, L. Gireaud, J.-M. Tarascon, and D. Gonbeau, *J. Electrochem. Soc.*, **154**, A689 (2005).

[3] M. Shikano, H. Kobayashi, S. Koike, H. Sakaebe, E. Ikegawa, K. Kobayashi, and K. Tatsumi, *J. Power Sources* **174**, 795 (2007).

[4] B. M. Meyer, N. Leifer, S. Sakamoto, S. G. Greenbaum, and C. P. Grey, *Electrochem.Solid State Lett.* **8**, A145 (2005).

[5] Y. Wang, V. Yufit, X. Guo, E. Peled, S. Greenbaum, *J. Power Sources* **94**, 230 (2001).

[6] Z. Wang, N. Dupre, L. Lajaunie, P. Moreau, J.-F. Martin, L. Boutafa, S. patoux, and D. Guyomard, *J. Power Sources* **215**, 170 (2012).

[7] J. Kikkawa, T. Akita, M. Tabuchi, K. Tatsumi, and M. Kohyama, *Electrochem.Solid State Lett.* **11**, A183 (2008).

[8] R. K. Marcus (Ed), *Glow Discharge Spectroscopies (Modern Analytical Chemistry)*, Plenum pub Corp, New York, p.128 (1993).

[9] M. Winchester and R. Payling, *Spectrochimica Acta B*, **59**, 607 (2004).

[10] Y. Saito and M. K. Rahman, *J. Power Sources*, **174**, 877 (2007).

[11] Masahiro Shikano, Hironori Kobayashi, Shinji Koike, Hikari Sakaebe, Yoshiyasu Saito, Hironobu Hori, Hiroyuki Kageyama, Kuniaki Tatsumi, *J. Power Sources* **196**, 6881 (2011).

[12] H. Kobayashi, Y. Arachi, S. Emura, H. Kageyama, K. Tatsumi, and T. Kamiyama, *J. Power Sources* **146**, 640 (2005).

[13] T. Neils and R. Payling (Ed), *Glow Discharge Optical Emission Spectroscopy: A Practical Guide*, The Royal Society of Chemistry, Cambridge, pp.40 - 43(2003).

[14] R. K. Marcus (Ed), *Glow Discharge Spectroscopies (Modern Analytical Chemistry)*, Plenum pub Corp, New York, pp.30-31 (1993).

[15] S. Malmgren, H. Rensmo, T. Gustafsson, M. Gorgoi, and K. Edstrom, *Electrochem. Society Transactions,* **25(36)**, 201 (2010).

4. Depth profiling of graphite electrode in lithium ion battery using glow discharge optical emission spectroscopy with small quantities of hydrogen or oxygen addition to argon

Depth profiling and quantification using GD–OES were applied to a graphite electrode in a lithium ion battery. To improve the measurement time and reliability beyond conventional argon discharge plasma, reactive sputtering with the respective addition of oxygen (0.50 % v/ v O_2 in Ar) and hydrogen (1.00 % v/ v H_2 in Ar) was investigated. Samples contained dispersed 0–5 wt% LiF or 0–0.5 wt% Li_3PO_4 in graphite electrodes. Adding oxygen to argon plasma increased the measurement time and the sensitivity in quantitative analysis of lithium drastically. That unexpected depth profile was obtained for graphite electrode samples possibly because chemical etching by oxygen was inhomogeneous. In contrast, adding hydrogen to argon plasma exhibited benefits both for depth profiling and for quantifying Li for graphite electrode samples with a shorter measurement time and higher sensitivity than that of conventional pure argon discharge. Molecular spectra showed strong C–H and C‑C bands, suggesting that formation of volatile material fragments of CH and CC increased with hydrogen addition during measurements. Surface analysis results with SEM and XPS showed that redeposition of sputtered materials and Ar^+ ion implantation that occurred in pure argon plasma was also suppressed.

4.1 Introduction

Lithium ion batteries (LIB) have been applied to portable electronics devices for the last decade. Recently, LIB application in the fields of energy vehicles and stationary energy storage systems has attracted considerable attention to enable the use of renewable energies such as solar and wind energies efficiently. Because higher energy capacity and power are required along with long-term stability, safety, and lower costs, further development and studies are being conducted world-wide. To attain this goal, extensive research into battery materials, configurations, and deterioration mechanisms is being conducted. Lithium ion cell comprises a positive electrode, a negative electrode, organic liquid electrolyte with lithium-ion conductivity, and an electrically insulating polymer separator. Lithium insertion oxides such as $LiCoO_2$, $LiNiO_2$, and $LiFePO_4$ are typically used as active materials for the positive electrode.

Carbon-based materials such as graphite and hard carbon are representatives of active materials used in negative electrodes, although Si or Sn alloy and $Li_4Ti_5O_{12}$ have also been considered recently for their respective benefits of higher energy capacity and safety. Lithium ion reversibly reacts in both electrodes during cell charge and discharge: during the charge process, lithium ions migrate from the positive electrode material to the negative electrode material through the electrolyte; the electrons flow through the external circuit from the positive electrode to the negative electrode. An inverse reaction occurs during the discharge process.

An important subject related to LIB development is cell deterioration that occurs through long-duration use or high-temperature use. The cell can be degraded for numerous and various reasons: formation of inactive layer so-called solid electrolyte interphase (SEI) [1], structural change of electrode materials, decomposition of organic liquid electrolytes, gas evolution, and so on. Especially, it is well known that SEI concerns with the cell performance and cell deterioration in LIB. The SEI is formed in the graphite electrode during charge-discharge cycling and storage. The numerous studies on characterization of SEI with XPS, FT-IR, and NMR have reported that SEI is composed of LiF, Li_2CO_3, lithium alkyl carbonates $ROCO_2Li$, and some decomposed solvents such as $Li_xPF_yO_z$ originated from $LiPF_6$.[2, 3] The SEI consumes Li ions as inactive states and fades the reversible Li ion transfer between electrodes. The formation of SEI could occur inhomogeneously in graphite electrode, so that we consider that radiofrequency glow discharge optical emission spectroscopy (rf-GD-OES) [4] will be powerful tool for in-depth and quantitative analysis of the distribution of SEI.

The positive and negative electrodes of LIB are typically formed by a 20–100 μm active layer consisting of an active material, carbon black of electric conductivity assistant, and a polymer binder on Al or Cu foil current collector. Depth profiling of positive electrodes was attempted previously using rf-GD-OES [5]. The lithium composition was analyzed from the surface to the interface of the current collector completely for various states of charge (SOC) of $LiNiO_2$-based electrode. The quantitative results agree well with inductively coupled plasma–mass spectroscopy (ICP-MS). Recent reports have also described that rf-GD-OES is applicable for the analysis of carbon-based negative electrodes [6, 7]. The hard carbon electrodes (30-μm active layer) were measured up to the Cu current collector. However, the measurements took a long time, 5000–8000 s, contrasted against 2000–3000 s for positive electrodes (30-μm active layer) because of a low sputtering yield of carbon (0.12 atoms/ion compared to 1.0 for Fe, at

400 eV Ar ions [8]). Moreover, redeposition was observed on the sputtered surface of an electrode sample, which could slow the sputtering rate further. To improve the measurement of carbon-based electrode faster and reliable without redeposition, the concept of plasma etching is examined in this study.

Plasma etching [9] is the removal of a material (while leaving other materials) from a sample surface using the chemical selectivity of a gas etchant. This technology is important for fabricating integrated circuits in the semiconductor industry. Etch chemistry is chosen to yield a volatile product. Halogen atom etchants (F, Cl, Br) are used to remove patterned Si and poly Si. Oxygen is commonly used to remove carbon-based materials and organic polymers presented by a photoresist mask.

$$\mathrm{C\ (s) + O\ (g) \rightarrow CO(g)} \quad \text{.....(1)}$$

$$\mathrm{Polymer\ (mostly\ C\ and\ H) + O\ (g) \rightarrow CO_2\ (g) + H_2O\ (g)} \quad \text{.....(2)}$$

In the industrial usage of GD-OES, pure Ar gas has usually been used as a discharge gas. However, other pure noble gases (He, Ne, Kr) and their binary gas mixtures (Ar–He, Kr–He, Ar–Kr, Ar–N_2, …) are known to modify the sputtering rate and optical emissions. Pure Ne gas enhanced the detection of fluorine with high excitation energy [10]. Gas mixtures changed the emission characteristics through collision energy transfer between the gases [11, 12]. The addition of activated gases such as oxygen and hydrogen in argon (0.5–10% v/v) was also widely investigated to assess discharge behaviors, sputtering rates, and emissions [13, 14]. When adding oxygen to argon, the electric current in glow discharge (GD) plasma decreased compared to pure argon, followed by the sputtering rate reduction of metallic materials (stainless steels and copper) and insulating materials (glass). According to a calculated model, metastable Ar (Ar^m), which had a large contribution to ionization process of materials as well as an electron impact, was quenched to a considerable degree by collision with O_2 molecules [15]. Simultaneously, an oxidation film was formed on material surface, which reduced the sputtering rate much more strongly in the metallic materials than in insulating glass samples [16]. For hydrogen addition to argon, the sputtering rate of the materials did not decrease so much irrespective of electrical current reduction because H_2 related species such as ArH^+ offset the decrease of Ar^+ ion flux to some extent [17]. Emission yields decreased in most analytical lines because of decreased Ar^m, but several lines such as Si I 288.1 nm, Mg I 383.3 nm, Zn I 330.2 nm, and Cu I 217.9 nm were enhanced, which is the so-called “hydrogen effect” [18].

This study investigated the addition of oxygen and hydrogen to Ar discharge gas in rf-GD-OES for carbon-based electrode materials, applying their reactive effects as an oxidant or a reductant to improve the sputtering rate and reliability on the depth profiling. Graphite electrodes for LIB were measured either with 0.50 % v/v O_2 in Ar and 1.00 % v/v H_2 in Ar. Variation of the sputtering rate by the additives was evaluated. The sputtered sample surfaces were observed using scanning electron microscopy (SEM) and XPS to characterize the effects of the additives. The depth profile and quantitative ability were investigated for LiF or Li_3PO_4 that had been distributed intentionally in the graphite electrode samples. The GD-OES measurements were examined for the distribution analysis of SEI for deteriorated graphite electrodes in commercially available LIB.

4.2 Experimental

The sample electrodes were prepared with organic−based and water−based systems which are widely used in LIB [19]. For the organic−based system, poly(vinylidene fluoride) (PVDF) binder was used. The 95 % graphite powder (MAG−D; Hitachi Chemical) and 5 % PVDF binder were mixed in N−methyl−2−pyrrolidone (NMP) solvent to prepare the slurry. For the water−based system, styrene−butadiene rubber (SBR) and carboxymethylcellulose (CMC) were used. A slurry was prepared by mixing 95 % graphite, 2 % carbon fiber of electronic−conductivity assistant (VGCF, Showa Denko), 2 % CMC and 1 % SBR in distilled water. The slurries were cast on 20 μm Cu foil, dried at 100 °C for one night, and roll−pressed to 1.0–1.4 g cm^{-3} and 55–90 μm for the active layer excluding Cu foil. LiF of 0‑5 wt% in the active layer was dispersed in organic−based slurry, considering the chemical stabilities of LiF in organic solvents. Then 0–0.5 wt% Li_3PO_4 was dispersed in water−based slurry because Li_3PO_4 is slightly soluble in water. The electrode samples were cut into 15 mm × 15 mm pieces and were pasted onto a brazen holder for GD−OES measurement.

GD−OES measurements were conducted on a spectrometer system (GDA750; Rigaku/Spectruma). High purity of argon (99.9999%) and high purity (99.9999%) of gas mixtures of 0.50% v/v O_2 and 1.00% v/v H_2 in argon were used as discharging gases. Radiofrequency power and pulsed glow discharge were applied under the following conditions: 550 V electric voltage, 200 Pa gas pressure, and 50% pulse rate at 2500 Hz frequency. The measurement spot was 4 mm diameter. The following elements and their emission lines were applied in this study: H 121.57 nm, Li 610.41 or 670.78 nm, C 156.14 nm, O 130.22 nm, P

177.49 nm, and Cu 327.39 nm. The emission line of fluorine was difficult to detect because of the lower sensitivity at Ar–based discharge gas10. The crater shape variation was recorded with a stylus profilometer (Surfcom 1500DX; Tokyo Seimitsu Co. Ltd.). Then SEM imaging and XPS surface characterization were conducted for the electrode samples before and after GD–OES measurements. The SEM micrographs were taken with 15 kV accelerating voltage (JSM 5500 LV; JEOL). The XPS data were collected using an Al Kα radiation source operated at 46.95 eV and an applied power of 25 W (PHI 5000 VersaProbe; Ulvac–Phi Inc.). The energies associated with each spectrum were calibrated to the C1s (284.6 eV), which is assigned mainly to C–C of graphite in the composite electrode. Li contents included in Li_3PO_4 sample electrodes were ascertained using induced coupled plasma – optical emission spectroscopy (ICP–OES, iCAP6200; Thermo Scientific).

Commercially available Al–laminated type cell samples were composed of LiM_2O_4–based positive electrode and graphite negative electrode [20]. A cycle test for 300 or 600 cycles under 2.5–4.0 V cut–off voltages and C/2 current rate at 25 or 45 ˚C was operated for them. After these tests, the cells were disassembled and the negative electrode samples were rinsed with dimethyl carbonate in an argon–filled glove box. The samples were transferred to the apparatus using an experimental vessel without exposing to the air, and then measured by rf–GD–OES with the same condition as described above. The negative electrode samples retained little deintercalation capacity (<1% in all cells), which means that the stored lithium has electrochemically inactive form as SEI.

4.3 Results and Discussion

4.3.1 Influences of oxygen and hydrogen addition on rf–GD–OES analysis for the carbon electrode

GD–OES analysis of graphite electrode was done for addition of small amount of oxygen or hydrogen in argon discharge gas, 0.50% O_2 v/v in Ar (Ar–O_2) and 1.00 % H_2 v/v in Ar (Ar–H_2). In order to understand the characteristics of the three discharge gasses, Cu foil, a typical metallic material, was chosen for a reference. Figures 4.1 and 4.2 show the crater shapes and the SEM micrographs of crater bottoms for Cu with pure Ar, Ar–H_2, and Ar–O_2. The sputtering time was 1000 s for all gas species. The sputtered depths of 30 μm for Ar–H_2 and 20 μm for Ar–O_2 were lower than 55 μm for pure Ar, which indicates that a small amount of addition of oxygen and hydrogen decrease the Cu sputtering rate. The addition of gases

also changes the crater shape to a flat bottom from rather concave in pure Ar. In the SEM micrograph of the surface of the crater bottom, projections resembling islands were formed for Ar–O_2 (Fig. 4.2(c)), although it was smooth for pure Ar and Ar–H_2 (Figs.4. 2(a) and 2(b)). The island–like areas were found to increase in oxygen contents (3.6–7.8 wt%) compared to the other parts (1.6–1.7 wt%) using energy–dispersive x–ray fluorescence spectroscopy (EDX) conducted by SEM, reflecting the promotion of surface oxidation for Ar–O_2. These influences of oxygen and hydrogen additives found on Cu metal, reduction of the sputtering rate, change in crater shape, and formation of oxide for Ar–O_2, are consistent with previous reports describing stainless steel samples [16].

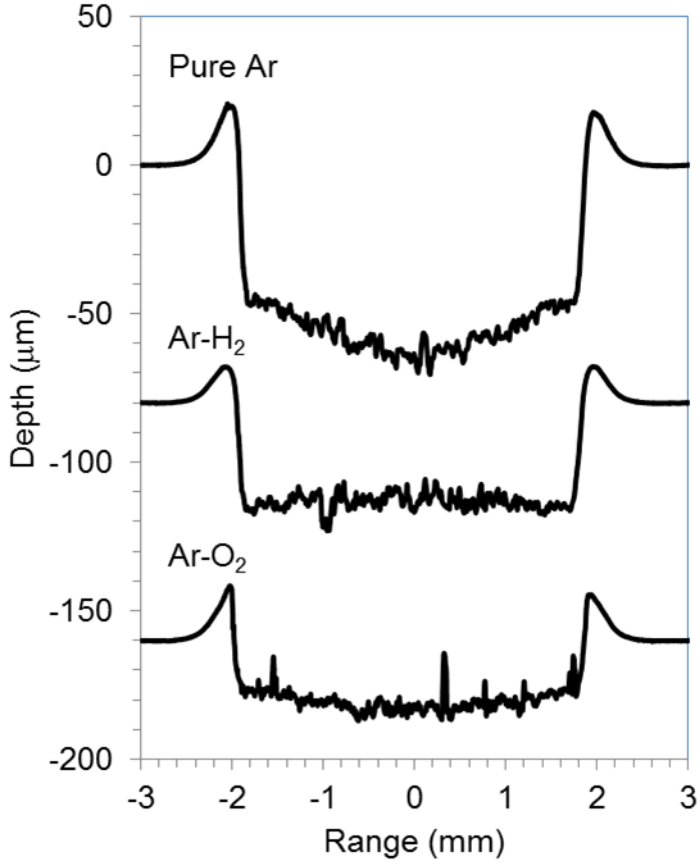

Figure 4.1. Crater shapes of Cu for 1000 s sputtering with pure Ar, 1.00% v/v H_2 in argon (Ar–H_2), and 0.50% v/v O_2 in Ar (Ar–O_2). Experimental conditions: 550 V electric voltage, 200 Pa gas pressure, 50% pulse rate at 2500 Hz.

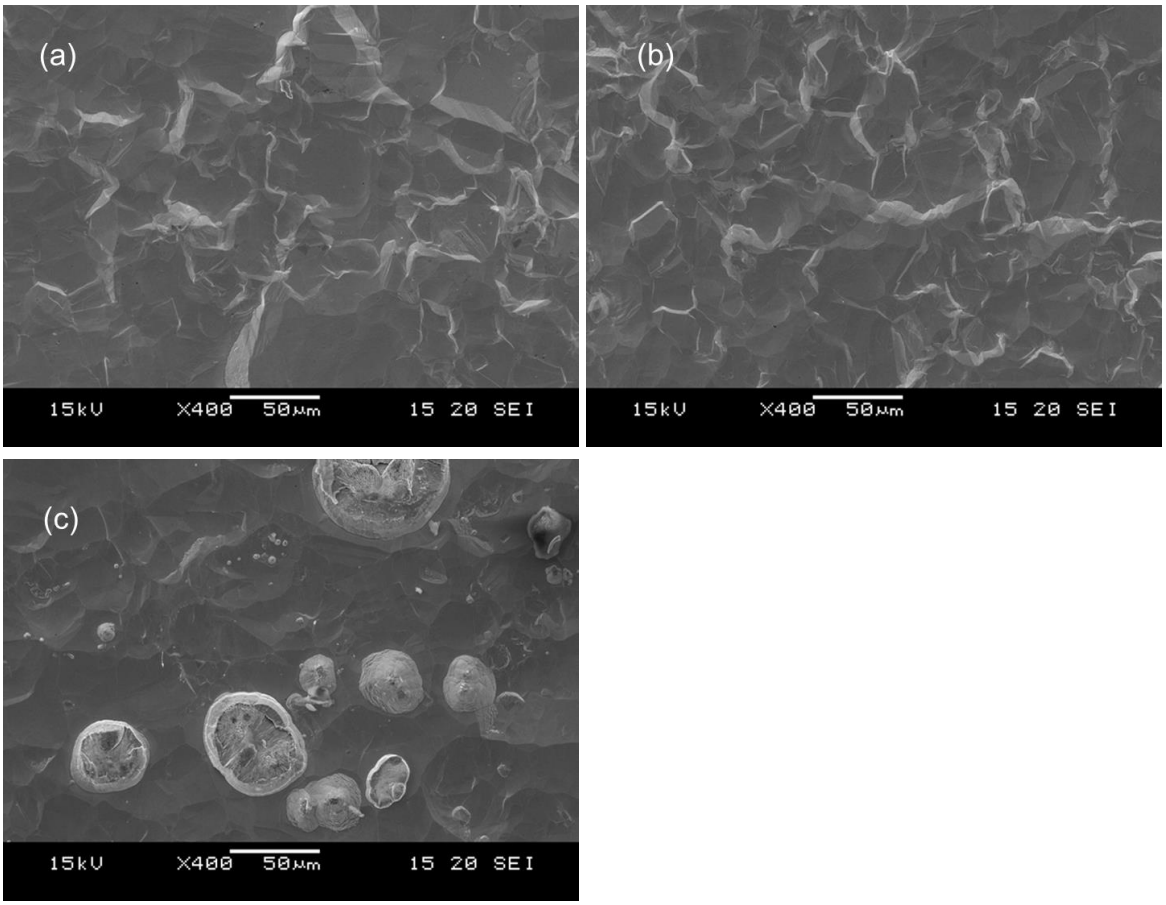

Figure 4.2. SEM micrographs of crater bottom of Cu sputtered with pure Ar (a), 1.00% v/v H_2 in argon (Ar–H_2) (b), and 0.50% v/v O_2 in Ar (Ar–O_2) (c).

The graphite electrode samples comprised graphite particles of around 10 μm size contiguously adhered with PVDF binder on Cu foil of a current collector. The SEM micrograph of the sample surface is portrayed in Fig. 4.3(a). The electrode active layer was 80 μm thick; the Cu foil was 20 μm thick. Figures 4.3(b)–4.3(d) and 4.4 respectively depict SEM micrographs and crater shapes for graphite electrode samples sputtered with pure Ar, Ar–H_2, and Ar–O_2. The measurement time was 3000 s for pure Ar and Ar–H_2, and 1000 s for Ar–O_2. The sputtered depth with pure Ar was 9 μm for 3000 s of sputtering time (Fig. 4.4). The sputtering rate is much lower than pure Cu (55 μm for 1000 s in the same measurement condition, in Fig. 4.1), because the sputtering yield of carbon (0.12 atoms/ion compared to 1.0 for Fe, at 400 eV Ar ions [8]) is much lower than that of Cu (1.65 atoms/ion compared to 1.0 for Fe, at 400 eV Ar ions [8]). Furthermore, the bottom of the crater shape was terribly jagged for pure Ar. The corresponding SEM micrograph reveals that redeposited materials are formed on the sputtered surface, which is probably

reflected by the rough bottom of the crater (Fig. 4.3(b)). When using Ar–H_2, the sputtered surface is smooth, indicating that the formation of redeposition is suppressed by the addition of 1% H_2 (Fig. 4.3(c)). The sputtering rate was enhanced several times to 20 μm for 3000 s in Ar–H_2 (Fig. 4.4). Using Ar–O_2, the sputtering rate became about ten times higher than that of pure Ar (30 μm for 1000 s, Fig. 4.4). This drastic enhancement of the sputtering rate can result from the chemical etching effect of carbon by oxygen in Ar–O_2, as described in chemical formulas (1) and (2). The SEM micrograph shows that the sputtered surface becomes rough and crisp, although redeposition did not occur (Fig. 4.3(d)).

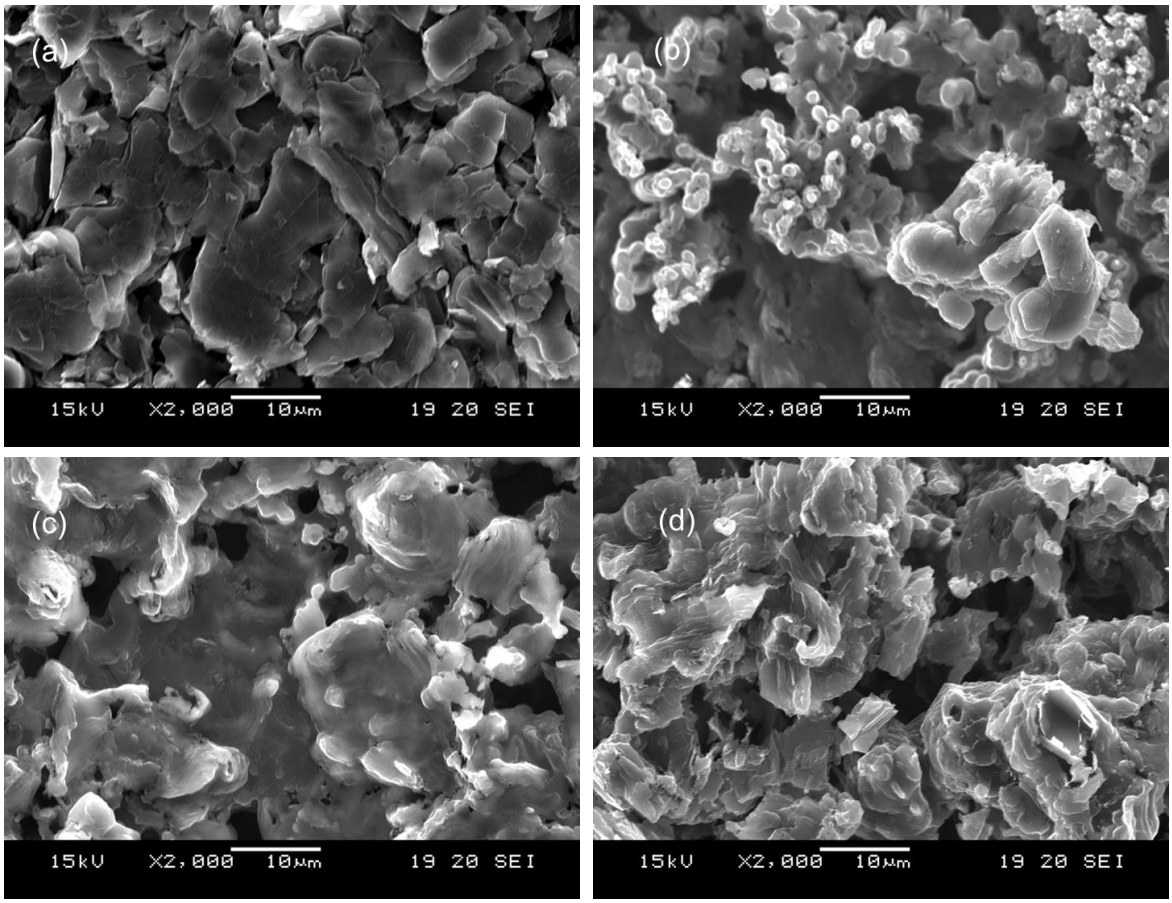

Figure 4.3. SEM micrographs of the crater bottom of graphite electrode samples before (a) and after sputtering with pure Ar (b), 1.00% v/v H_2 in argon (Ar–H_2) (c), and 0.50% v/v O_2 in Ar (Ar–O_2) (d).

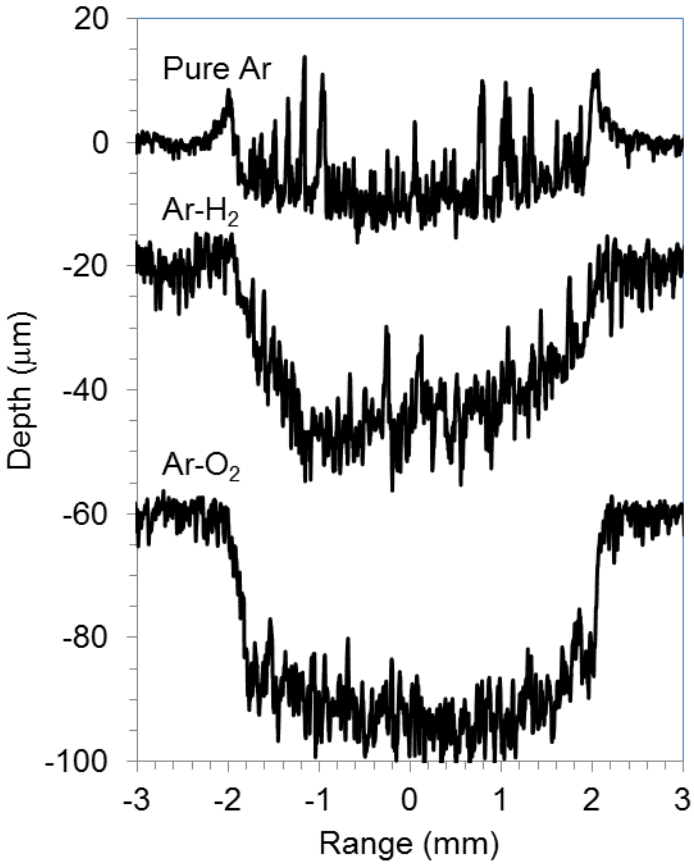

Figure 4.4. SEM micrographs of the crater bottom of graphite electrode samples before (a) and after sputtering with pure Ar (b), 1.00% v/v H_2 in argon (Ar–H_2) (c), and 0.50% v/v O_2 in Ar (Ar–O_2) (d).

To investigate details of the sputtered surface, XPS measurement was performed. Figure 4.5 shows XPS C 1s, F 1s, and Ar 2p spectra for the sample surface sputtered with pure Ar, Ar–H_2, and Ar–O_2. The electrode sample comprises graphite and PVDF, so that C, F, and H are the intrinsic elemental components. In C1s spectra (Fig. 4.5(a)), only a peak appeared at 284.6 eV, which is assigned to C–C bond in graphite. Peaks corresponding to C–F and C–H of PVDF (290.8 and 286.1 eV, respectively) [21] were not observed clearly because of small constituent of PVDF. However, a peak originated from C–F of PVDF (687 eV) [21] is apparent in F 1s spectra (Fig. 4.5(b)). The peak intensity is much higher in Ar–O2 than in pure Ar and Ar–H2, suggesting preferential sputtering; C would be selectively sputtered with oxygen to enhance the concentration of F on the sputtered surface in Ar–O_2. In the corresponding SEM micrograph, portrayed in Fig. 4.3(d), the surface appears to be partly unetched and partly eroded to the inner layer. Therefore it was considered that the fluorine compound could be left on the sputtered surface if the graphite particle is

removed preferentially. In Ar 2p spectra (Fig. 4.5(c)), a peak is found at 242 eV for pure Ar and Ar–O_2. This peak is responsible for Ar^+ ion implantation that occurred unintentionally on the sample surface during the GD–OES measurement. The Ar peak disappears for Ar–H_2, implying that the addition of hydrogen might prevent impinging of Ar^+ ions into C matrix. Argon has some reactive interaction with H^+ in the argon–hydrogen plasma to form ArH^+ [17]. This kind of interaction might remove argon from the sputtered sample surface though it is a supposition.

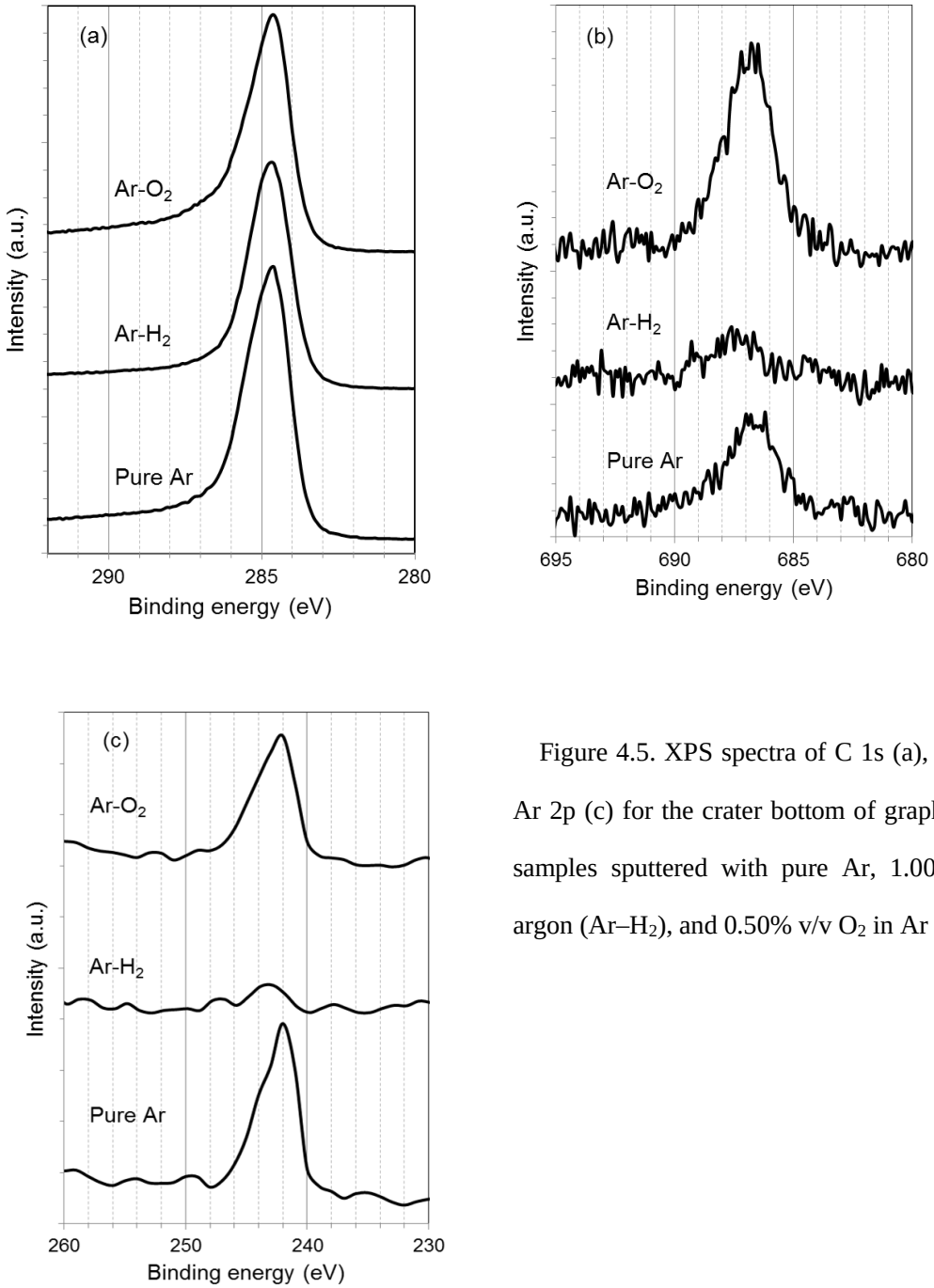

Figure 4.5. XPS spectra of C 1s (a), F 1s (b), and Ar 2p (c) for the crater bottom of graphite electrode samples sputtered with pure Ar, 1.00% v/v H_2 in argon (Ar–H_2), and 0.50% v/v O_2 in Ar (Ar–O_2).

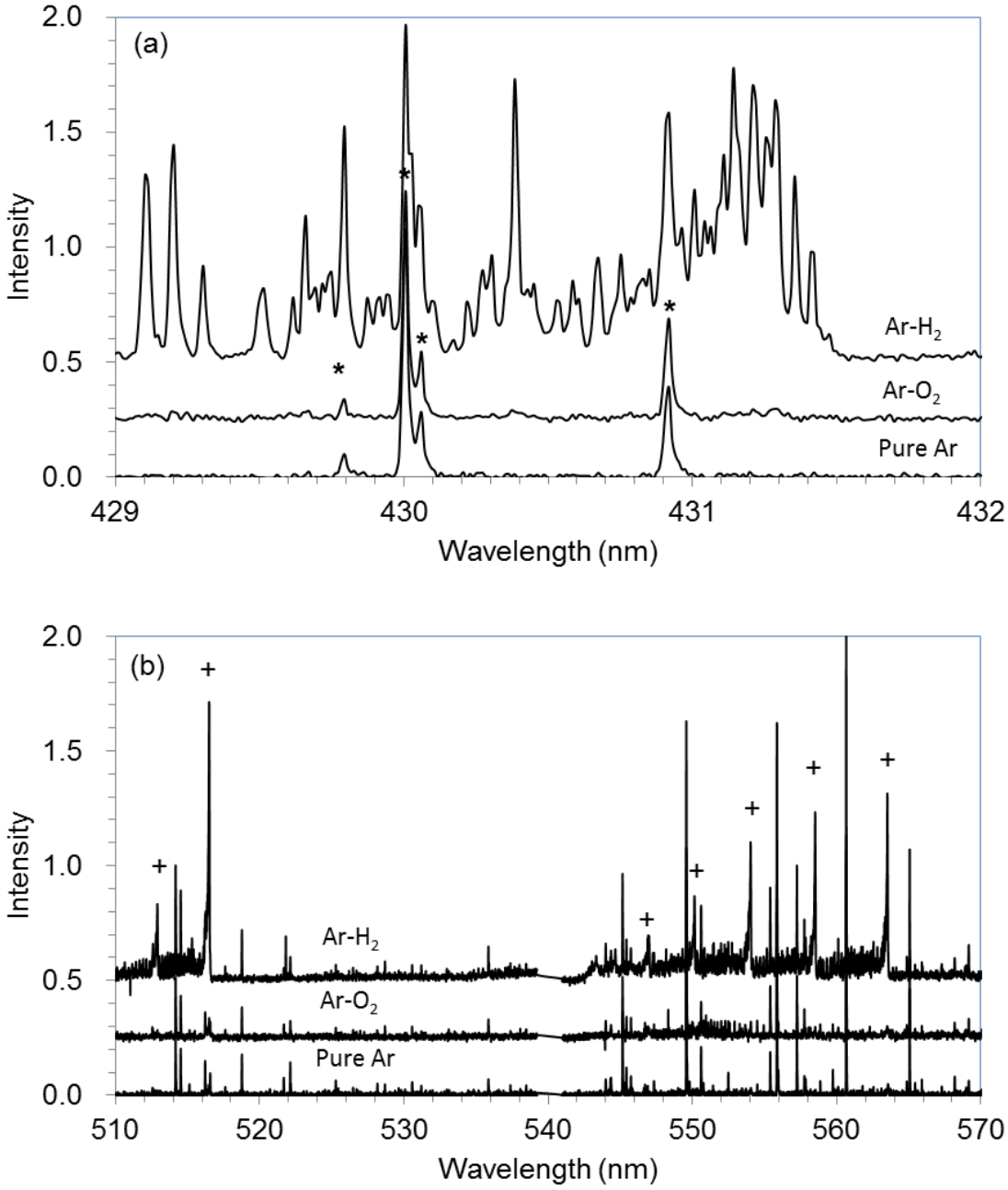

Figure 4.6. Molecular spectra recorded with CCD mounted on GD-OES for pure Ar, 1.00% v/v H_2 in argon ($Ar–H_2$), and 0.50% v/v O_2 in Ar ($Ar–O_2$): (a) The CH molecular band and overlapping Ar peaks are marked with *. (b) The CC molecular band is marked with +; the others are assigned to Ar.

The molecular spectra can help to elucidate the effects of hydrogen addition, although the mechanism could not be explained clearly yet. Figure 4.6 (a) and (b) show molecular spectra of C–H and C–C, respectively, which were recorded with spectrometer equipped with a CCD detector in GD–OES

measurement for pure Ar, Ar–H_2, and Ar–O_2. The C–H molecular band structure is observed in the range of 429–432 nm [22–23] (Fig. 4.6(a)). The strong C–H band is shown in Ar–H_2. This indicates that CH radical is formed in the plasma by the reaction between carbon in the sample and hydrogen in discharge gas. Additionally, C–C band in 510–570 nm is also strong for Ar–H_2, whereas the signals are slight for Ar and Ar–O_2 (Fig. 4.6(b)). This indicates that CC radical is also formed in the plasma by hydrogen addition. It could be considered that C_nH_m type of radicals were formed first in Ar–H_2, and then CC radicals involved in them possibly contributed to the optical emission. Thus hydrogen addition could be recognized as a sort of reactive sputtering for carbon–based materials and the formation of volatile material fragments such as CH and C_nH_m can increase the sputtering rate.

4.3.2 Depth profiling of carbon electrode with oxygen and hydrogen addition

Figure 4.7(a) shows rf–GD–OES depth profiles with pure Ar for a graphite electrode sample including 1% LiF (PVDF binder, 55 μm thickness of graphite layer). The rapid increase of Cu intensity indicates that sputtering penetrates the graphite layer to reach Cu foil. Consequently, it took 15,000 s to measure the depth profile from the surface of the graphite layer to the bottom. The intensities of C increased drastically around the rapid increase of Cu because the sputtering rate of the carbon electrode layer is influenced by the presence of Cu, which has a high sputtering yield (1.6 atoms/ion at 400 eV Ar ions [8]) [7]. For Ar–H_2, the sputtering time of the electrode layer was diminished to 3500 s. Moreover, the C and Li intensities increased several times, which reflects the reactive effect and the higher sputtering rate with the benefit of hydrogen addition (Fig. 4.7(b)).

For Ar–O_2, the sputtering rate was accelerated further compared to the results in Ar–H_2: sputtering to the bottom of the graphite layer took only 1500 s (Fig.4. 7(c)). This effect is predominantly attributable to chemical etching by oxygen, as described in chemical formulas (1) and/or (2). The C intensity for Ar–O_2 did not increase, compared to pure Ar, despite its ten–times higher sputtering rate. This lack of increase can be attributed to the strong absorption of oxygen in vacuum–ultraviolet below 195 nm, although it should not be affected in Ar–H_2 by the absorption band of hydrogen appeared below 110 nm [24]. The lithium emission at 610 nm is hardly affected by the absorption of oxygen. Therefore, the Li intensity increases, as expected, from the enhancement of sputtering rate in Ar–O_2. However, the depth profile of Li sloped toward the longer sputtering time, although it was flat for pure Ar and Ar–H_2. Results show that the

sputtering rate was almost constant in progress by checking the crater shape in the course of the measurement. Therefore the slope in the Li intensity profile was unlikely to be increased by the sputtering rate variation. Preferential etching of C in Ar–O_2, as described in section 4.3.1, might occur to become lower emission intensities of co–existing elements in the carbon matrix, especially at the initial stage of sputtering. This phenomenon seemed rather intrinsic for Ar–O_2, independently of glow discharge conditions. We regard further detailed study as necessary to understand the reason for the unexpected slop of Li intensity when Ar–O_2 sputtering is applied for carbon electrode samples.

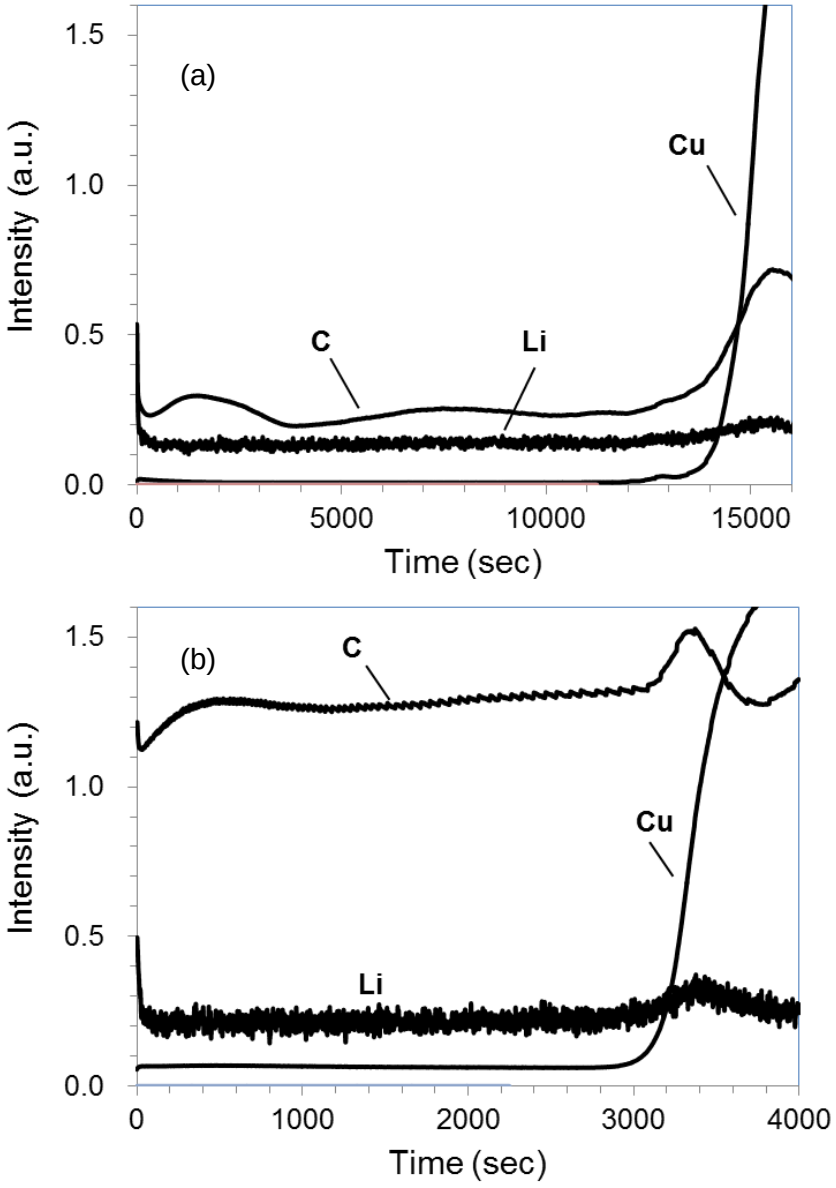

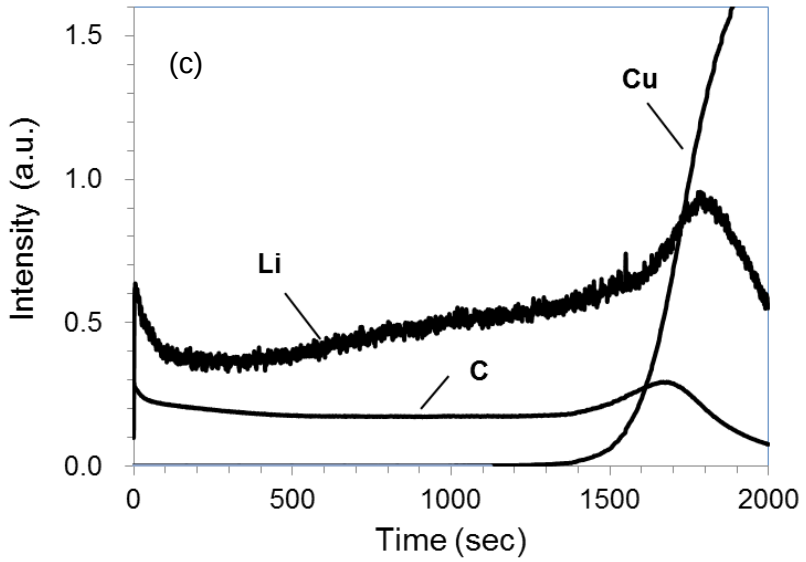

Figure 4.7. Rf-GD-OES depth profiles for 1% LiF included graphite electrode sample (55 μm thickness of graphite layer on in argon (Ar–H_2), and 0.50% v/v O_2 in Ar (Ar–O_2).

4.3.3 Quantification ability of lithium with oxygen and hydrogen addition

Quantitative ability for Ar–H_2 and Ar–O_2 plasmas was evaluated with the use of carbon electrode samples varied with LiF or Li_3PO_4 concentration. Figure 4.8 depicts Li intensities obtained from GD–OES versus Li contents. The inset was on an expanded scale to facilitate examination of a series of Li_3PO_4 with lower concentration range than the series of LiF. The Li content for the series of Li_3PO_4 samples was determined using ICP–OES to confirm the correlation between GD–OES and ICP–OES, whereas that for LiF was the amount added in the preparation. A linear relation between Li intensity and Li content was obtained for all of pure Ar, Ar–H_2 and Ar–O_2. The intensity of Li for a series of Li_3PO_4 samples seemed to be larger than that expanded from the calibration curves for LiF, which might be responsible for sample characteristic dependence. Sputtering of the carbon–based samples is likely to proceed reactively with oxygen of a constituent of Li_3PO_4, even for pure Ar. Figure 4.9 presents crater shapes for 0–0.4 wt% Li_3PO_4 including carbon electrodes. The sputtering rate increased concomitantly with increasing Li_3PO_4 amount in carbon matrix samples. The crater shape was also changed to concave, whereas it was mostly unchanged over the whole concentration range (0–2 wt%) in the LiF samples. It was reported previously that the effect of hydrogen addition is similar when hydrogen is induced in gaseous form and when it is sputtered from the sample [13, 25]. The same phenomenon would occur if oxygen was added to the discharge gas of argon. Even including the error found between Li_3PO_4 and LiF on the correlation curves,

the correlation coefficient r^2 for Ar–H_2 and Ar–O_2 (0.98 and 0.995, respectively, in the Li concentration range of 0.0–1.4 wt%) was equivalent to that of pure Ar (0.98), which suggests that both Ar–H_2 and Ar–O_2 are acceptable for quantitative analysis of carbon–based materials. Moreover, the correlation curve slopes were 2.5 and 10 times larger than those of pure Ar, respectively for Ar–H_2 and Ar–O_2, from the benefit of the faster sputtering rate, which promises advantages for sensitivity in quantitative analysis.

Table 4.1 presents a summary about the characteristics in GD–OES analysis of graphite electrode samples with pure Ar, Ar–H_2 and Ar–O_2. The Ar–H_2 discharge shows benefits for quantifying lithium in graphite electrode samples with shorter measurement time and higher sensitivity than that of conventional pure Ar discharge. The Ar–O_2 enabled ten–times higher sensitivity and good correlation in quantification within a shorter measurement time, although it possibly brought about a different depth profile for the samples.

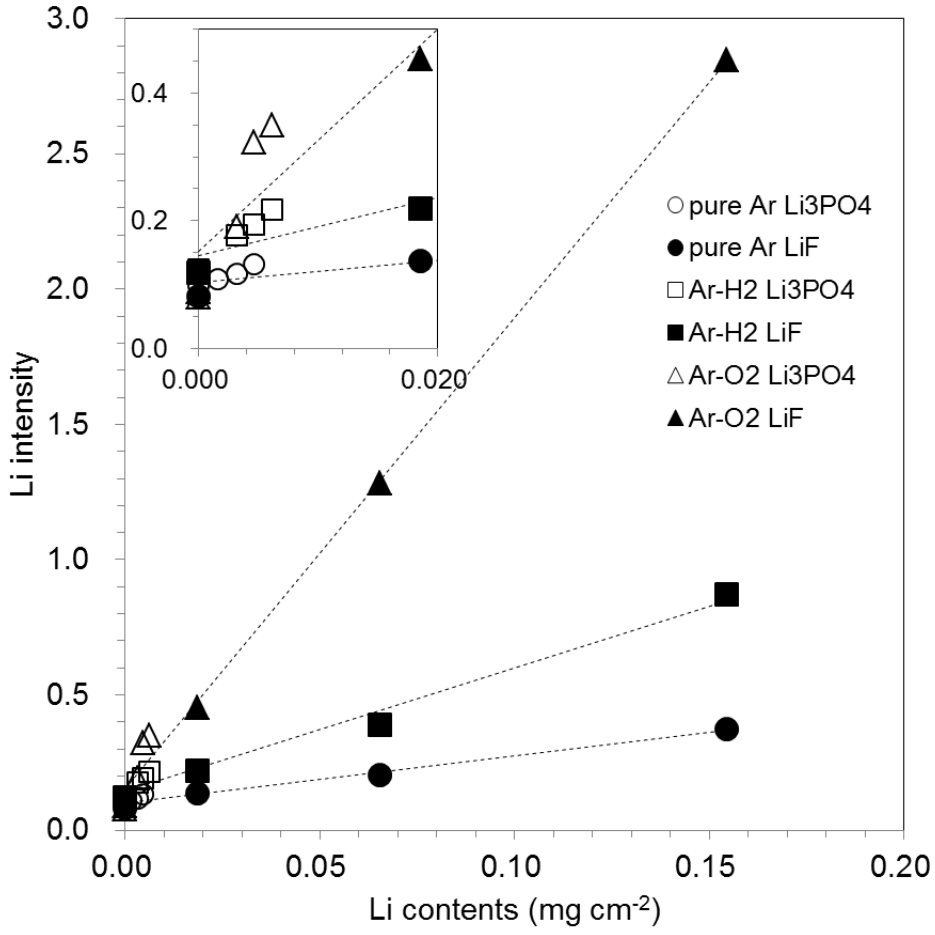

Figure 4.8. Relation between GD-OES Li intensity and Li contents in graphite samples with pure Ar, 1.00% v/v H_2, and 0.50% v/v O_2 in Ar (Ar–O_2).

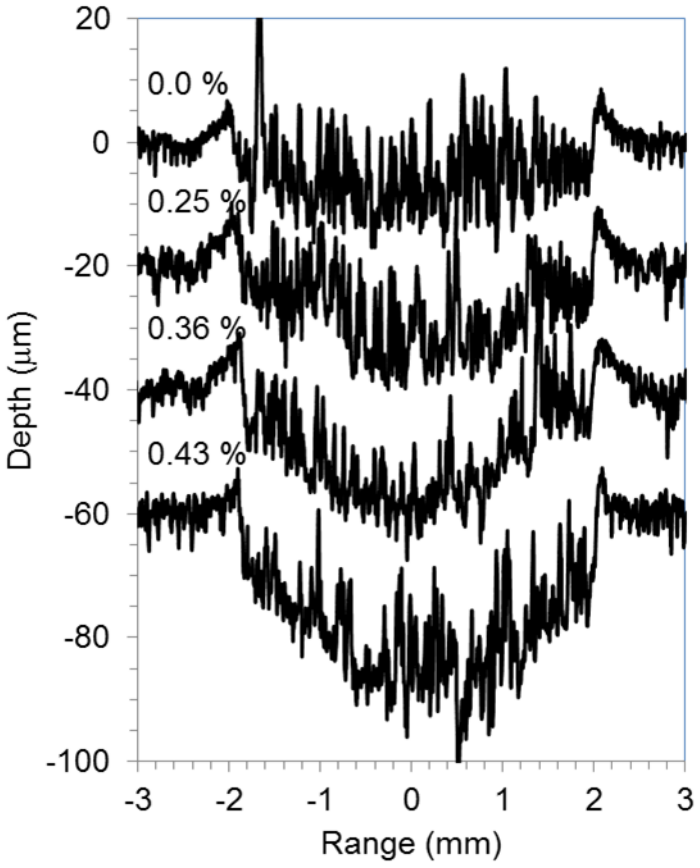

Figure 4.9. Crater shapes of graphite electrode samples included various Li_3PO_4 contents after 1000 s sputtering with pure Ar. Experimental conditions: 550 V electric voltage, 200 Pa gas pressure, 50% pulse rate at 2500 Hz.

Table 4.1 Characteristics of rf-GD-OES with pure Ar, 1.00% v/v H2 in argon (Ar- H_2), and 0.50% v/v O_2 in Ar (Ar–O_2). Sample: 1 wt% LiF included graphite electrode, 55 μm thickness. Experimental conditions: 550 V electric voltage, 200 Pa gas pressure, 50% pulse rate at 2500 Hz. Relative sensitivity was estimated by normalizing the slopes of the correlation curves shown in Fig. 4.9.

	Sputtering rate	Relative sensitivity of Li	Correlation coefficient r^2 of Li	Depth profile of Li	Surface analysis by SEM / XPS	Note
Pure Ar	15000 s / 55 μm	1.0	0.98	Flat	Redeposition / Ar immersion	
Ar-H_2	3500 s / 55 μm	2.7	0.98	Flat	Smooth / Less Ar immersion	Absorption below 110 nm
Ar-O_2	1500 s / 55 μm	10	0.995	Sloping	Rough and crisp / Rich F	Absorption below 195 nm

4.3.4 Depth Profiling of degraded LIB Electrodes

GD–OES measurements with Ar–H_2 and Ar–O_2 were practically applied to degraded graphite electrodes in commercially available LIB [20]. Table 4.2 summarizes the test conditions and obtained cell capacity. The sample named New was as–prepared one before deterioration. The other samples were tested by charge–discharge cycles under the various conditions. The capacity retention means the relative cell capacity after the cycle test with New; the smaller value indicates the higher deterioration degree. Figure 4.10 (a) shows a depth profile of a graphite electrode sample for New with use of Ar–H_2. The profile was quantified with the calibration curve shown in Fig. 4.8. The sputtering time of the electrode layer was shorten to about 3500 s for 50–60 μm thickness, comparing with more than 10000 s in the case of conventional pure Ar. The electrode mainly consisted of C and included a small amount of Li which could be attributed to a SEI component. The Li concentration was almost constant except for the surface region (0–10 μm). The surface concentration of Li could be high because SEI is likely deposited on the electrode surface [26]. Figure 4.10 (b) portrays Li profiles for all electrode samples. The Li concentration increased with deterioration degree of the samples. The decreasing slope was moderated in the outer layer (0–10 μm) with the deterioration degree and slightly declined still in the inner layer (10–40μm). This suggested that Li of a SEI component relatively increased in the inner layer with the cell degradation.

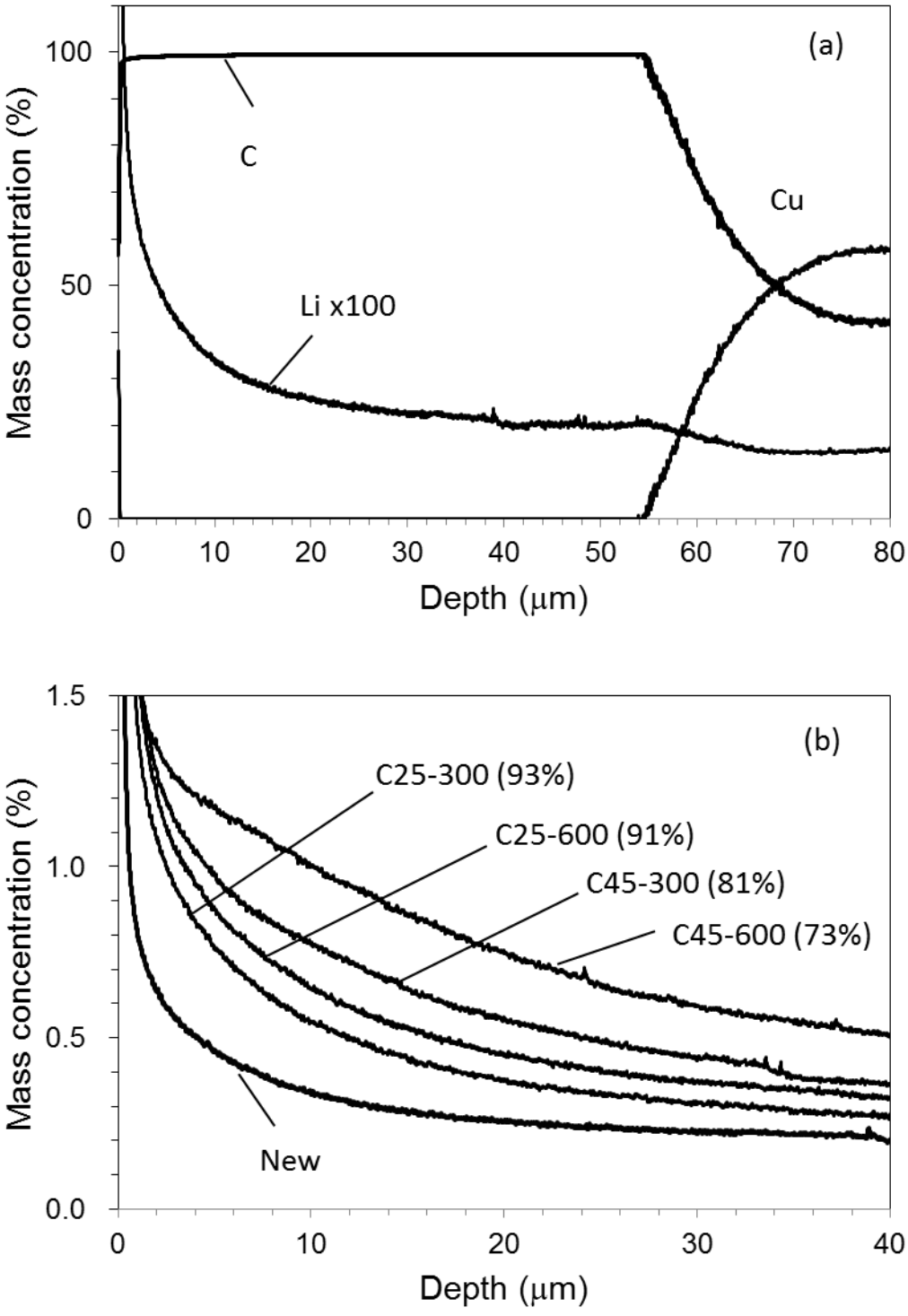

Figure 4.10. Depth profile for [New] electrode (a) and Li profiles for all electrode samples (b) with 1.00% v/v H_2 in argon (Ar–H_2).

Table 4.2 Tested charge-discharge cycle conditions and obtained cell capacity. The capacity retention indicates the relative discharge capacity after the cycle test with [New]. All the cycle tests were performed under 2.5-4.0 V cut-off voltages and C/2 current rate.

	Temperature (°C)	Cycle	Capacity (Ah)	Capacity retention (%)
[NEW]	–	–	5.20	100
[C25-300]	25	300	4.82	93
[C25-600]	25	600	4.73	91
[C45-300]	45	300	4.23	81
[C45-600]	45	600	3.79	73

Figures 4.11 (a) and (b) show a depth profile of a graphite electrode sample for New and Li profiles for all electrode samples in the case of Ar–O_2, respectively. It took only 700 s for sputtering the electrode layer. The Li concentration gradually declined throughout the entire depth even for New sample. For the deteriorated samples, the profiles did not monotonously decrease and had a local increase in the outer layer (0–10 μm). Monotonous decrease indicated in Ar–H_2 (Fig. 4.10(b)) seemed more reasonable considering the electrochemical reaction in the cell, though we could not describe clearly because overall depth distribution of SEI in electrode has not been investigated yet in our knowledge. The systematic variation with the deterioration degree was not obtained among samples in Ar–O_2 profiles (Fig. 4.11(b)), unlike in Ar–H_2 profiles (Fig. 4.10(b)). Figure 4.12 plots the averaged Li concentrations for all samples obtained with Ar–H_2 and Ar–O_2 to those determined by ICP–OES. A linear relationship with the correlation coefficient $r^2 = 0.95$ was obtained for Ar–O_2. This suggested that quantitative analysis was possible in Ar–O_2, whereas the depth profiles might be ambiguous. The Ar–H_2 result showed a better linear relationship with the correlation coefficient $r^2 = 0.995$. Therefore we considered that Ar–H_2 was prominent in both respects of depth profiling and quantitative analysis for carbon electrodes in LIB.

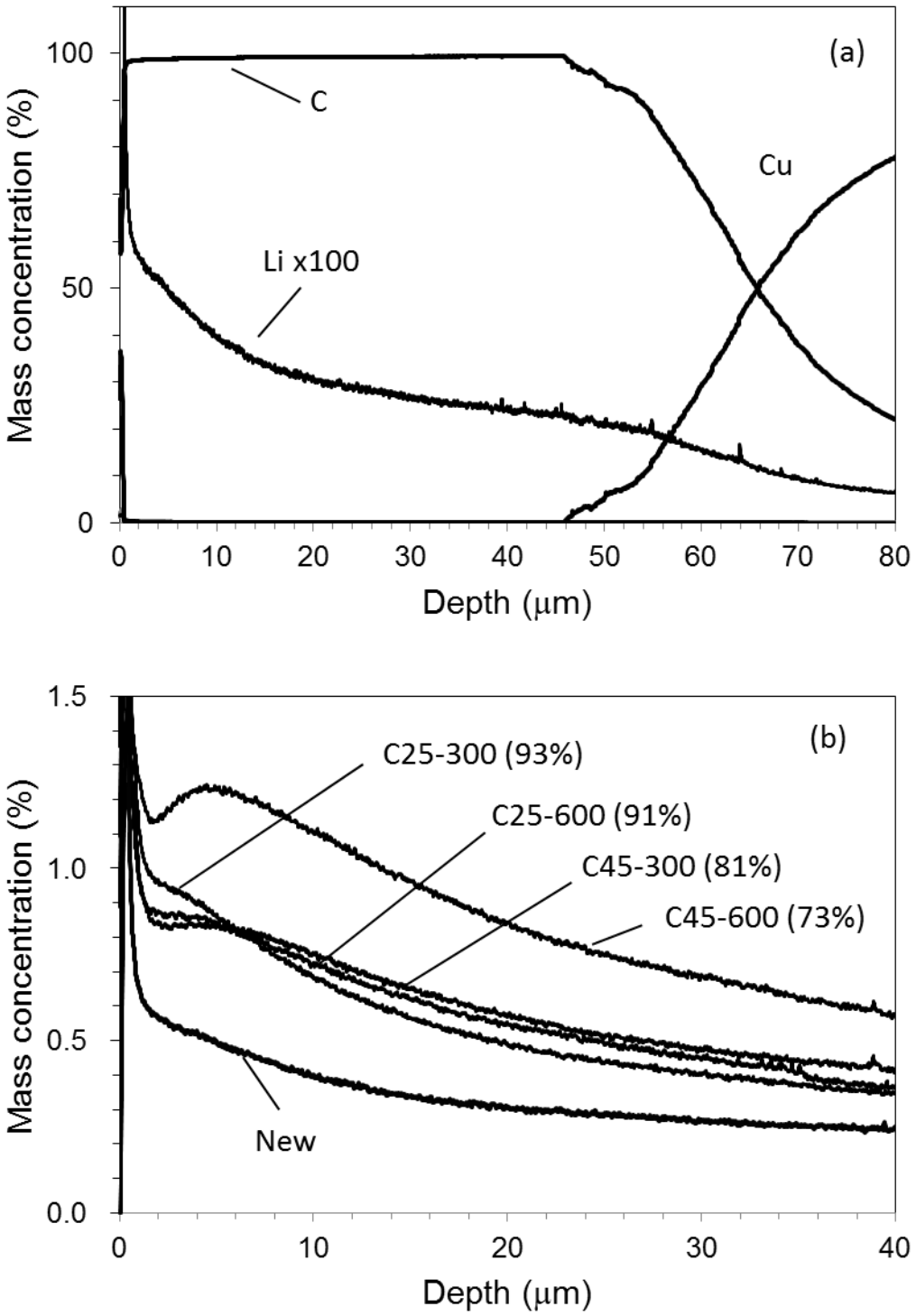

Figure 4.11. Depth profile for [New] electrode (a) and Li profiles for all electrode samples (b) with 0.50% v/v O_2 in argon (Ar–O_2).

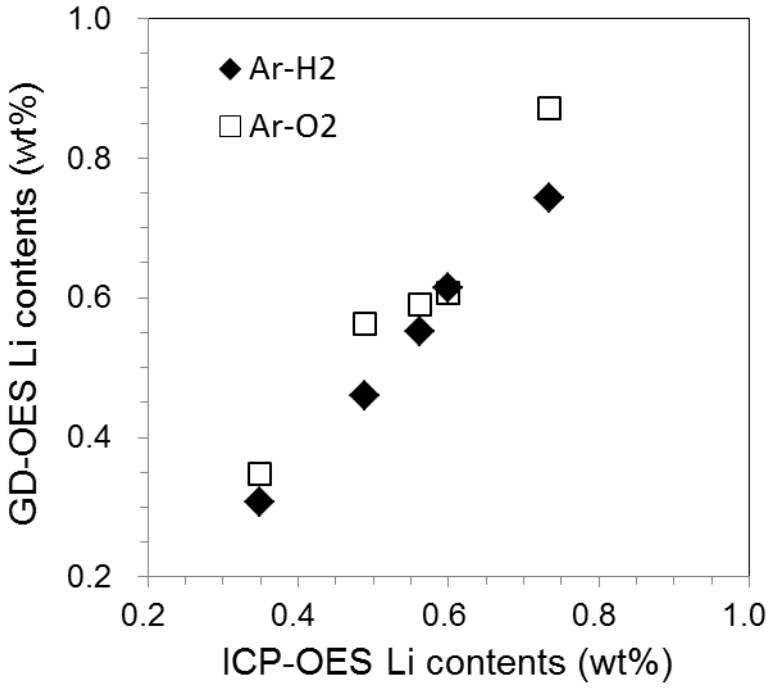

Figure 4.12. Relationship of Li concentrations obtained by GD-OES with Ar–H_2 and Ar–O_2 to those determined by ICP-OES.

4.4 Conclusion

Rf–GD–OES with small addition of oxygen (0.50 % v/ v O_2 in Ar) and hydrogen (1.00 % v/ v H_2 in Ar) was applied and characterized for a graphite electrode in LIB. For oxygen addition, the sputtering rate was enhanced drastically: ten–fold compared to conventional pure argon discharge. This outcome is attributed to chemical etching effects of oxygen in argon plasma. The depth profile of lithium dispersed in a graphite electrode sample differed from that with pure Ar. Surface analysis results obtained using SEM and XPS suggest that the etching reaction progresses inhomogeneously to the inner layer. For adding hydrogen to argon plasma, shorter measurement time and higher sensitivity were brought about compared to those for pure argon, which indicated benefits for both depth profiling and for quantifying Li for graphite electrode samples. Molecular spectra with a CCD spectrometer showed strong C–H and C–C bands, suggesting that the formation of volatile material fragments of CH and CC increased sputtering rate. Surface analysis results indicate that redeposition and Ar^+ ion implantation were suppressed, which can also enhance the sputtering rate and reliability of depth profiling. For practical applications of LIB graphite electrodes, we recommend Ar–H_2 plasma which could give shorter measurement time and more reliable depth–profile

with a good quantitativity.

4.5 References

[1] D. Aurbach, E. Zinigrad, Y. Cohen, and H. Teller, *Solid State Ionics*, **148**, 405 (2002).

[2] D. Aurbach, B. Markovsky, I. Weissman, E. Levi, and Y. Ein-Eli, *Electrochim Acta*, **45**, 67 (1999).

[3] B. M. Meyer, N. Leifer, S. Sakamoto, S. G. Greenbaum, and C. P. Grey, *Electrochem. Solid-State Lett*, **8**, A145 (2005).

[4] M. Winchester and R. Payling, *Spectrochemica Acta B*, **59**, 607 (2004).

[5] Y. Saito and M. K. Rahman, *J. Power Sources*, **174**, 877 (2007).

[6] H. Takahara, M. Shikano, and H. Kobayashi, *J. Power Sources*, **244**, 252, (2013).

[7] H. Takahara, H. Miyauchi, M. Tabuchi, T. Nakamura, *J. Electrochem. Soc.*, **160**, A272 (2013).

[8] R. K. Marcus (Ed), *Glow Discharge Spectroscopies (Modern Analytical Chemistry)*, Plenum pub Corp, New York, pp.30−31 (1993).

[9] M. A. Lieberman and A. J. Lichtenberg, *Principle of Plasma Discharge and Materials Proceeding*, p.571−579, John Wiley & Sons, Inc., New Jersey (2005).

[10] K. Wagatsuma, K. Hirokawa, N. Yamashita, *Analytica. Chimica*. Acta, **324**, 147 (1996).

[11] K. Wagatsuma, K. Hirokawa, *Spectrochimica Acta*, **B 42**, 523 (1987).

[12] K. Wagatsuma, K. Hirokawa, *Anal. Chem*., **61**, 326 (1989).

[13] A. Martine, A. Menendez, R. Pereiro, N. Bordel, and A. Sanz−Medel, *Anal. Bioanal Chem* **388**, 1573 (2007) .

[14] E. B. M. Steers, P. Smid, V. Hoffman, and Z. Weiss, *Journal of Physics: Conference Series*, **133** 012020 (2008).

[15] A. Bogaerts, *Spectrochimica Acta*, **B 64**, 1266 (2009).

[16] B. Fernandez, N. Bordel, R. Pereiro, and A. Sanz−Medel, *J. Anal. At. Spectrom*, **18**, 156 (2003).

[17] A. Bogaerts, *J. Anal. At. Spectrom*, **23**, 1476 (2008).

[18] V. D. Hodoroaba, E. B. M. Streers, V. Hoffmann, W. E. S. Unger, W. Paatsch, K. Wetzig, *J. Anal. At. Spectrom*, **18**, 521 (2003).

[19] C. C. Li and Y. W. Wang, *J. Electrochem. Soc.*, **158**, A1361 (2011).

[20] Y. Kobayashi, T. Kobayashi, K. Shono, Y. Ohno, Y. Mita, and H. Miyashiro, *J. Electrochem. Soc.*,

160, A1181 (2013).

[21] A. M. Andersson, D. P. Abraham, R. Haasch, S. MacLaren, J. Liu, and K. Amine, *J. Electrochem. Soc.*, **149**, A1358 (2002).

[22] A. Bengtson, *J. Anal. At. Spectrom.*, **18**, 1066 (2003).

[23] R. W. B. Pearse and A. G. Gaydon, *The Identification of Molecular Spectra, Chapman and Hall*, London, 1976.

[24] G. Herzberg, *Molecular Spectra and Molecular Structure I: Spectra of Diatomic Molecules (2nd Ed.)*, Krieger, Malabar, Florida (1989).

[25] A. Bengston and S. Hanstrom, *Steel Met. Ind.*, 47, 1998.

[26] M. Winter, K–C. Moeller, and J. O. Besenhard, *Lithium Batteries Science and Technology*, G. Nazri and G. Pistoia, Editors, pp.171–179, Springer, New York (2009).

5. Analysis of solid electrolyte interphase in Mn–based cathode/graphite Li–ion battery with glow discharge optical emission spectroscopy (GD–OES)

Solid electrolyte interphase (SEI) and Mn deposition formed on capacity-degraded graphite electrodes in commercially available Mn-based/Graphite lithium ion batteries were characterized using glow discharge-optical emission spectroscopy (GD-OES). The depth profile of the whole electrode showed a homogeneous distribution of Li and Mn except for the surface region at the initial state. With the progress of degradation, Li and Mn concentrations increased inhomogeneously in the depth-direction of the electrode; the Li and Mn concentrations were high in the outer layer and decreased with depth to the current collector in the degraded electrodes. The SEI layer deposited on the electrode surface was separately analyzed in detail. The GD-OES surface profile was explained by comparing to the XPS analysis results. The amount of Li deposited on the electrode surface was almost constant with the capacity degradation, though the Li concentration in the whole electrode increased along with the capacity degradation. In contrast, the amount of Mn deposition increased with the capacity degradation both in the surface deposition layer and in the whole electrode.

5.1 Introduction

Lithium ion batteries (LIBs) have been applied to portable power sources and then extensively to various uses of electric vehicles and stationary devices. An important subject related to LIBs is deterioration during long–term and high–temperature operations. The deterioration mechanism has been studied extensively to date. Solid electrolyte interphase (SEI) growth on the negative electrode is well known to contribute strongly to capacity fading during cycles [1, 2]. Formation of the SEI layer on the negative electrode causes irreversible capacity loss in the first few cycles. Even in additional cycles, lithium is consumed continuously as a result of continuous reduction of the electrolyte on the electrode.

Lithium manganese oxide spinel, $LiMn_2O_4$ (LMO), has been regarded as a promising positive electrode material for large–scale commercial battery because of its low–cost and environmentally friendly characteristics. In the case of LMO cathode, manganese dissolution is a critical factor for deterioration, just as SEI growth is for it [3, 4]. Manganese dissolution probably results from acid that is generated by

oxidation of the solvent. The dissolved manganese is migrated to the negative electrode. Then it is reduced and deposited as Mn metal on the negative electrode. Finally, it presumably forms manganese compounds such as $MnCO_3$ [5]. The deposited manganese can enhance the electrolyte decomposition to accelerate SEI growth on the negative electrode [6]. These deposited manganese compounds and SEI growth promote lithium consumption and enhance cell resistance.

Recently, capacity fading in commercially available Mn−based/Graphite ($LiMn_2O_4$/$LiNi_{0.8}Co_{0.2}Al_{0.05}O_2$ mixed cathode and graphite anode) batteries was investigated by Kobayashi et al. [7, 8] They performed long−term charge−discharge cycling at the operation temperature of 25 and 45 °C for the cells. They carefully disassembled the degraded cells under 3.0 V in OCV and then analyzed the cell operation balance for the cathode and anode capacities by assembling the half cells with them. The capacity degradation was explained from the capacity loss in the positive electrode and the shift in the operation valance of electrodes, so−called electrode slippage [9, 10]. They estimated quantitatively that the contribution of the electrode slippage was equivalent to the capacity loss in the graphite electrode as SEI growth. In the results, the SEI growth was a dominant factor for the capacity degradation under 25 °C, whereas the capacity loss in the positive electrode was drastically accelerated and got dominated for the capacity degradation at the operation temperature of 45 °C. Additionally, the contribution of Mn deposited in the graphite electrode corresponded to around 10% for the capacity loss of the positive electrode, which was similar to the previous report [11]. We further investigated the results of capacity fading in Mn−based cathode/Graphite battery with the use of depth profiling in this study.

Glow discharge optical emission spectroscopy (GD−OES) is an elemental analysis technique in the depth direction with nm to 100 μm scale using Ar ion sputtering. A few previous reports describe depth profiling of LIB electrodes using GD−OES [12−15]. The lithium composition was analyzed for various states of charge (SOC) of oxide−based cathode and carbon anode. The quantitative results agreed well with those obtained using inductively coupled plasma – mass spectroscopy (ICP−MS). The capacity−fading of $LiFePO_4$ (LFP)/Graphite cells was characterized with GD−OES in our previous study [13]. Depth profiling results showed that lithium was distributed homogeneously regardless of depth for the positive and negative electrodes in cells with 85–100% capacity retention after cycling tests. Decrease of lithium amount in the inner layer of LFP electrode was suggested for the highly deteriorated cell of 44% only. Furthermore, homogeneous lithium distribution in depth was shown in the graphite electrode while large

amounts of Li were deposited on the surface, which might cause a partial shortage for the sudden deterioration. In the GD−OES measurement of the graphite electrode, the long measuring time is attributed to the intrinsic low sputtering yield of carbon, which leads to low−analysis sensitivity. Furthermore, the redeposition of C−related material on the sample surface reduced the sputtering efficiency [14]. Then the emission profile of C became unstable near the Cu current collector. Reportedly, the addition of a small amount of hydrogen into a discharge argon gas can improve the measuring time and reliability in GD−OES measurement for a graphite electrode [15]. The sputtering rate was enhanced several−fold compared to that using conventional pure argon gas (Ar−H_2). That redeposition was suppressed efficiently by the benefit of reactive sputtering with Ar−H_2 discharge. Favorable quantitative performance of Li was also confirmed from the experimental graphite electrode samples including several concentration levels of Li_3PO_4 and LiF.

This study investigates capacity fading in commercially available Mn−based/Graphite batteries with GD−OES. Depth profiles of SEI growth and Mn deposition in the graphite electrode were analyzed for various capacity fading levels. The distributions of Li and Mn were taken with the Ar−H_2 discharge for the whole electrode from surface to the current collector. Separately, the SEI and Mn deposited on the graphite electrode surface were analyzed carefully with much slower sputtering measurement with a low−rate pulse mode. The deposition layer structure was characterized and the depth resolution of the GD−OES measurement was discussed in comparison with X−ray photoelectron spectroscopy (XPS) results.

5.2 Experimental

Commercially available Al−laminated type cells were used. The positive and negative electrodes of the cell were composed of $LiMn_2O_4$/$LiNi_{0.8}Co_{0.2}Al_{0.05}O_2$ (8/2) and graphite respectively. The cycle tests were operated for 300 or 600 cycles under 2.7–4.2 V cut−off voltages and C/2 current rate at 25 ℃ or 45 ℃. Table 5.1 presents a summary of the abbreviations, test conditions and the obtained cell capacities. The New sample corresponded to the initial state of the tests. The discharge capacity in the real first cycle was difficult to determine, because a proper charge−discharge cycling was already set before shipment in the commercial cells. Therefore, in this study, the degradation ratio of capacity was calculated with respect to the initial capacity of this New sample untested. The cells were discharged at 3.0 V for over 10 h to de−intercalate lithium completely from the negative electrodes. Subsequently, the cells were disassembled. Then the negative electrode samples were rinsed with dimethyl carbonate in an argon−filled glove box. Li

and Mn contents included in the electrode samples were ascertained using induced coupled plasma – optical emission spectroscopy (ICP–OES, iCAP6200; Thermo Scientific). The ICP–OES results are presented in Table 5.1. More details related to the preparation of the degradation test and sample preparation are described in an earlier report. [7]

Table 5.1 Tested charge–discharge cycle conditions and obtained cell capacities. Degradation ratio indicates the loss ratio of the cell capacity after cycle test to the initial capacity estimated from New sample. All cycle tests were performed under 2.5–4.0 V cut-off voltages and C/2 current rate. The Li and Mn contents were determined using ICP-OES after the test.

	Temperature (°C)	Cycle	Capacity (Ah)	Degradation ratio (%)	ICP-OES Li(mg cm^{-2})	ICP-OES Mn(mg cm^{-2})
New	–	–	5.20	0	0.067	0.0029
C25-300	25	300	4.82	7	0.094	0.0075
C25-600	25	600	4.73	9	0.11	0.011
C45-300	45	300	4.23	19	0.12	0.016
C45-600	45	600	3.79	27	0.14	0.025

GD–OES measurements were conducted for the degraded negative electrode samples on a spectrometer system (GDA750; Rigaku Corp./Spectruma). A high–purity gas mixture of 1.00% v/v H_2 in Ar (99.9999%) (Ar–H_2) was used as discharging gas for the whole electrode analysis. Radiofrequency power and pulsed glow discharge were applied under the following conditions: 550 V electric voltage, 200 Pa gas pressure, and 50% pulse rate at 2500 Hz frequency. Alternative gas of high purity Ne (99.9999%) was used for detailed surface analysis under 750 V electric voltage, 2.0 kPa gas pressure, and 10% pulse rate at 2500 Hz frequency. Ne gas was chosen for analyzing fluorine because the Ne gas discharge provides much higher sensitivity for fluorine analysis than Ar gas discharge does. The mixture gas of Ne and H_2 was not available commercially because the composition analysis was difficult as a result of the peak overlapping between Ne and H_2 in conventional gas chromatography. Therefore we used Ar–based gas, Ar–H_2, not Ne–H_2 for rapid whole–electrode analysis. The measurement spot was of 4 mm diameter. The electrode samples were cut into 15 mm × 15 mm pieces and were pasted with glue onto a brazed holder for

GD–OES measurements. The following elements and their emission lines were applied in this study: Li 610.41, C 156.14, O 130.22, F 685.60, P 177.49, Mn 403.45, and Cu 327.39 nm. The emission intensity was quantified with reference samples. For whole–electrode analysis with Ar–H_2, the reference electrode samples were prepared because reactive sputtering depends on the sample matrix, whereas conventional metallic reference materials were used for the surface analysis. The reference sample electrodes were prepared with 0–0.5 wt% Li_3PO_4 or 0.5–1% $LiNi_{0.33}Mn_{0.34}Co_{0.33}O_2$ as dispersed in water–based slurry of 95 % graphite, 2 % carbon fiber of electronic–conductivity assistant (VGCF; Showa Denko K.K.), 2 % carboxymethylcellulose CMC, and 1 % styrene–butadiene rubber (SBR) in distilled water [15]. The slurries were cast on 20 μm Cu foil, and then dried at 100 °C for one night. Then the coated film was roll–compacted to 1.0–1.4 g cm^{-3} and 55–90 μm for the active layer excluding Cu foil.

Scanning electron microscope (SEM) imaging and XPS surface characterization were conducted for electrode samples before and after GD–OES measurements. The SEM micrographs were taken with 15 kV accelerating voltage (JSM 5500 LV; JEOL). The XPS data were collected using an Al Kα radiation source operated at 46.95 eV and applied power of 25 W (PHI 5000 VersaProbe; Ulvac–Phi Inc.). The energies associated with each spectrum were calibrated to the C1s (284.6 eV), which is assigned mainly to C–C of graphite in the composite electrode.

5.3 Results and Discussion

5.3.1 SEI growth and Mn deposition on graphite electrode surface

The surface deposition on the degraded electrode was characterized with a slow sputtering method using pulse discharge. Figure 5.1 shows the GD–OES sputtering time–intensity profile of the graphite electrode surface for New and C45–300. The intensity peaks appeared to 150 s for Li, C, O, F, P, and Mn. Actually, Li is a component to form SEI with C, O, F, and P such as lithium alkyl carbonate, Li_2CO_3, LiF, and $Li_xPF_yO_z$ [17–19]. Mn can be attributed to the Mn deposition resulting from dissolution and migration from the positive electrode. The SEI formation was already indicated in New sample, because a proper charge–discharge cycling was carried out in the commercial cell before we get. It is likely that the depth profiles of those elements behave independently. In Fig. 5.1(b), C and P peaks appeared at the top surface at 0 s (D1). First, Mn and O peaks appeared at 15 s (D2). The second P peak followed them at 20 s (D3). Wide peaks of Li and F and the second Mn peak were centered at 50 s (D4). These peaks were settled at

120 s (D5). The curves for all elements were likely stable at 200 s (D6). To investigate the phenomena taking place in the GD–OES profile, XPS measurements were performed at depths of D1–D6. Samples were prepared separately for C45–300 by stopping GD–OES measurement at the predetermined times and then transferred to XPS measurement chamber without exposure to the air. Using point–to–point comparison of the chemical shifts, the materials reflected in GD–OES profiles can be inferred.

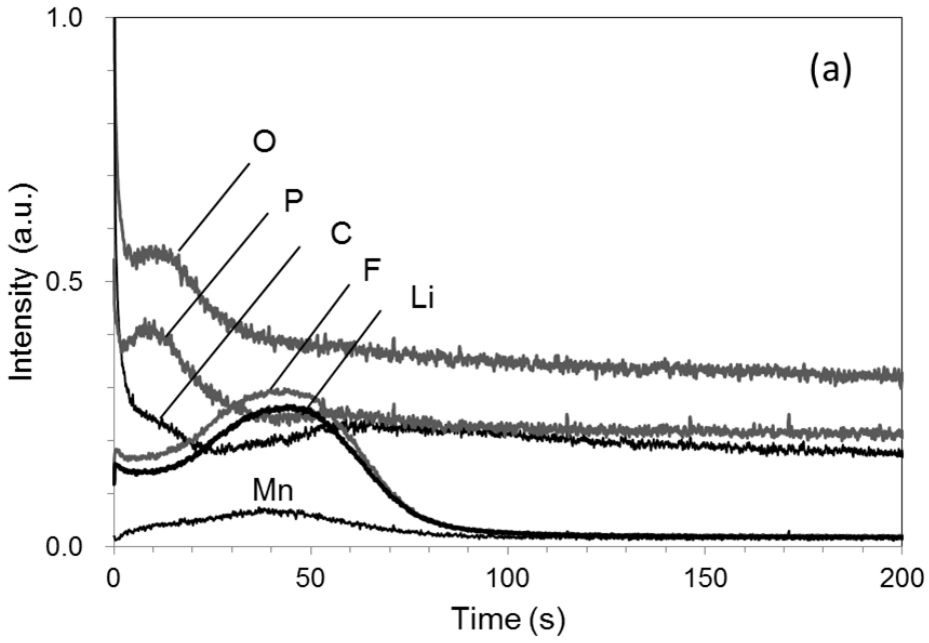

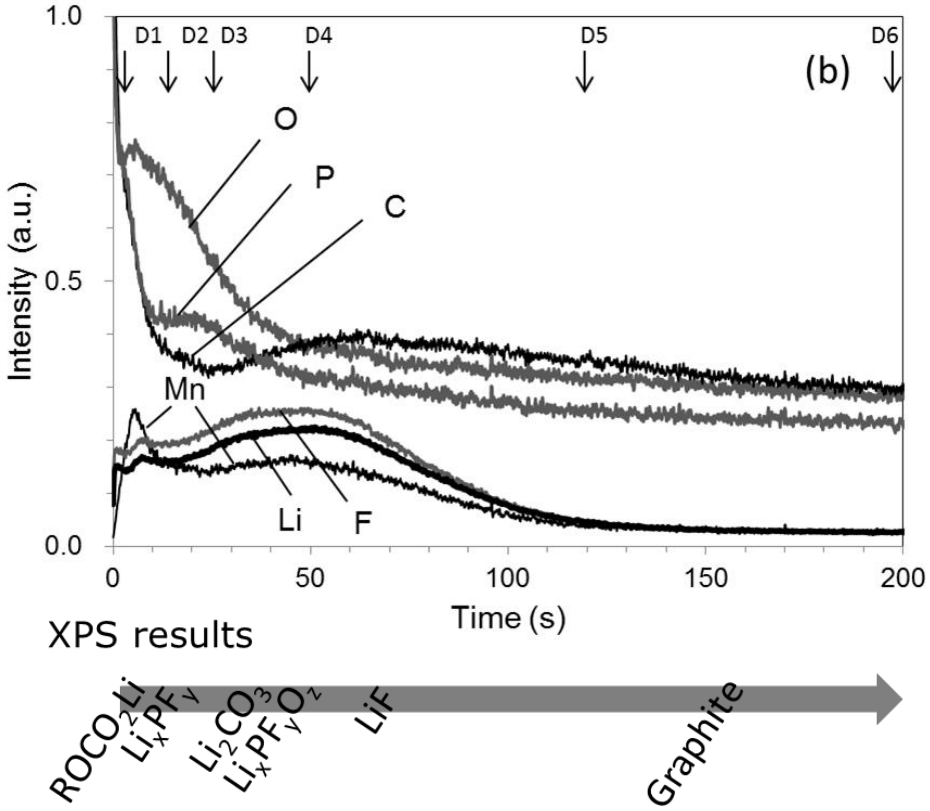

Figure 5.1. GD-OES detailed surface profiles obtained for degraded graphite electrodes of New (a) and C45-300 (b). XPS measurements were performed at the times marked with D1 to D6 and the result is summarized at the bottom of (b).

Figure 5.2 presents XPS spectra of C 1s, F 1s, P 2p, Li 1s, O 1s, and Mn 2p at D1–D6. At the initial surface (D1), there was an O=C–O peak at 290 eV and a C–O peak at 288–286 eV in the C 1s spectrum, which revealed the presence of lithium alkyl carbonate $ROCO_2Li$ [20]. The presence of Li_xPF_y and $Li_xPF_yO_z$ was also indicated by peaks, located respectively at 137 and 135 eV in the corresponding P 1s spectrum [21, 22]. At the depths marked with D2 and D3, a peak attributed to Li_2CO_3 at 291 eV appeared in the C 1s spectrum. The peaks from $Li_xPF_yO_z$ and Li_xPF_y were remarkable not only in P 2p spectrum but also in F 1s spectrum (689 eV) [23]. The strong peak at 686 eV was attributed to LiF [20]. The peaks at 533 eV in O1s, 57 eV in Li 1s, and 654 and 642 eV in Mn 2p originate from inorganic compounds such as fluorides and oxides [22, 23], although they were difficult to assign precisely because the chemical shifts were not clear (Fig. 5.2(d)–(f)). Those peaks from LiF and the inorganic compounds in F 1s, O 1s, Li 1s,

and Mn 2p were strong at D2 and D3. Then they decreased gradually and concomitantly with increasing depth. At D5, the C–C peak at 284.6 eV increased remarkably in C 1s spectrum, suggesting the original surface of the graphite electrode. Therefore, it was concluded that the region from D1 to D5 covers the whole layer deposited over the graphite electrode. Actually, SEM micrographs for D1 and D5 taken before and after the GD–OES measurement show that the sample surface is little changed (Fig. 5.3), which suggests that the deposition layer is mildly sputtered by the pulse discharge without damaging the graphite particles. The sputtering rate of this measurement is estimated as sub–nanometer per second, assuming that the thickness of the deposition layer is several tens of nanometers. Summarizing XPS results from D1–D6 at the bottom of Fig. 5.1(b), the GD–OES profile reflects that alkyl carbonate is present at top surface of the deposition layer. Then Li_2CO_3 appeared. Then LiF, $Li_xPF_yO_z$ and Li_xPF_y increased to the inner of the layer. It is well known from numerous previous reports that SEI comprises organic components such as alkyl carbonate in the outer layer and inorganic components such as Li_2O and LiF in the inner layer close to the graphite particle. The trend is described in GD–OES results. This might constitute evidence that GD–OES sustains sufficient depth resolution to analyze the surface deposition on graphite electrode. In GD–OES data, the emission intensity is related directly to the number of radiating atoms. It is possible to convert the sputtering time to the thickness if the atomic density is known or if it is theoretically available. However, in the case of the deposited layer, it was difficult to estimate the thickness because the atomic density cannot be ascertained and it should vary according to depth. Therefore, we discussed the depth profile qualitatively as time–intensity data. To quantify the amount, the integrated intensity of peak area was considered. That will enable us to discuss the total amount of the elements in the deposited layer.

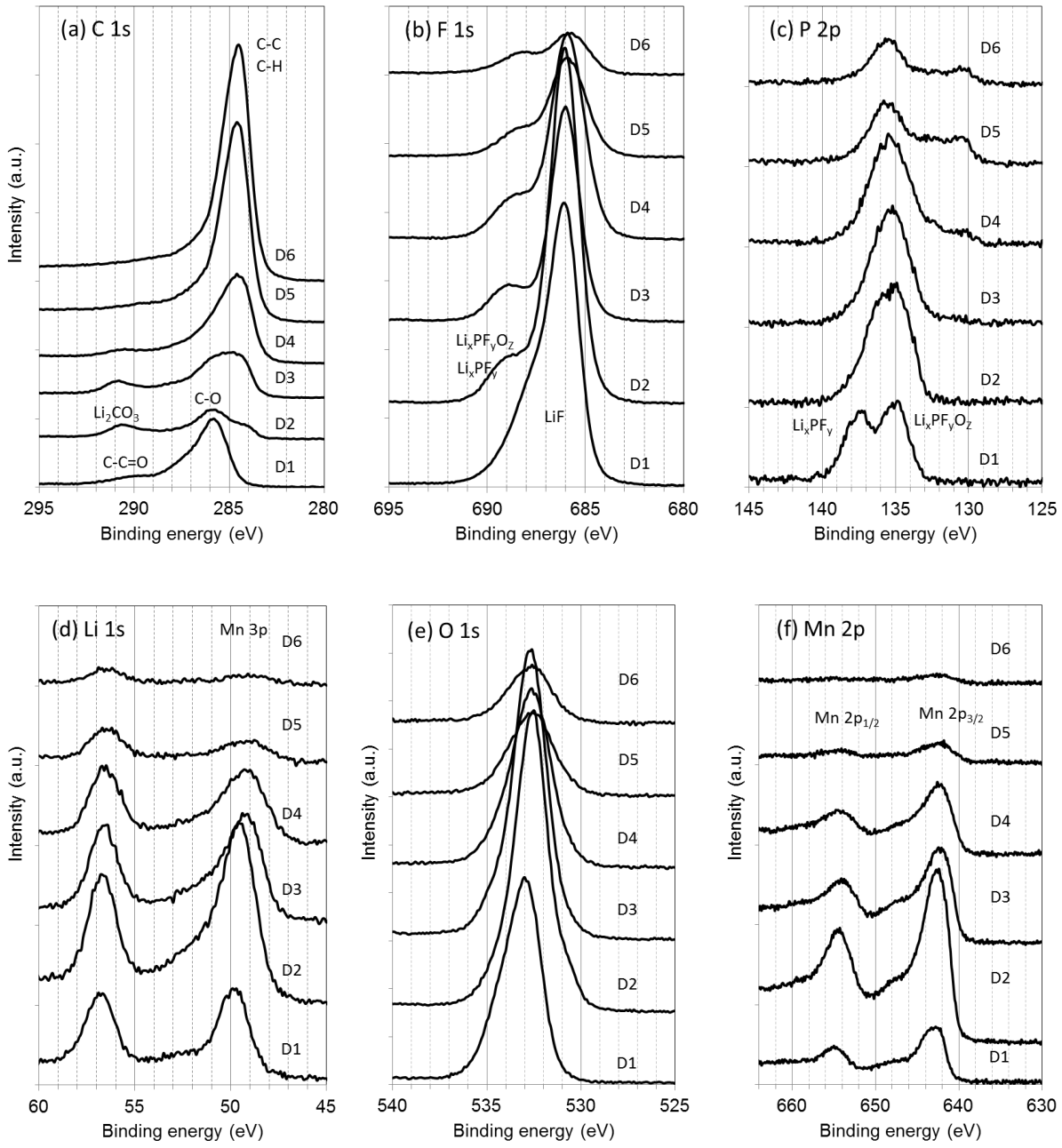

Figure 5.2. XPS spectra from D1 to D6 during the GD-OES measurement in Fig. 5.1(b).

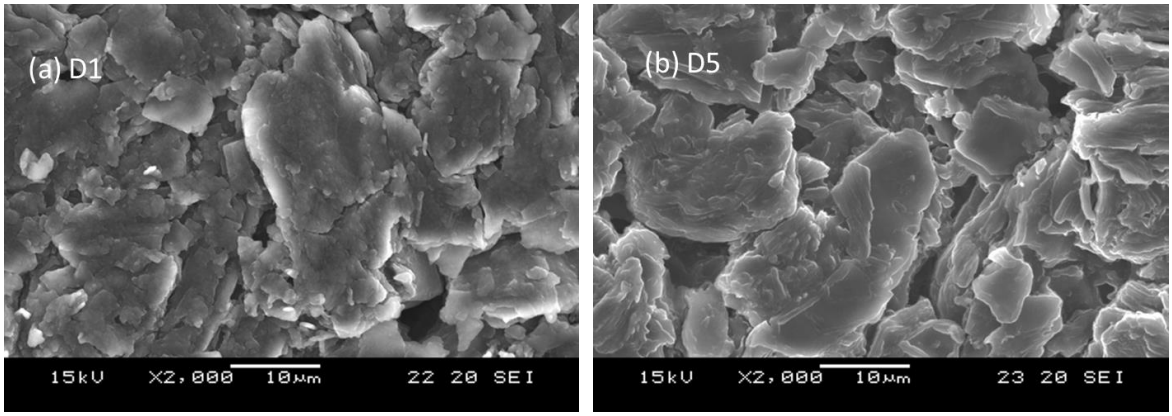

Figure 5.3. SEM micrographs of C45-300 at D1 (a) and D5 (b).

Figure 5.4 presents profiles of Li, F, Mn, O, and P for graphite electrode samples with various degrees of degradation. In the Li profile, the peak area intensity increased for degraded samples. The area intensity was the highest for C25–300 (7% in degradation ratio). The profiles were little changed for the further degradation of C25–600 (9%), C45–300 (17%), and C45–600 (19%). The F profile showed a similar trend to that of Li, suggesting that Li is mainly deposited as LiF. In the Mn profile, the peak intensity clearly increased concomitantly with increase of the degradation degree. This trend was different from those of Li and F. The rising edge of the Mn peak was observed in the outer position of the decomposition layer compared to those of Li and F. This can be recognized clearly as a separate peak in the top surface for C25–300 (7%), C25–600 (9%), and C45–300 (17%). This suggested that Mn could be located in the outer layer of the surface deposition. The O peak showed a similar rising edge to that of Mn, implying that Mn might form oxide or carbonate with O. To obtain the total amount of the materials deposited on the electrode as a function of the degradation ratio of the cell, the peak area was numerically integrated from 0 to 250 s and quantified in Fig. 5.5. The amount of Mn and O increased monotonously and concomitantly with increasing degradation. However, the amounts of Li and F likely increased for the low degradation degree, but they became almost constant for the further degradation. In the profile variations shown in Fig. 5.5, both the O and P peak intensities seemed to increase remarkably under 45 °C operating conditions (C45–300 and C45–600), though Li, F, and Mn intensities showed no such an obvious dependence on the operating temperatures. The origins of O and P could be attributed to the decomposition

of electrolyte and positive electrode material Therefore the result suggested that the decomposition of electrolyte and positive electrode material was drastically accelerated at high–operating temperature at 45 ℃. On the contrary, the unclear temperature dependences of Li, F, and Mn suggested SEI formation and Mn deposition occurred rather independently of the operating temperature. This might be related with the preceding results that the contribution of capacity loss in the positive electrode was dominant factor for the capacity degradation at the operating temperature of 45 ℃, and that SEI formation was dominant for the degradation for the operation at 25 ℃ [7].

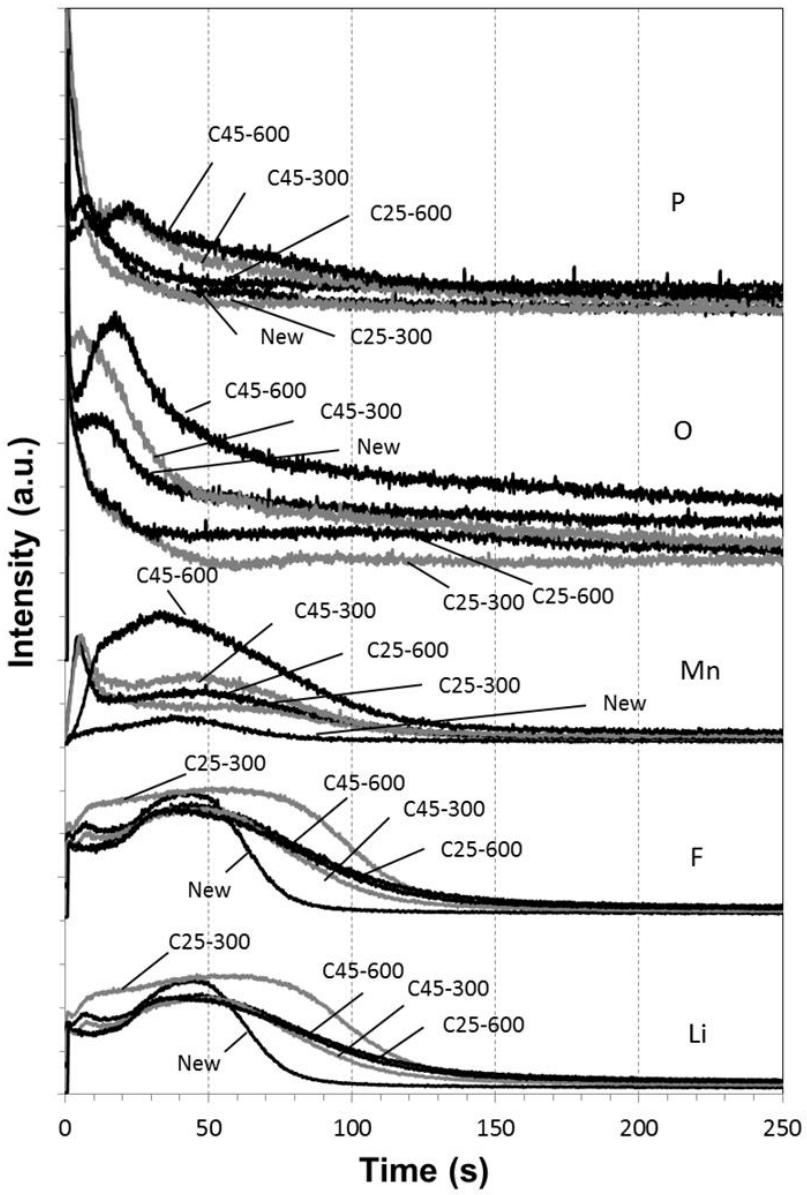

Figure 5.4. Detailed surface profiles of Li, F, Mn, O, and P for New and the degraded samples.

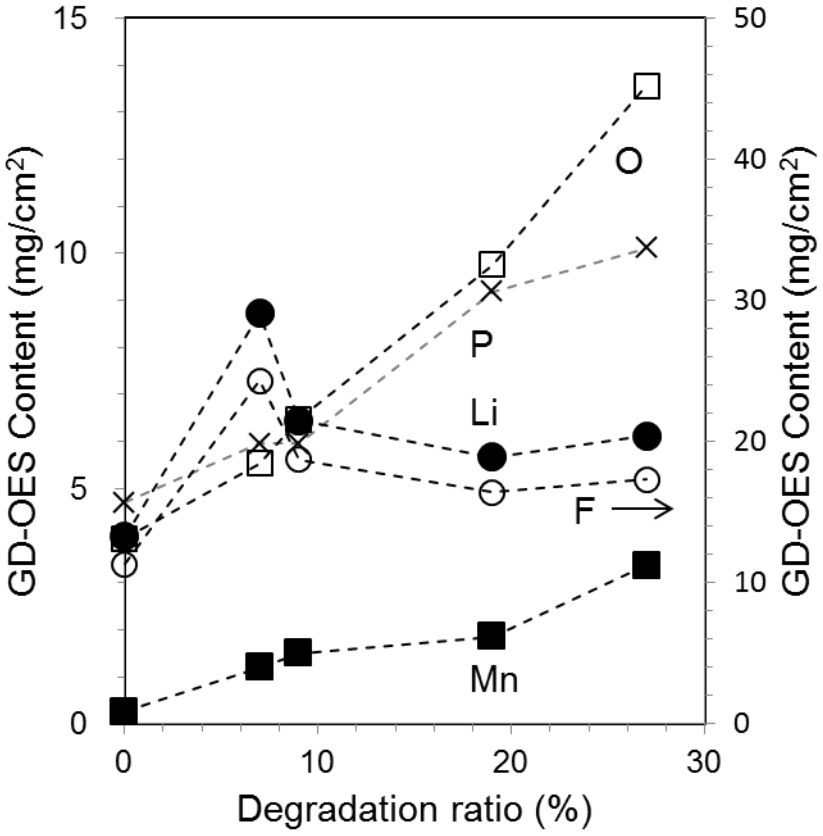

Figure 5.5. The contents of Li, F, Mn, O, and P in the surface deposition are shown as a function of deterioration ratio for New and the degraded samples.

5.3.2 Depth profile of the whole graphite electrode layer

Figure 5.6 presents qualitative and quantitative GD–OES depth profiles of the whole graphite electrode layer for C45–600. Data were taken using 1.00 % H_2 v/v added Ar gas (Ar–H_2). In the qualitative depth profile (sputtering time–intensity plot) in Fig. 5.6(a), good depth resolution was found between the electrode layer and substrate Cu foil, as reflected by the rapid increase of Cu intensity around 3500 s. The sputtering time of the electrode layer was shortened to about 3500 s for 50 μm thickness by reactive sputtering with Ar–H_2, compared with about 16,000 s in the case of conventional pure Ar sputtering[15]. Additionally, the Cu profile was stably flat until the sputtering reached the current collector layer, whereas the Cu signal was increased gradually by impulsive sputtering with pure Ar sputtering[13]. Both the sputtering rate and the stability are improved by the benefits of reactive sputtering with the use of Ar–H_2.

The time–intensity data were quantified with the standard samples that had been prepared previously by adding known amounts of Li, P, O, and Mn into graphite electrode slurries.

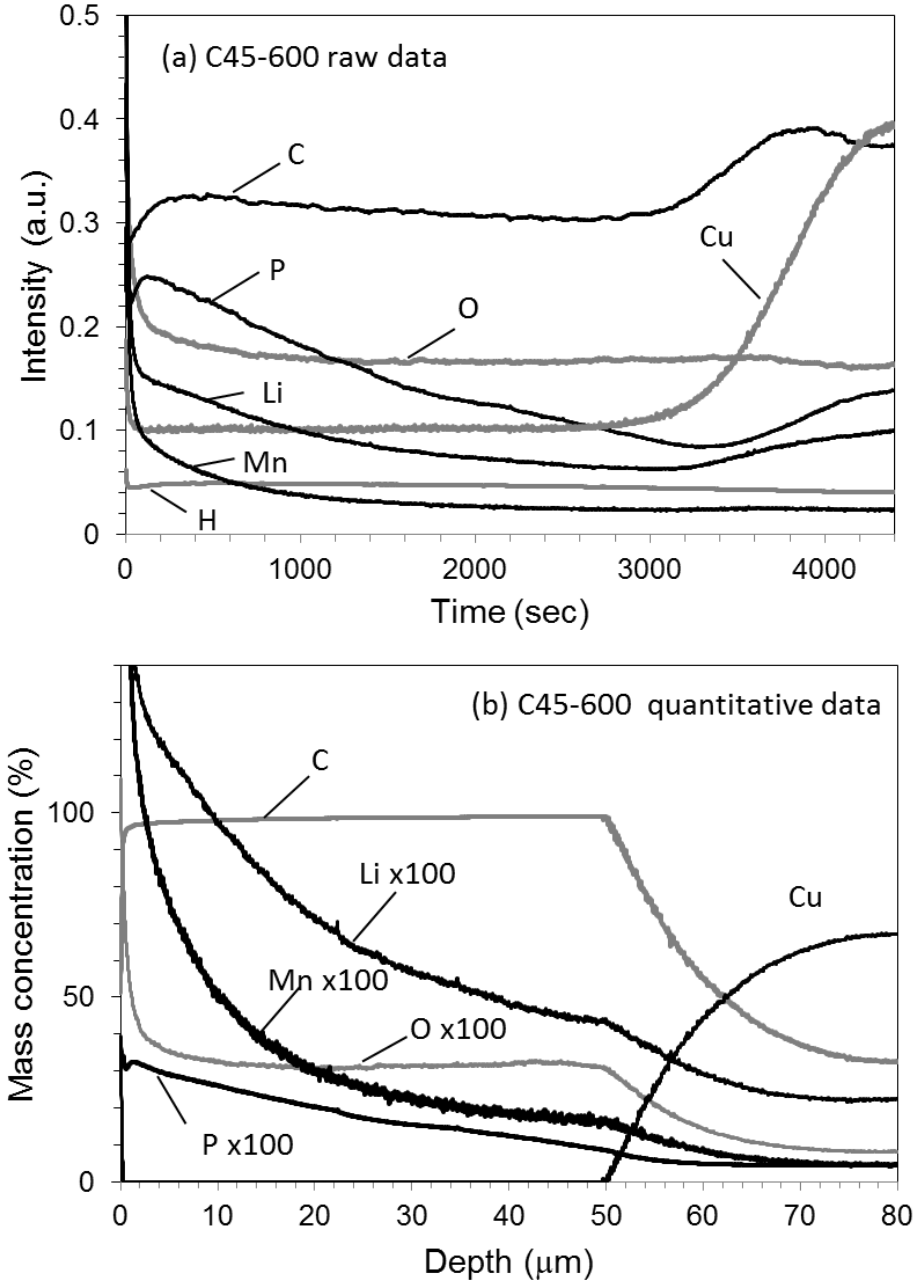

Figure 5.6. GD-OES depth profile of the whole electrode for C45-600. The time-intensity plot (a) was quantified to depth-concentration plot (b) where Li, Mn, O, P are under 100-times magnification.

In the quantitative depth profile depicted in Fig. 5.6(b), the main component C originates mainly

from graphite particles, although a polymer binder component might give a slight contribution. The Li, Mn, P, and O show small concentrations (the curves for their concentration are visualized under 100−times magnification). The test cell was fully de−intercalated by discharge at 3.0 V for over 10 h. The remaining discharge capacity was estimated as a very low value below 0.3%, as estimated with re−assembly of a half cell. Therefore, the remaining Li in the electrode is regarded as the SEI component rather than reversible Li. The P was also regarded as attributed to the SEI component such as $LiP_xF_yO_z$. Figure 5.7 shows Li, Mn, O, and P profiles for the initial and the degraded electrode samples. The concentration of Li increased with the degradation degree and showed a more inhomogeneous distribution in the graphite anode. In the New sample, the Li concentration was almost constant with depth in the middle region (10–50 μm). This fact suggests that homogeneous SEI formed during the initial cycles, except in the outer surface region (0–10 μm). With the progress of that degradation, SEI growth depends on the depth. The Li concentration is high in the outer layer and decreased with depth all the way down to the current collector. Unlike the initial sample, the Li concentration was less at the inner layer for the other degraded samples. Furthermore, the slope in the middle region became steeper as the degree of deterioration increased. The Mn concentration increased with the degree of deterioration as well as that of Li. The Mn profiles showed a decreasing trend to the inner layer. The Mn concentration in the inner layer increased with the degree of cell deterioration. Comparison with the profile of Li shows that the Mn concentration dropped more rapidly in the outer layer. In other words, Mn was precipitated in the outer layer and Li deposition spread to the inner layer. The concentration of P and O also showed an increasing trend with the degradation degree and their concentrations were higher in the outer layer for C25−300, C25−600 and C45−300. In C45−600, the O profile exhibited much higher concentration, and both P and O profiles had a decrease in the slope of depth profiles. This suggested that the decomposition reaction, which could contribute to the presences of P and O, might spread to the inner layer of the electrode. It was a similar trend to the surface deposition analysis where P and O behaved differently at the operation of 45 °C.

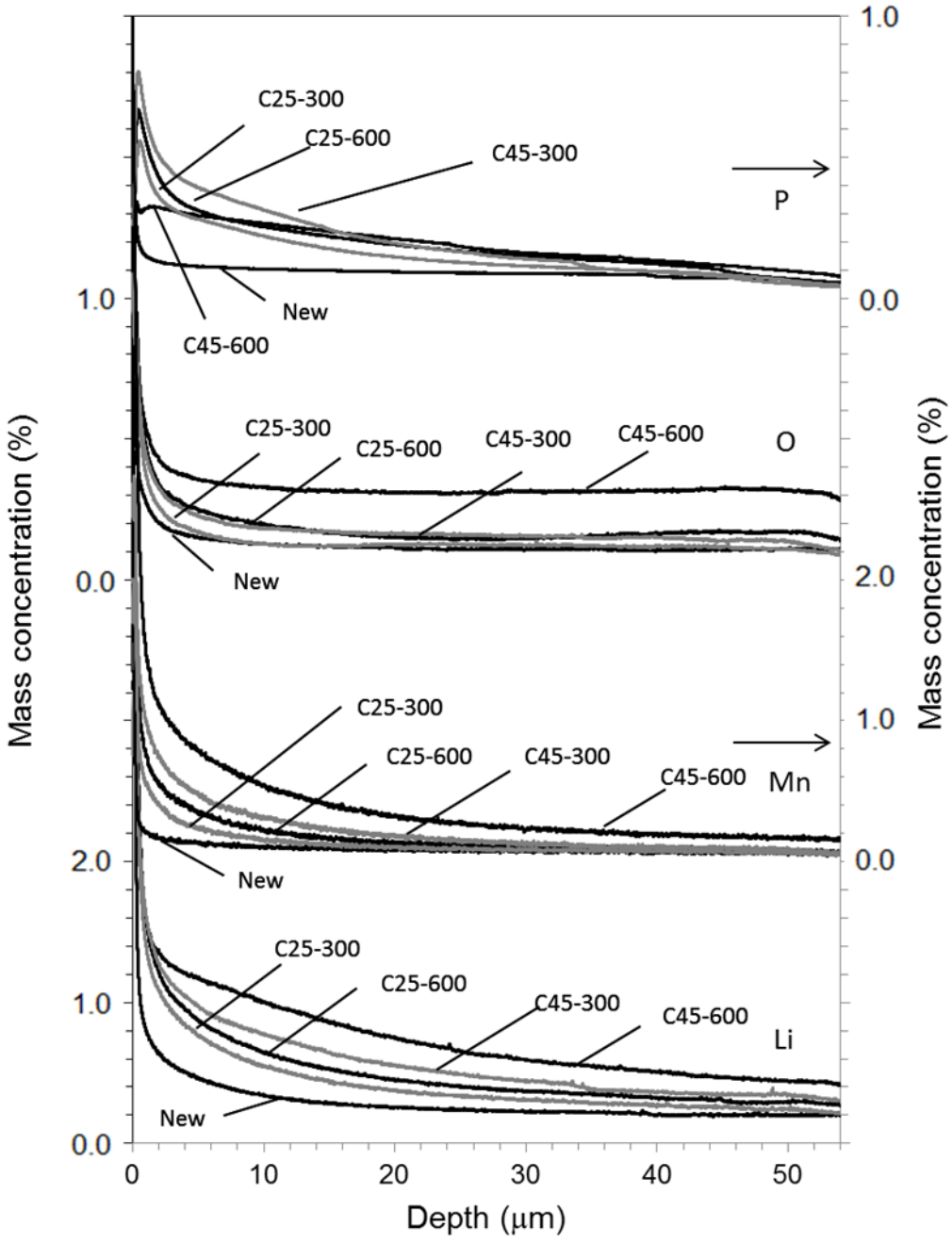

Fig.5.7. Depth profiles of the whole electrode for Li, Mn, O, and P for New and the degraded samples.

In addition to these experiments, another series of experimental laminate cell of $LiFePO_4$(LFP)/graphite was evaluated similarly. The cell capacity was faded to the degradation rate of 29% after 300 cycles at 45 °C under 2.5–4.0 V cut–off voltage and 1C current rate. Figure 5.8 shows the depth profile obtained for the degraded graphite electrode. Contrary to the results of Mn–based cathode cells (Fig. 5.6), Li concentration was almost constant throughout in the electrode, implying homogeneous SEI growth

regardless of depth for capacity fading. Therefore, the distribution of SEI growth was considered to vary with battery system components such as cathodes, anodes, and electrolytes and the operating conditions. Fe was not detected in the whole electrode, so that the Mn deposition in this study might trigger inhomogeneous SEI formation for the Mn–based battery.

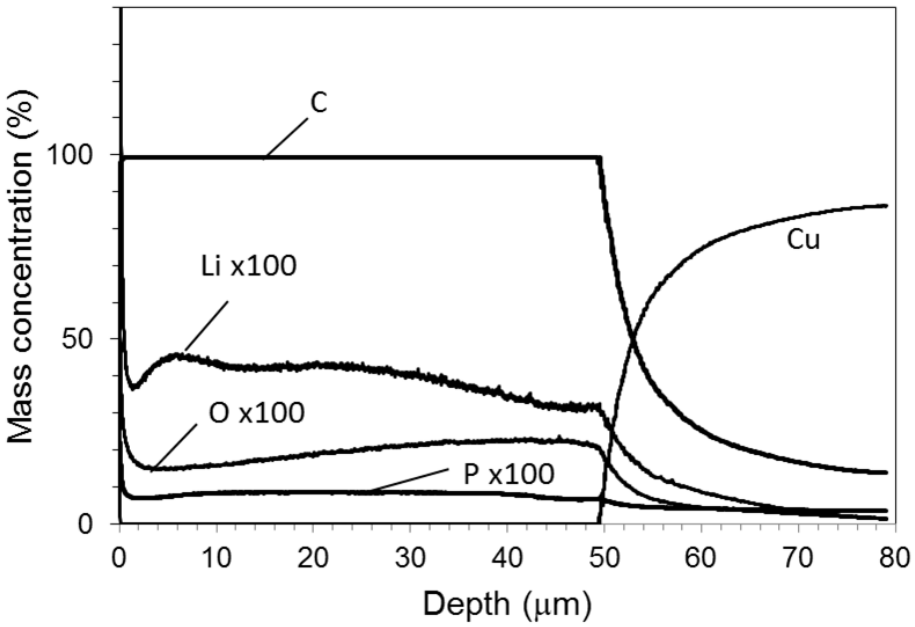

Fig. 5.8. GD-OES depth profile of the whole electrode for the graphite electrode from a degraded LFP/graphite cell.

Figure 5.9 presents quantification results for Li and Mn from both the whole electrode and the surface deposition. The total amount was quantified from the integrated intensity in each datum to compare the contributions of the surface to the whole layer. In the case of Li (Fig. 5.9(a)), the amount in the whole electrode increases concomitantly with the increasing degradation ratio. This trend for the whole electrode was similar to ICP–OES results (Table 5.1). However, GD–OES showed higher values overall than ICP–OES did. This fact was also shown for the case of Mn, as explained later. It is considered that the difference between the quantified values of GD–OES and ICP–OES originated from a slightly different background among electrode samples in GD–OES in principle. Contrary to the amount in the whole electrode, the amount of Li in the surface deposition was almost constant for the degraded samples, which meant that the Li deposition did not increase in the surface for degradation but increased in the inner part of

electrode. The amount of O and P in the surface deposition gradually increased with degradation ratio as shown in Fig. 5. In the corresponding whole electrode profiles, however, the O concentration was extremely high only in C45-600 and the P concentration was lower for C45-600 than for C45-300 (Fig. 7). Therefore, it is considered that the trend of variation could not be always consistent between in the surface deposition and in the whole electrode, as is shown in the variation of Li content in the surface deposition and in the whole electrode (Fig. 5.9(a)). In the case of Mn, the amount of Mn increased for the degraded samples on both the surface deposition and the whole electrode (Fig. 5.9(b)). The ratio of the surface likely increased concomitantly with increasing degree of degradation. The depth profiles of the whole electrode (Fig. 5.6) also showed preferable deposition of Mn in the outer layer comparing to Li. Such Mn distribution lying extremely on the surface can enhance the interface resistance, engendering degradation of the cell capacity, as reported previously [5, 6].

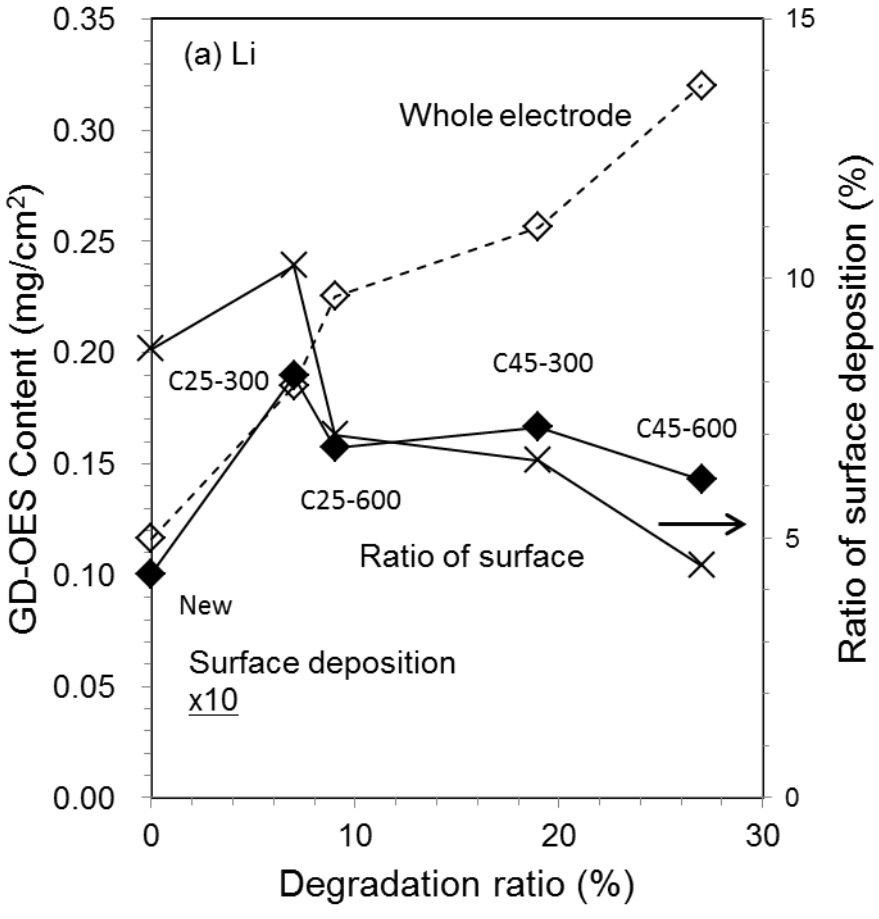

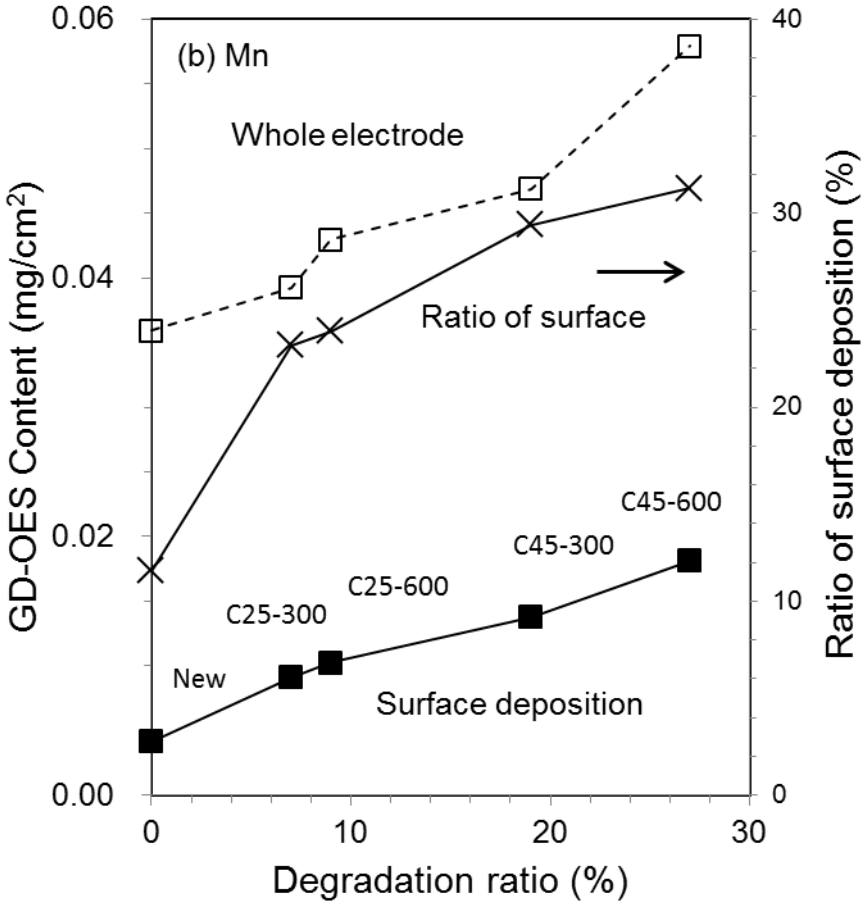

Fig. 5.9. The Li (a) and Mn (b) contents included in the whole electrode and the surface deposition are shown as a function of deterioration ratio for New and the degraded samples.

5.4 Conclusion

GD–OES was applied to characterize SEI and Mn deposition formed on the graphite electrodes for capacity degraded Mn–based cathode/Graphite Li–Ion Battery. Measurements were performed separately for the whole electrode from the surface to the current collector and for the surface deposition in detail. The measurement for the whole electrode was improved in the sputtering rate and stability with reactive Ar–H_2 discharge. Results show that Li was distributed homogeneously in the electrode except for the surface region for the initial state, but it was highly concentrated in the outer layer for the degraded states. This fact

suggests that the initial cycles formed homogeneous SEI except for the surface region, but additional cycles caused inhomogeneous SEI growth. The Mn deposition was apparently lower towards the current collector for the capacity degradation. Detailed surface measurements, confirmed the depth resolution with comparison to XPS analysis. The amount of Li deposited on the graphite electrode surface was almost constant after degradation. In contrast, the amount of Mn increased with the degree of degradation. Therefore it was considered that Mn deposition was more distributed in the outer layer than Li was.

5.5 References

[1] D. Aurbach, E. Zinigrad, Y. Chohen, and H. Teller, *Solid State Ionics*, **148**, 405 (2002).

[2] *Lithium–Ion Batteries Solid Electrolyte Interphase*, P. B. Balbuena and Y. Wang, Editors, Imperial College Press, USA (2007).

[3] S. Komaba, B. Kaplan, T. Ohtsuka, Y. Kataoka, N. Kumagai, and H. Groult, *J. Power Sources*, **119**–**121**, 378 (2003).

[4] D. H. Jang, Y. J. Shin, and S. M. Oh, *J. Electrochem. Soc.*, **143**, 2204 (1996).

[5] M. Ochida, Y. Domi, T. Doi, S. Tsubouchi, H. Nakagawa, T. Yamanaka, T. Abe, and Z. Ogumi, *J. Electrochem. Soc.*, **159**, A961 (2012).

[6] S. Komaba, N. Kumagai, and Y. Kataoka, *Electrochim. Acta*, **47**, 1229 (2002).

[7] Y. Kobayashi, T. Kobayashi, K. Shono, Y. Ohno, Y. Mita, and H. Miyashiro, *J. Electrochem. Soc.*, **160**, A1181 (2013).

[8] Y. Kobayashi, T. Kobayashi, K. Shono, Y. Ohno, Y. Mita, and H. Miyashiro, *J. Electrochem. Soc.*, **160**, A1415 (2013).

[9] A. J. Smith, J. C. Burns, and J. R. Dahn, *Electrochemical and Solid–State Letters*, **14**, A39 (2011).

[10] S. Krueger, R. Kloepsch, J. Li. S. Nowak, S. Passerini, and M. Winter, *J. Electrochem. Soc.*, **160**, A542 (2013).

[11] T. Tsujikawa, K. Yabuta, T. Matsushita, M. Arakawa, and K. Hayashi, *J. Electrochem. Soc.*, **158**, A322 (2011).

[12] Y. Saito and M. K. Rahman, *J. Power Sources*, **174**, 877 (2007).

[13] H. Takahara, H. Miyauchi, M. Tabuchi, and T. Nakamura, *J. Electrochem. Soc.*, **160**, A272 (2013).

[14] H. Takahara, M. Shikano, and H. Kobayashi, *J. Power Sources*, **244**, 252 (2013).

[15] H. Takahara, A. Kojyo, K. Kodama, T. Nakamura, K. Shono, Y. Kobayashi, M, Shikano, and H. Kobayashi, *J. Anal. At. Spectrom.*, **29**, 95 (2014).

[16] D. Fang and R. K. Marcus, *Glow Discharge Spectroscopies*, R. K. Marcus Editors, p. 30–31, Plenum Press, New York (1993).

[17] P. Verma, P. Maire, P. Novak, *Electrochim. Acta*, **55**, 6332 (2010).

[18] K. Xu, A. Cresce, *J. Mater. Chem.*, **21**, 9849 (2011).

[19] M. Nie, D. Chalasani, D. P. Abraham, Y. Chen, A. Bose, B. Lucht, *J. Phys. Chem*, **117**, 1257 (2013).

[20] A. M. Anderson, A. Henningson, H. Siegbahn, U. Jansson, and K. Edstrom, *J. Power Sources*, **119**–**121**, 522 (2003).

[21] M. Shikano, H. Kobayashi, S. Koike, E. Ikenaga, K. Kobayashi, and K. Tatsumi, *J. Power Sources*, **174**, 795 (2007).

[22] A. M. Anderson, D. P. Abraham, R. Haasch, S. MacLaren, J. Liu, and K. Amine, *J. Electrochem. Soc.*, **149**, A1358 (2002).

[23] S. K. Martha, J. Nanda, G. M. Veith, and N. J. Dudney, *J. Power Sources*, **216**, 179 (2012).

6. Conclusion

In this study, GD−OES method was studied for characterization of LIB electrodes. The measurement conditions of GD−OES were optimized in both positive and negative electrodes, at first. This enables us to see the depth profile of elemental compositions, including Li, from the surface to the interface of the current collector throughout. The quantitative ability of GD−OES was also evaluated with use of a series of positive and negative electrode samples including various Li concentrations controlled by states of charge (SOCs). The Li intensities obtained by GD−OES were correlated with Li components determined using ICP− MS. This confirmed that GD−OES is a potential technique for quantitative analysis of Li in the electrode.

There was a serious subject that the measurement of carbon−based anode took long time, which followed to lower the analytical sensitivity. This is because the sputtering yield of carbon is low and the sputtered carbon is partially redeposited on the sample surface. To solve the problem of low sputtering rate in carbon−based anode, the reactive sputtering with small quantities of hydrogen or oxygen addition to argon was investigated. For oxygen addition, the sputtering rate was enhanced drastically: ten−fold compared to conventional pure argon discharge. This outcome is attributed to chemical etching effects of oxygen in argon plasma. However, the depth profile of Li dispersed in a graphite electrode sample differed from that with pure Ar, which is likely because the etching reaction progresses inhomogeneously to the inner layer by SEM and XPS analyses. For adding hydrogen to argon plasma, not only shorter measurement time and higher sensitivity, but fine depth profile was brought about compared to those for pure argon. The benefits of hydrogen addition were indicated for both depth profiling and quantifying Li in graphite electrode samples.

Finally, the practical GD−OES was applied to characterize SEI and Mn deposition formed on the graphite electrodes for capacity degraded Mn−based cathode/Graphite batteries. Measurements were performed separately for the whole electrode with reactive Ar−H_2 discharge and for the surface deposition in detail. Results show that Li was distributed homogeneously in the electrode except for the surface region for the initial state, but it was highly concentrated in the outer layer for the degraded states. This fact suggests that the initial cycles formed homogeneous SEI except for the surface region, but additional cycles caused inhomogeneous SEI growth in the whole electrode. Mn deposition was more distributed in the outer layer than Li was. The depth profiling with GD−OES visualized the behavior of Li and Mn in the negative

electrodes to discuss the degradation mechanism.

Thus, quantifying and depth profiling capabilities of GD–OES are applicable and useful for characterization of LIB electrode. This could give us knowledge which we have not revealed clearly with other surface analysis techniques such as XPS and FT–IR. Uniformity of materials in electrode becomes more important factor to improve the cell performance and reduce the deterioration these days. This study indicates how GD–OES can contribute to research and development in LIB.

Acknowledgement

I am deeply grateful to Professor Tetsuya Nakamura of University Hyogo for his guidance for me to advance my study. I am grateful to Assistant professor Yoshihiro Oka and their students in the laboratory. I am also grateful to Professor Masaru Shimizu, Professor Shin−ichi Honda, and Professor Etsuo Fujiwara for their help to complete this thesis.

I would like to thank Dr. Hironori Kobayashi, Dr. Masahiro Shikano, Dr. Mitsuharu Tabuchi, Dr. Hiroyuki Kageyama, Dr. Tomonari Takeuchi, and Dr. Hikari Sakaebe of AIST. I received generous supports and warm encouragement from them always.

I would also like to thank Dr. Yo Kobayashi, Dr. Hajime Miyashiro and Ms. Kumi Shono of CRIEPI. Their cooperation to my study is greatly appreciated.

I would like to express my gratitude to Rigaku corporation for giving me an opportunity to study as a doctoral student. I would like to particularly thank Dr. Takashi Yamada, Dr. Hisashi Kohno, Mr. Kazuaki Okuda, late Mr. Noboru Yamashita, Mr. Atsushi Kojyo and Dr. Kenji Kodama for their supporting my study in many ways.

I would also like to thank Technos corporation, especially Mr. Kazuo Nishihagi (currently Horiba, Ltd.) and Mr. Yasuhiko Yoshida (currently Techno−X Co., Ltd.). They allowed me to continue my career as a researcher when I belonged to my unfamiliar field of analysis in semiconductor industry. At that time I had support and encouragement from TXRF working group of ISO TC201. I would like to thank Professor Yohichi Gohshi (Tsukuba University), Dr. Yoshihiro Mori (Horiba, Ltd.) and all members of the working group.

At the very end, I would like to offer special thanks to my teachers when I studied at Kobe University, Professor Yoji Kawamono, Professor Ryoji Kanno (currently Tokyo Institute of Technology), and Professor Masahide Takahashi (currently Osaka Prefecture University). I would like to offer thanks to Professor Kohei Kadono (currently Kyoto Institute of Technology) and Professor Junji Nishii (currently Hokkaido University) of AIST. Without their persistent guidance when I started my career, this thesis would not have been possible.

Publication list

Original articles

1. Hikari Takahara, Hironari Miyauchi, Mitsuharu. Tabuchi, Tatsuya. Nakamura, *J. Electrochem. Soc*., **160**, A272 (2013).
2. Hikari Takahara, Masahiro Shikano, Hironori Kobayashi, *J. Power Sources*, **244**, 252 (2013).
3. Hikari Takahara, Atsushi Kojyo, Kenji Kodama, Tatsuya Nakamura, Kumi Shono, Yo Kobayashi, Masahiro Shikano, Hironori Kobayashi, *J. Anal. At. Spectrom.*, **29**, 95 (2014).
4. Hikari Takahara, Yo Kobayashi, Kumi Shono, Hironori Kobayashi, Masahiro Shikano, Tatsuya Nakamura, *J. Electrochem. Soc*., **161**, A1716, (2014).

Presentations

1. グロー放電発光分析法によるリチウムイオン二次電池電極の表面分析，深さ方向分析，高原晃里, 古城篤志, 山下昇, 宮内啓成, 島裕也, 中村龍哉，第51回電池討論会，名古屋 (2010).
2. グロー放電発光分析（GD–OES）によるLIB電極中リチウムの定量分析の検討，高原晃里，小林弘典，第52回電池討論会，東京 (2011).
3. 市販リチウムイオン電池の劣化機構解明(II)－参照極導入と電圧微分解析による劣化過程の考察，小林 剛，小林 陽，庄野 久実，大野 泰孝，高原 晃里，山中 厚志，宮代 一，三田裕一，第52回電池討論会，東京 (2011).
4. 市販リチウムイオン電池の劣化機構解明(II)－温度測定と表面分析による劣化要因の考察，小林 陽，小林 剛，庄野久実，大野泰孝，高原晃里，山中厚志，宮代 一，三田裕一，第52回電池討論会，東京 (2011).
5. グロー放電発光法によるリチウム電池電極材料の深さ方向分析，高原晃里，電気化学セミナー（依頼講演），東京 (2011).
6. Depth profiling and Li quantification for Li-ion battery electrodes by glow discharge optical emission spectroscopy (GD–OES), Hikari Takahara, Hironari Miyauchi, Yo Kobayashi, Mitsuharu Tabuchi, Tatsuya Nakamura, 220th ECS meeting, Boston (2011).
7. Capacity fading process of $LiFePO_4$/graphite cells studied by depth profiling with glow discharge optical emission spectroscopy (GD–OES)，Hikari Takahara, Hironari Miyauchi, Mitsuharu

Tabuchi, Tatsuya Nakamura, 16th IMLB, Jeju (2012).

8. Quantification of lithium in LIB electrode by glow discharge optical emission spectroscopy (GD–OES), Hikari Takahara, Hironori Kobayashi, 16th IMLB, Jeju (2012).
9. Electrochemical performance of cathodes prepared on current collector with different surface morphology, Tatsuya Nakamura, Shingo Okano, Noriko Yaguma, Yukari Morinaga, Hikari Takahara, Yoshihiro Yamada, 16th IMLB, Jeju (2012).
10. Analysis of solid electrolyte interphase by glow discharge optical emission spectroscopy for Li–ion battery electrodes, Hikari Takahara, Hironari Miyauchi, Hironori Kobayashi, Yo Kobayashi, Tatsuya Nakamura, 222nd ECS meeting, Honolulu (2012).
11. グロー放電発光分析法（GD–OES）による劣化炭素負極の分析，高原晃里，庄野久実，小林弘典，鹿野昌弘，中村龍哉，小林陽，第53回電池討論会，福岡 (2012).
12. グロー放電発光分析法（GD–OES）によるLIB劣化炭素負極の分析，高原晃里，庄野久実，小林弘典，鹿野昌弘，中村龍哉，小林陽，第80回電気化学会，仙台 (2013).
13. Quantitative analysis of capacity fading mechanism in Mn-based cathode/graphite anode lithium-ion battery, Yo Kobayashi, Takeshi Kobayashi, Kumi Shono, Hikari Takahara, Yuichi Mita, Hajime Miyashiro, 223rd ECS meeting, Toronto (2013).
14. Depth profiling of solid electrolyte interphase in Li-ion battery electrodes with glow discharge optical emission spectroscopy, Hikari Takahara, Kumi Shono, Yo Kobayashi, Masahiro Shikano, Hironori Kobayashi, Tatsuya Nakamura, 224th ECS meeting, San Francisco (2013).
15. グロー放電発光分析法（GD–OES）によるLIB劣化炭素負極のSEI分析，高原晃里，庄野久実，小林陽，鹿野昌弘，小林弘典，中村龍哉，第54回電池討論会，大阪 (2013).
16. Mn系市販リチウムイオン電池の劣化要因定量分析，小林陽，加藤尚，大内崇広，工藤貴司，小林剛，庄野久実，高原晃里，大野泰孝，宮代一，三田裕一，第54回電池討論会，大阪 (2013).
17. 全固体リチウムイオンポリマー電池の開発–炭素系負極における不可逆リチウム量と電池劣化の関係，庄野久実，小林剛，田渕雅人，高原晃里，小林陽，大野泰孝，宮代一，第54回電池討論会，大阪 (2013).
18. グロー放電発光分析法によるリチウムイオン電池材料分析，高原晃里，平成25年度第2回関西分析研究会，（特別講演），京都 (2014).

19. グロー放電発光分析法（GD–OES）によるDLCの水素定量の検討, 高原 晃里, 石神 龍哉, 児玉 憲治, 古城 篤志, 安田 啓介, 中村 龍哉, 岡 好浩, 第61回応用物理学会春季大会, 東京 (2014).
20. High–temperature cycling performance of cathode with DLC protective film, Yoshihiro Oka, Taiki Obata, Hikari Takahara, Tatsuya Nakamura, 17th IMLB, Como (2014).

Literary work

1. リチウム二次電池性能向上への電極・電解質の表面処理/界面制御技術, 第6章リチウム二次電池用炭素負極の劣化とグロー放電発光分析によるSEI分析, 高原晃里（分担執筆）, 技術情報協会, 2014年発刊予定.